GEOSCIENCE CANADA

JOURNAL OF THE GEOLOGICAL ASSOCIATION OF CANADA
JOURNAL DE L'ASSOCIATION GÉOLOGIQUE DU CANADA

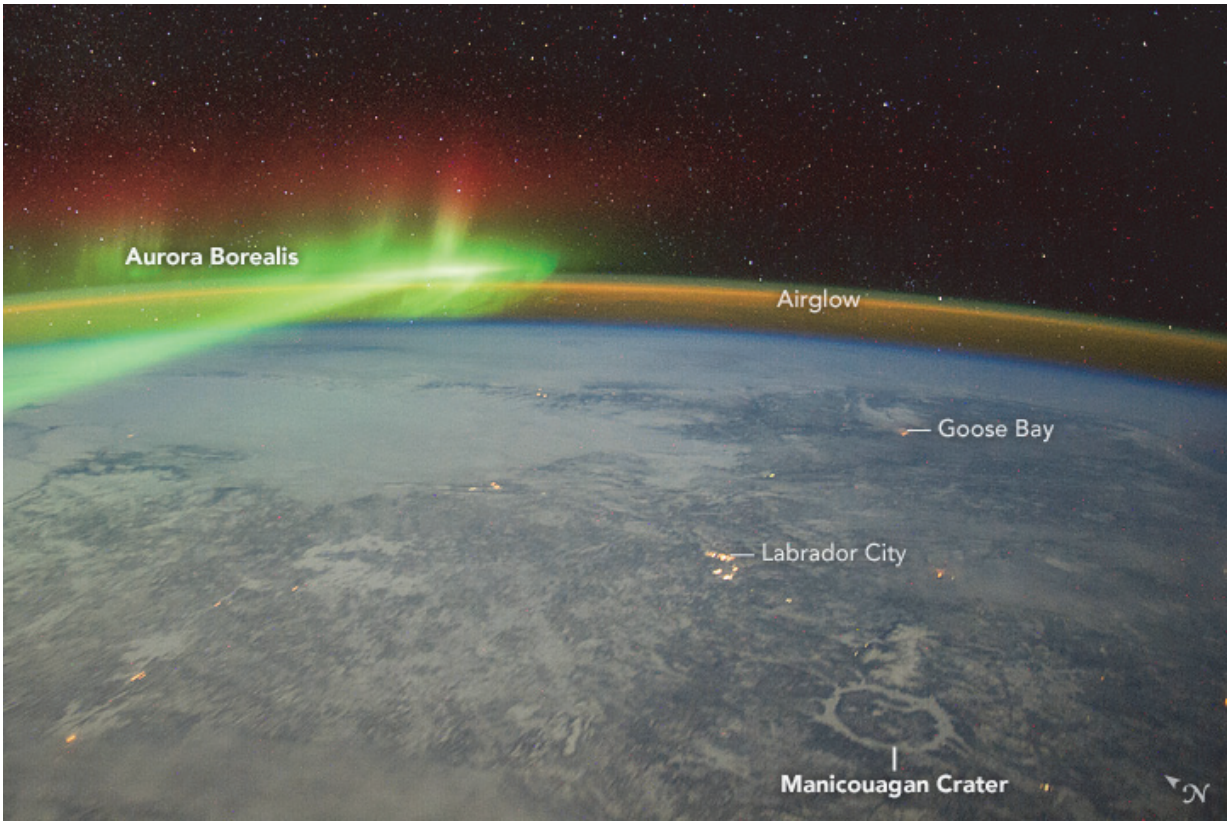

Inevitable impact events: The collateral benefits of catastrophes

Changing the shape of metamorphic petrology in phases

Pondering a possible Pliocene polar paradise

The clergyman, the lawyer, and the soft-bodied impression

2017 VOLUME 44

Publisher/Éditeur
Geological Association of Canada
c/o Department of Earth Sciences
Memorial University of Newfoundland
St. John's NL Canada A1B 3X5
Tel: (709) 864-7660
Fax: (709) 864-2532
gacpub@mun.ca
gac@mun.ca
www.gac.ca

Print Edition: ISSN 0315-0941
Online Edition: ISSN 1911-4850

Volume 44

A journal published quarterly by the Geological Association of Canada, incorporating the Proceedings.
Une revue trimestrielle publiée par l'Association géologique du Canada et qui en diffuse les actes.

Subscriptions: Receiving four issues of Geoscience Canada per year for $50 is one of the benefits of being a GAC member. To obtain institutional subscriptions, please contact Érudit: www.erudit.org

Abonnement: Recevoir quatre numéros par année pour 50,00 $ du magazine Geoscience est l'un des avantages réservés aux membres de l'AGC. Pour les abonnements institutionnels, s'il vous plaît contacter Érudit: www.erudit.org

Those wishing to submit material for publication in Geoscience Canada should refer to the Instructions to Authors on the journal's website, www.geosciencecanada.ca

AUTHORS PLEASE NOTE:
Please use the web address http://journals.hil.unb.ca/index.php/GC/index for submissions; please do not submit articles directly to the editor.

The Mission of the Geological Association of Canada is to facilitate the scientific well-being and professional development of its members, the learned discussion of geoscience in Canada, and the advancement, dissemination and wise use of geosciences in public, professional and academic life. Articles in Geoscience Canada are freely available two years after their publication date, unless authors have arranged for immediate open access. Opinions expressed and interpretations presented are those of the authors and do not necessarily reflect those of the editors, publishers and other contributors. Your comments are welcome.

Cover Image: A large asteroid impacted Earth some 214 MYA, creating the 100 km Manicouagan impact structure in Quebec. The impact caused a shock wave to radiate across Earth's surface, followed closely by high-velocity winds. Near the impact point, wind speeds would have exceeded 1000 km/hr. The shock wave and air blast would have severely damaged and killed plants and animals out to distances of ca. 600 km, as far as Goose Bay. After erosion by glaciers and other processes over millions of years, the Manicouagan crater is now visually dominated by the Manicouagan hydroelectric reservoir some 60 km in diameter.
Image credit: NASA, International Space Station.

GAC MEDALLIST SERIES

Logan Medallist 4.
Large-Scale Impact and Earth History

Richard A.F. Grieve

Department of Earth Sciences
University of Western Ontario
1151 Richmond Street, London
Ontario, N6A 5B7, Canada
Email: richard.grieve@canada.ca

SUMMARY

The current record of large-scale impact on Earth consists of close to 200 impact structures and some 30 impact events recorded in the stratigraphic record, only some of which are related to known structures. It is a preservation sample of a much larger production population, with the impact rate on Earth being higher than that of the moon. This is due to the Earth's larger physical and gravitational cross-sections, with respect to asteroidal and cometary bodies entering the inner solar system. While terrestrial impact structures have been studied as the only source of ground-truth data on impact as a planetary process, it is becoming increasingly acknowledged that large-scale impact has had its effects on the geologic history of the Earth, itself. As extremely high energy events, impacts redistribute, disrupt and reprocess target lithologies, resulting in topographic, structural and thermal anomalies in the upper crust. This has resulted in many impact structures being the source of natural resources, including some world-class examples, such as gold and uranium at Vredefort, South Africa, Ni–Cu–PGE sulphides at Sudbury, Canada and hydrocarbons from the Campeche Bank, Mexico. Large-scale impact also has the potential to disrupt the terrestrial biosphere. The most devastating known example is the evidence for the role of impact in the Cretaceous–Paleocene (K–Pg) mass extinction event and the formation of the Chicxulub structure, Mexico. It also likely had a role in other, less dramatic, climatic excursions, such as the Paleocene–Eocene–Thermal Maximum (PETM) event. The impact rate was much higher in early Earth history and, while based on reasoned speculation, it is argued that the early surface of the Hadean Earth was replete with massive impact melt pools, in place of the large multiring basins that formed on the lower gravity moon in the same time-period. These melt pools would differentiate to form more felsic upper lithologies and, thus, are a potential source for Hadean-aged zircons, without invoking more modern geodynamic scenarios. The Earth-moon system is unique in the inner solar system and currently the best working hypothesis for its origin is a planetary-scale impact with the proto-Earth, after core formation at ca. 4.43 Ga. Future large-scale impact is a low probability event but with high consequences and has the potential to create a natural disaster of proportions unequalled by other geologic processes and threaten the extended future of human civilization, itself.

RÉSUMÉ

Le bilan actuel de traces de grands impacts sur la Terre se compose de près de 200 astroblèmes et d'une trentaine d'impacts enregistrés dans la stratigraphie, dont seulement certains sont liés à des astroblèmes connus. Il s'agit d'échantillons préservés sur une population d'événements beaucoup plus importante, le taux d'impact sur Terre étant supérieur à celui de la lune. Cela tient aux plus grandes sections transversales physiques et gravitationnelles de la Terre sur la trajectoire des astéroïdes et comètes qui pénètrent le système solaire interne. Alors que les astroblèmes terrestres ont été étudiés comme étant la seule source de données avérée d'impacts en tant que processus planétaire, de plus en plus on reconnaît que les grands impacts ont eu des effets sur l'histoire géologique de la Terre. À l'instar des événements d'énergie extrême, les impacts redistribuent, perturbent et remanient les lithologies impliquées, provoquant dans la croûte terrestre supérieure des anomalies topographiques, structurelles et thermiques. Il en a résulté de nombreux astroblèmes à l'origine de ressources naturelles, dont certains exemples de classe mondiale tels que l'or et l'ura-

Geoscience Canada, v. 44, https://doi.org/10.12789/geocanj.2017.44.113 pages 1–26

nium à Vredefort en Afrique du Sud, les sulfures de Ni–Cu–PGE à Sudbury au Canada, et les hydrocarbures du Banc de Campeche au Mexique. Les grands impacts peuvent également perturber la biosphère terrestre. L'exemple le plus dévastateur connu nous est donné des indices du rôle de l'impact dans l'extinction de masse au Crétacé–Paléogène (K–Pg) et la formation de la structure de Chicxulub, au Mexique. Il a également probablement joué un rôle dans d'autres événements climatiques extraordinaires moins dramatiques, comme le Maximum thermal du Paleocène–Eocène (PETM). Le taux d'impact était beaucoup plus élevé au début de l'histoire de la Terre et, tout en étant basé sur une spéculation raisonnée, on fait valoir que la surface précoce de la Terre à l'Hadéen était tapissée de grands bassins en fusion, au lieu de grands bassins à couronnes multiples tels ceux qui se sont formés à la même période sur la lune ayant une gravité inférieure. Ces bassins en fusion se seraient différenciées pour constituer des lithologies plus felsiques sur le dessus, devenant ainsi une source potentielle de zircons d'âge Hadéen, sans qu'il soit nécessaire d'invoquer des scénarios géodynamiques plus récents. Le système Terre-lune est unique dans le système solaire interne. Actuellement la meilleure hypothèse de travail pour son origine est un impact planétaire avec la proto-Terre, après la formation du noyau à env. 4,43 Ga. La probabilité d'un futur grand impact est faible mais comporte des conséquences capables d'engendrer un désastre naturel aux proportions inégalées comparé à d'autres processus géologiques, menaçant l'avenir de la civilisation humaine elle-même.

Traduit par le Traducteur

INTRODUCTION

Planetary exploration has clearly demonstrated that impact is a ubiquitous process throughout the solar system. Impact was dominant in early planetary history and its effects are most obvious on smaller, airless bodies. For example, even a casual examination of orbital imagery of the Earth's moon clearly illustrates the importance of impact in lunar geologic history (Fig. 1a). The same can not be said for imagery of the Earth (Fig. 1b). The Earth's physical cross-section, however, is ~ 3.5 times larger than that of the moon. More importantly, from the point of view of incoming extraterrestrial bodies, its gravitational cross-section is even larger (~ 50 times larger for an average asteroidal impact velocity). Thus, the Earth has presented a much larger target to asteroidal and cometary bodies entering the inner solar system and, therefore, must have received many more impacts than the moon throughout geologic time. The simplest explanation for the apparent contradiction in the appearance of the surface of the Earth compared to that of the moon in orbital imagery lies in the fact that the results of the impact, impact structures and their attendant ejecta, are surface features. The Earth is the most active of the terrestrial, or silicate, planets in terms of endogenic geologic processes. Its surface is constantly being reworked and reshaped through tectonic, erosional and depositional processes. Through this resurfacing, the Earth's impact record has been obscured and largely removed. As a result, the Earth's known share of impact structures is not a production population, as on many areas of the moon, but is a preservation sample of an originally much larger population.

Unlike some other geologic processes, such as volcanic eruptions, earthquakes and inundation and erosional events, major terrestrial impact events have not occurred on the recorded human time-scale. Impact is also unlike other geologic processes in terms of the extreme pressures and temperatures generated and the very high strain rates and short timescales involved. These may be among the reasons that the geoscience community was relatively late in recognizing the occurrence of terrestrial impact structures. The first terrestrial structure to be suggested as the result of impact was the now famous 1.2 km diameter Meteor or Barringer crater in Arizona, USA (Barringer 1905). Its origin was controversial and remained largely so for over 50 years, until the discovery of coesite, the high pressure polymorph of quartz, at Barringer (Chao et al. 1960). A major increase in the scientific interest into the nature of terrestrial impact structures occurred leading up to and during the Apollo missions by NASA, where they served as terrestrial analogs for lunar impact craters. It was in this period when the diagnostic effects of impact on rocks and minerals, known as shock metamorphism, were firmly established (e.g. French and Short 1968). At that time, the study of impact processes was the domain of a relatively small number of 'specialists' and impact was still generally regarded by the larger community as a significant process in the geologic history of other planetary bodies but not of particular significance to that of the Earth.

This perception remained largely in place until, initially, geochemical, and, later, physical evidence began to emerge for the role of impact in the Cretaceous–Paleogene (K–Pg) mass extinction event (e.g. Alvarez et al. 1980; Ganapathy 1980; Bohor et al. 1984). As with the initial suggestion that the Barringer crater was produced by a terrestrial impact event, this working hypothesis was not without controversy, particularly in some segments of the geoscience community. As additional and equivalent evidence for impact was forthcoming from other K–Pg boundary sites world-wide, however, the working hypothesis gained more acceptance. It received a major increase in credibility with the eventual identification of the actual K–Pg impact site, namely the buried 180 km diameter Chicxulub impact structure in the Yucatan, Mexico (Hildebrand et al. 1991). Although Chicxulub was not without its own initial controversies, e.g. its exact size and morphology, these have largely dissipated through the results of extensive geophysical, particularly, reflection seismic, campaigns (e.g. Morgan et al. 1997, 2011). In addition, there have been accompanying drilling programs by the International Continental Drilling Program (ICDP), National Autonomous University of Mexico (UNAM), and most recently the completion of a joint Integrated Ocean Drilling Program (IODP)-ICDP drilling of Chicxulub's peak-ring structure off-shore (Morgan et al. 2015, 2016). The working hypothesis relating the K–Pg boundary sites world-wide and the mass extinction to a major impact event on Earth and the ensuing debate and studies moved the perception of impact from one of it being almost exclusively a planetary process to one of also being a process of some

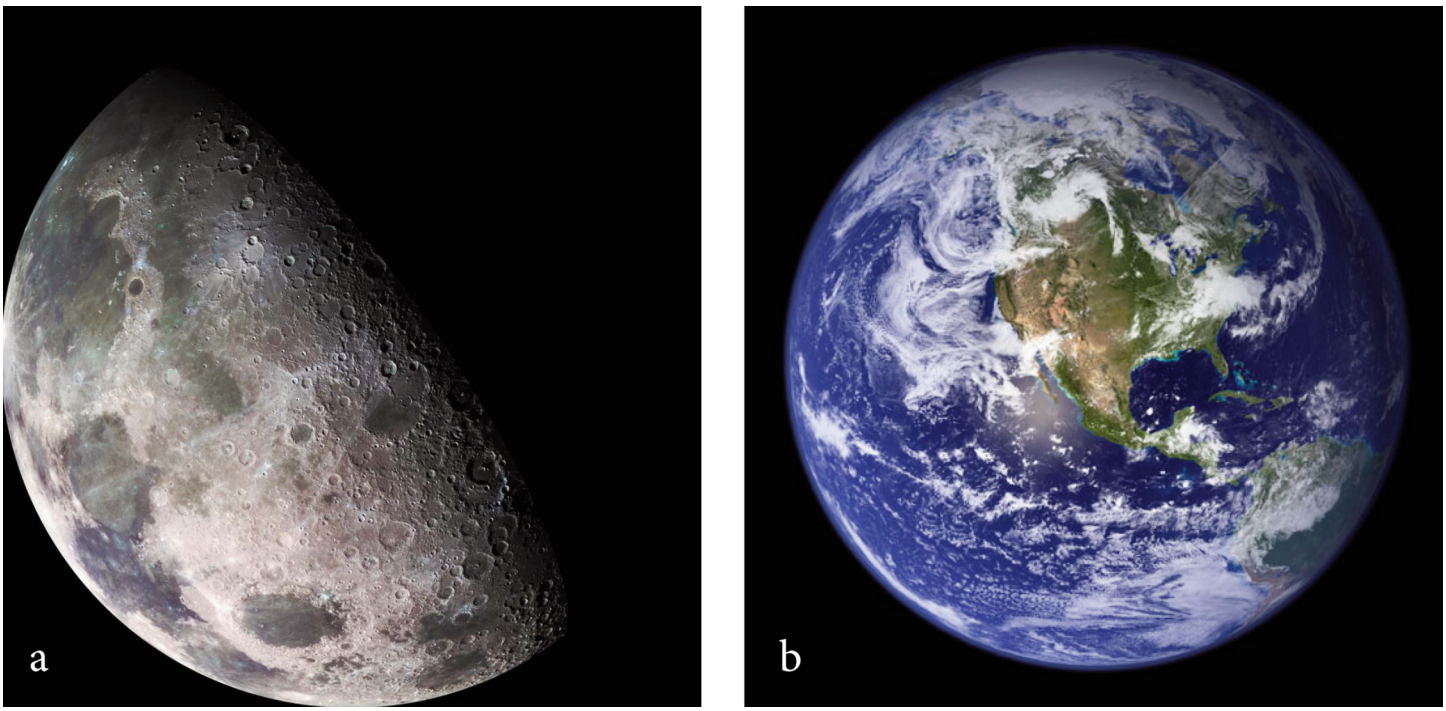

Figure 1. a) Orbital image of the moon, indicating its highly cratered surface. b) Orbital image of the Earth, indicating its apparently uncratered surface. NASA imagery.

potential importance in the context of terrestrial geologic history. It also had the effect of broadening the interest in and knowledge of impact processes to the larger, and more general, geoscience community. So much so that today, the discovery and documentation of a new terrestrial impact structure or impact event are as likely to be authored by workers from the larger geoscience community, as by those specializing in impact studies.

While the K–Pg boundary remains currently the sole example of a terrestrial mass extinction, with demonstrable evidence for the role of a major impact event on Earth, it is the thesis of this contribution that the role of large-scale impact in Earth history is much more diverse and goes well beyond this apparently singular event. As most of the terrestrial impact record has been destroyed by endogenic geologic processes, some of what is presented is based on planetary analogies and reasoned speculation.

THE TERRESTRIAL IMPACT RECORD: AN OVERVIEW

Small extra-terrestrial objects enter the Earth's atmosphere, which retards their cosmic velocity, every day and either burn-up in the atmosphere as meteors or land on Earth, at relatively low velocities, as meteorites. Larger objects ($> 9 \times 10^7$ kg), however, do not have their velocity reduced by atmospheric passage and impact the Earth with a velocity that is a combination of their cosmic velocity and the Earth's gravitational attraction. The minimum impact velocity of such objects is 11.2 km.s^{-1}, the escape velocity of the Earth. Asteroidal bodies are the most common of such objects and impact with an average velocity of ~ 18 km.s^{-1}. Less common are impacts by short-period comets, with an average impact velocity of ~ 30 km.s^{-1}. Long-period comets are even less common but impact with a higher average velocity of ~ 50 km.s^{-1} (e.g. http://impact.ese.ic.ac.uk/ImpactEffects/).

On impact, these asteroidal and cometary bodies transfer their considerable kinetic energy to the target rocks. For example, a 1 km diameter, stony asteroidal body impacting the Earth at 18 km.s^{-1} contains some 2.5×10^{20} J of kinetic energy. This essentially instantaneous energy release is of the same order as the annual release of internal energy of the entire Earth from crustal heat flow, volcanic eruptions and earthquakes. Impact events of this scale, however, occur on the million year time-scale. The impacting body transfers its kinetic energy to the target rocks via a shock wave, which propagates into the target rocks and back into the impacting body. In the target rocks, the kinetic energy of the impacting body is partitioned into kinetic energy, which sets the target rocks in motion and leads to the formation of a craterform, and into internal energy, which leads to shock metamorphic effects. Since stress can not be maintained at free surfaces (edges of the impacting body, the surface of the target rocks), rarefaction or release waves follow the propagating shock wave. The particle velocity vectors from rarefaction combine with those induced by the passage of the shock wave to produce the so-called 'cratering flow-field,' which results in the ejection of material from the upper and outer reaches of the target and downward displacement of material in the lower and central reaches of the target. The maximum radial extent of ejected and displaced materials in the target by the cratering flow-field defines the so-called transient cavity in an impact event. The transient cavity is a conceptual construct and only exists as an entity in the smallest of impacts. It is generally taken to be approximately parabolic in cross-section but, as indicated by its name, it represents an unstable situation due to gravitational

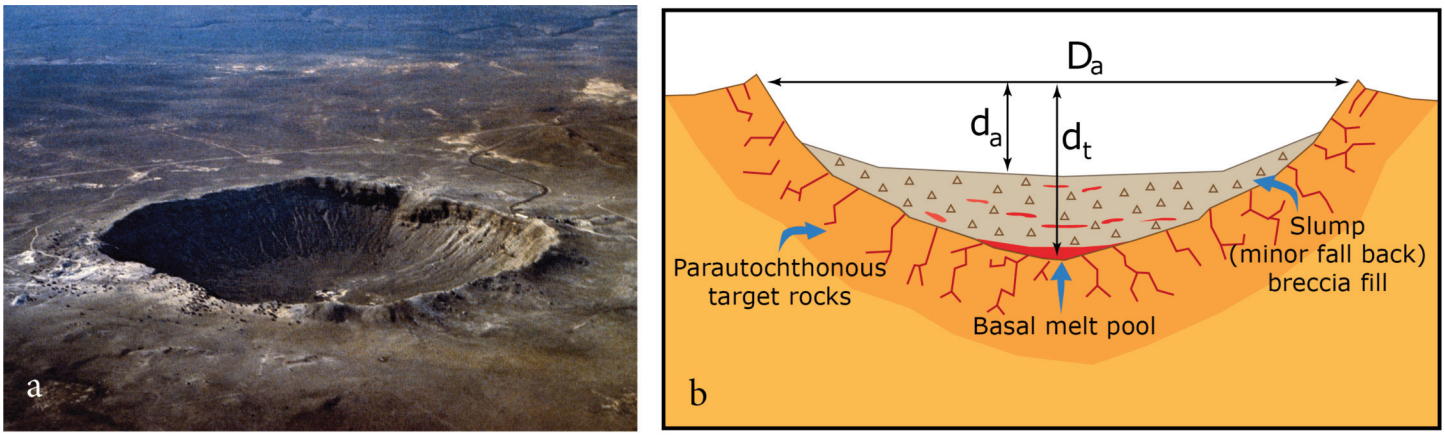

Figure 2. a) Barringer (Meteor) crater, USA, is a 1.2 km diameter (D_a) simple crater (bowl-shaped). Note rather square outline of rim, due to the effects of pre-existing regional jointing. b) Schematic cross-section of a simple crater. Note visible surface, as seen at Barringer (above), defines the apparent crater, with depth (d_a), and is underlain by a breccia lens, the base of which defines the true crater, with depth (d_t).

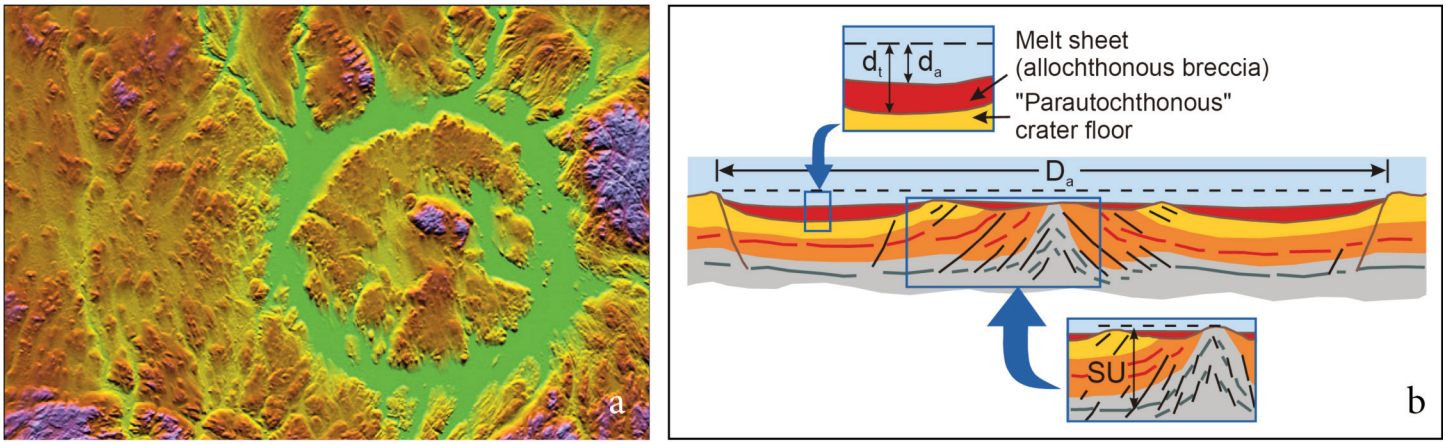

Figure 3. a) Colour image of topography of the complex Manicouagan structure, Canada, based on NASA SRTM data. Reds and blues are high, yellows and greens are low. Manicouagan has an estimated original diameter of ~ 100 km. Note the smooth annulus ~ 55 km in diameter that corresponds to the Manicouagan hydroelectricity reservoir, the slightly off-centre topographic peak (horst of uplifted anorthosite target rocks) and the topographic lineations that reflect the effects of glaciation, particularly within the annulus where the coherent impact melt sheet outcrops. b) Schematic cross-section of a complex impact structure, with a central peak and ring. Note the structural uplift (SU) of parautochthonous target rocks in the centre and that d_a and d_t are much shallower with respect to D_a, compared to a simple crater, reflecting the greater modification with respect to the initial transient cavity. As with simple crater, the interior of complex structures are partially filled with allochthonous impact lithologies (impact melt rock, breccia).

forces and collapses and is modified, almost as it forms and grows, resulting in the final craterform.

The final craterform is a function of the size of the impact event, planetary gravity and the dynamic strength of the target rocks. Smaller impact structures are so-called simple structures (Fig. 2a). When fresh, they are bowl-shaped in form, with an upraised and overturned rim, which is overlain by ejecta. They are partially filled, to approximately half the depth of the original transient cavity, with impact lithologies, such as various types of breccias and impact melt rocks (Fig. 2b). These lithologies largely represent fractured and brecciated transient cavity wall rocks and their lining that collapsed inward under gravity, during the modification of the transient cavity. Larger impact structures are so-called complex structures (Fig. 3a, b). Complex structures occur at diameters > 2–5 km on Earth, depending on the nature of the target rocks (crystalline, sedimentary or both). They are characterized by a complex, faulted and collapsed rim area, a relatively flat floor and some form of uplifted structure in the centre (Fig. 3b). They represent a much more highly modified craterform, with respect to the transient cavity, than simple structures. The uplifted central structure consists of parautochthonous target rocks from the transient cavity floor. It has the form of an emergent topographic peak or ring, above the crater-fill products lining the parautochthonous crater floor, depending on the size of the impact event. The vertical amount of this 'structural uplift' in the centre of complex structures is approximately 0.1 of the rim diameter (Fig. 4). The largest impact structures, which have an internal topographic ring structure, are often referred to as impact basins. As with simple structures, the crater-fill products at complex structures consist of various breccias and impact melt rocks, the latter being a dominant lithology in impacts into crystalline targets (Fig. 3b). The crater-fill products represent material that failed to be ejected from the transient cavity.

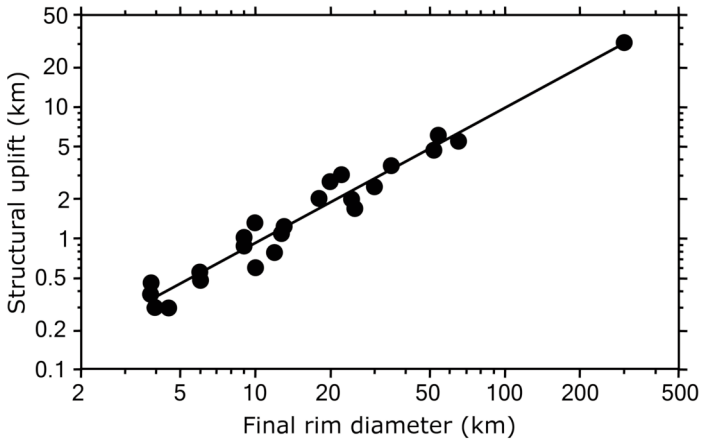

Figure 4. Logarithmic plot of apparent diameter (D_a) against structural uplift (SU) for terrestrial complex impact structures, indicating that uplift varies as ~ 0.1 D_a.

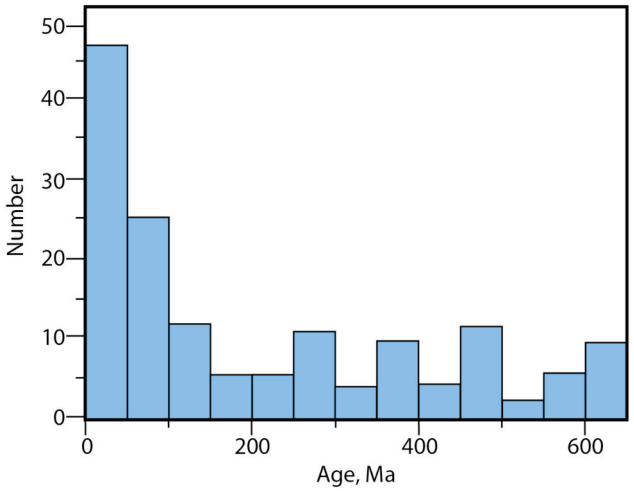

Figure 5. Histogram of the ages of Phanerozoic terrestrial impact structures, with < ± 10 m.y. age uncertainty and binned by 50 Ma. Note temporal bias towards 'young' ages, reflecting the effects of endogenic terrestrial geologic processes in removing and obscuring 'older' impact structures.

The preservation sample of impact structures that constitutes the terrestrial impact record is biased, compared to that, for example, of the moon. It is biased towards larger and younger structures (Fig. 5). This is a reflection of the fact that not only are such larger structures more likely to be preserved in the very active terrestrial geologic environment but they are also more likely to be recognized. Their spatial distribution is also biased towards the more geologically stable cratonic areas of the Earth, where they are more likely to be preserved (Fig. 6). In some cases, terrestrial impact structures have been eroded below the original crater floor and no longer have an associated negative topographic expression. In several cases, differential erosion has resulted in their present topographic expression being positive, relative to the surrounding terrain (e.g. only an erosionally resistant central structure remains). Thus, it is more appropriate, and encompassing, to refer to them as terrestrial impact 'structures' as opposed to 'craters.'

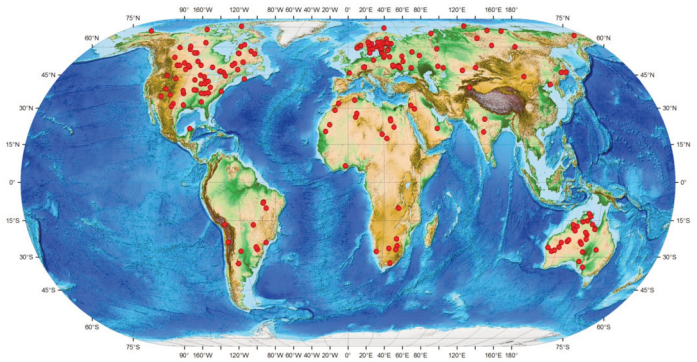

Figure 6. Spatial distribution of known terrestrial impact structures. Note bias towards preservation and recognition of impact structures on stable cratonic areas, particularly where there have been active programs to identify impact structures (e.g. North America, Fennoscandia, Australia). Image from G. Osinski, Western University.

The known terrestrial impact record currently stands at ~ 200 impact structures, with several new discoveries per year. Basic information (name, size, age, location, etc.) on known terrestrial impact structures can be found at http://www.passc.net/EarthImpactDatabase/. They range in size from metres to ~ 300 km in diameter and in age from Recent to Precambrian. Approximately 30% of known terrestrial impact structures are buried by post-impact sediments. They were detected originally as geophysical anomalies and subsequently drilled for economic or scientific purposes. In addition, there are ~ 30 impact events recorded in the stratigraphic column, in the form of ejecta deposits, spherule layers, tektites and microtektites, only some of which are related to known impact structures.

Given the effects of erosion and the very active endogenic geologic environment, the confirmation of the occurrence of a terrestrial impact structure is not based on its topographic expression, although that may be the reason for its initial interest as a potential impact structure. Confirmation of an impact origin is based on the occurrence of irreversible changes in the target rock and minerals by shock metamorphism or the physical or chemical evidence of meteoritic material. Shock metamorphic effects are a direct result of the shock wave increasing the internal energy of the target rocks and are, thus, diagnostic of impact. They do not occur below shock pressures of several GPa and continue up to pressures of 100's of GPa (Fig 7). They include the formation of: shatter cones, the only known megascopic shock effect; microscopic so-called planar deformation features (PDFs), best known in quartz and feldspar; so-called diaplectic or thetomorphic solid-state glasses in quartz and feldspar; impact melt rocks and glasses; and various high pressure polymorphs, such as coesite and stishovite from quartz and diamond from graphite (Fig. 8).

Shock metamorphic effects are not produced directly by the passage of the shock wave and compression of the target rocks but rather after the shock pressure is released, following the passage of the rarefaction wave. With increasing pressure, the net effect of shock compression and pressure release is to increase the entropy and degree of disorder in the target rocks

https://doi.org/10.12789/geocanj.2017.44.113

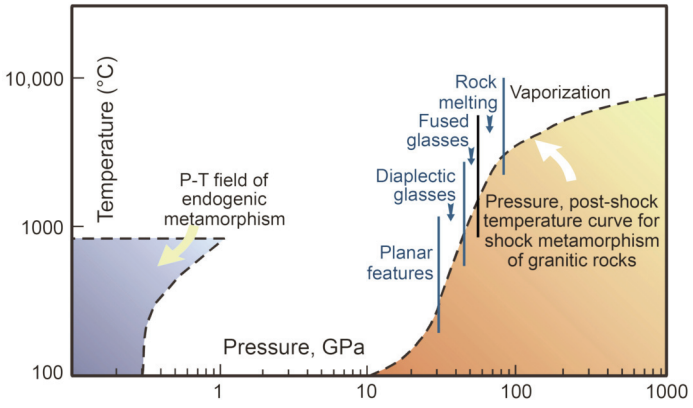

Figure 7. Logarithmic pressure–temperature curve for shock metamorphism in granitic rocks, with the attendant pressure–temperature range of some specific shock metamorphic features, compared with field of endogenic metamorphism.

and their constituent minerals, such that still crystalline shocked rocks and minerals are less dense than their original state. Impact melting (and even vaporization and ionization) occur as a result of the fact that considerable pressure–volume work is performed on the target rocks during shock compression but pressure release is adiabatic and not all this pressure–volume work is recovered. The work not recovered on pressure release is manifested as waste heat, which leads to increased post-shock temperatures and, ultimately, mineral and whole rock melting of target materials. This melting is not the same as in igneous processes and does not correspond to the standard phase diagram behaviour of rocks and minerals. It is a function of the compressibility of minerals, with more compressible minerals retaining more waste-heat and, thus, melting when subjected to lower shock pressures than less compressible minerals.

Although there are secondary effects due to target type (e.g. crystalline versus sedimentary), impact is a scale-dependent process that is very much governed by physics. The above has been the briefest of summaries regarding impact processes, and readers interested in more detail, particularly in regard to the physics behind impact cratering, are referred to Melosh (1989). Further entrance to literature can be made through a series of Geological Society of America Special Papers, based on conferences on "Large-scale impact and planetary evolution", the latest of which was edited by Osinski and Kring (2015). The most recent synopsis of current knowledge on impact process and products can also be found in Osinski and Pierazzo (2012).

The effects of large-scale impact on the Earth are discussed below, in the order of decreasing empirical evidence and increasing reasoned speculation, i.e. from the present back through the Phanerozoic to the earliest times in Earth's history, for which no substantive record remains. There is also an accompanying thematic focus. The present and historical time illustrate the economic benefits of impact to human civilization, with the focus on the observation that a number of impacts have resulted in the concentration of exploitable natural resources. The Phanerozoic geologic record highlights the potential for major impacts to affect the terrestrial biosphere, with emphasis on the working hypothesis that a major impact

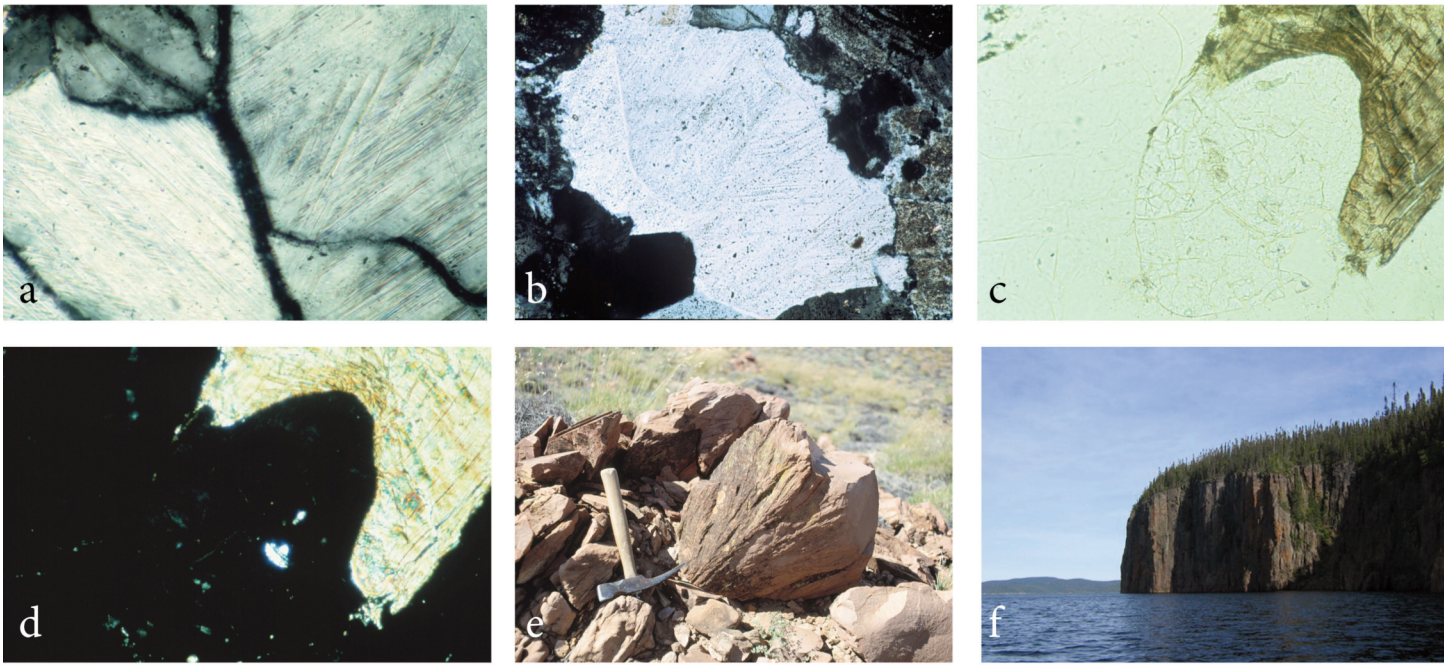

Figure 8. a) Photomicrograph of relatively fresh (undecorated) planar deformation features (PDFs) in quartz in target rocks at the 36 ± 4 Ma Mistastin structure, Canada. Crossed polars, field of view 1 mm. b) Photomicrograph of partially annealed (decorated) planar deformation features in quartz in target rocks at 1.85 Ga Sudbury structure. Crossed polars, field of view 1 mm. c) Photomicrograph of granodiorite target rocks at Mistastin structure, with quartz (white, high relief), feldspar (white, low relief) and biotite (brown). Plane light, field of view 1 mm. d) As c) but with crossed polars. Both quartz and feldspar are isotropic (black), as they are solid-state diaplectic glasses that have retained their original crystal forms. e) Shatter cones at the Gosses Bluff structure, Australia. Hammer for scale. f) Cliffs of coherent impact melt rock at the Manicouagan structure, Canada. Current thickness of melt rocks is ~ 200 m.

event was the cause of the K–Pg mass extinction event. The earliest times of Earth history are the most speculative, with respect to the effects of impact on Earth history, but some reasoned potential consequences of major impacts and their role in the earliest crustal evolution of the Earth and the formation of the Earth's moon are presented.

NATURAL RESOURCES AND IMPACT

Some 20% of known terrestrial impact structures have some form of associated natural resources and, of these, about half are being exploited or have been historically. Reimold et al. (2005) list 56 impact structures with 'economic interests,' including structures that provide sites for recreational activities and/or serve as tourist attractions. In addition, several structures have been, or are being, exploited as a source of building materials (e.g. Ries, Germany; Rochechouart, France), or sources of groundwater or as reservoirs for hydro-electric power generation (e.g. Puchezh-Katunki, Russia; Manicouagan, Canada). The economic value of such resources, however, can be considerable. For example, the electricity generated by the Manicouagan reservoir is of the order of 5000 $GWh.a^{-1}$, which is sufficient to supply a small city (~ 500,000 households with average consumption) and worth approximately $700 million per year (at 2016 Ontario electricity rates).

Natural resource deposits at terrestrial impact structures are considered under the headings of progenetic, syngenetic and epigenetic (Grieve and Masaitis 1994). Commercial accumulations of hydrocarbons at terrestrial impact structures result from a number of processes related to impact and are considered separately. Some generalities of the types of deposits are given in Table 1 and only a few examples of the larger and more important deposits are given here. For more comprehensive coverage of the full range of natural resources occurring in association with terrestrial impact structures, the reader is referred to Reimold et al. (2005) and Grieve (2012).

Progenetic Deposits

Progenetic economic deposits originated prior to the impact event by endogenic terrestrial concentration mechanisms. The impact event itself subsequently resulted in the spatial redistribution of these deposits and, in most cases, brought them to a surface or near-surface stratigraphic position, from where they can be exploited. Progenetic economic deposits in impact structures include iron, uranium, gold, hydrocarbons and others (Table 1). In many cases, the deposits are relatively small. For illustration, a Canadian (Carswell) and a world-class (Vredefort) example are presented here.

Uranium at Carswell

The Carswell structure in northern Saskatchewan, Canada, is a complex impact structure in the Athabasca Basin. The Proterozoic-aged Athabasca Basin is the richest known and second largest uranium-producing region in the world. The Carswell structure has been eroded to below the original crater floor and is apparent in Shuttle Radar Topography Mission (SRTM) imagery as two circular ridges, corresponding to the outcrop of the dolomite of the Carswell Formation (Fig. 9a, b). The outer ridge is ~ 39 km in diameter and is generally quoted as the diameter of the structure; although it may well be an underestimate. Interior to this, there is an annular trough, occupied by sandstone and conglomerate of the Athabasca Group. This trough is ~ 5 km wide and rises to a core, ~ 20 km in diameter, of mixed gneisses of the basement, which are believed to have been structurally uplifted by > 2 km (Baudemont and Fedorowich 1996). The inner contact of the Athabasca Group sedimentary rocks with the basement is faulted and truncated in places and offset by radial faults. The outcrops of the sedimentary rocks are unique to the area and owe their preservation to having been down-faulted > 1 km in the impact. Brecciation is common at Carswell and affects all lithologies. So-called 'Cluff Breccias,' after exposures near Cluff Lake, include autochthonous monomict, allochthonous polymict clastic and melt-bearing breccias, as well as clast-rich impact melt rocks.

The known commercial uranium deposits (Fig. 9) occur in two main settings: at the unconformity between the Athabasca Group and the uplifted crystalline basement core, and in mylonites and along faults in the crystalline core. These deposits had grades from 0.3 to > 4% uranium oxide (Jefferson and Delaney 2007). The original uranium mineralization in the Athabasca Basin, and at Carswell, occurred during regolith development in the Precambrian, with later remobilization due to hydrothermal activity (Lainé et al. 1985). The original commercial uranium deposit discovered at Carswell, the Cluff Lake D deposit, was, at the time of mining, the richest known uranium ore body in the world. It closed in 2002, having produced 28.1 kt of 'yellow cake,' an intermediate milling product consisting mostly of uranium oxide, over its 22 year lifetime.

Baudemont and Fedorowich (1996) recognized four episodes of deformation at Carswell, with the third episode related to mineralization and the final episode related to the impact event. They noted that Carswell-related deformation reactivated earlier faults, associated with the main mineralization, and that the association was "striking". It is not clear to what extent the Carswell impact event was involved in remobilizing the uranium ores, beyond physical movement related to structural uplift. The basement-hosted ores are all associated with extensive regional alteration and hydrothermal fluid movement. All known commercial uranium deposits within the Carswell structure are currently closed. There are, however, active exploration targets, including reactivated faults, with pseudotachylitic breccia and/or 'Cluff Breccias' and uranium mineralization. In addition to bringing ore bodies to the surface, Carswell serves as a unique window into the nature of basement beneath the Athabasca Basin and, as such, serves as a guide to uranium exploration through out the entire basin.

Gold and Uranium at Vredefort

The Vredefort impact structure, South Africa (Fig. 10a, b) consists of a 44 km diameter uplifted central core of predominantly Archaean granitic gneisses, surrounded by an 18 km wide collar of steeply dipping to overturned Proterozoic sedimentary and volcanic rocks of the Witwatersrand and Ventersdrop Supergroup. This, in turn, is surrounded by a 28 km wide

https://doi.org/10.12789/geocanj.2017.44.113

Table 1. Natural Resources at Terrestrial Impact Structures.

Crater Name	Lat.	Long.	Country	Apparent Diameter (km)	Age (Ma)	Resource
Ames	36°15'N	98°12'W	USA	16	470 ± 30	Hydrocarbons
Avak	71°15'N	156°38'W	USA	14	< 95	Hydrocarbons
Boltysh	48°45'N	32°10'E	Ukraine	24	65.2 ± 0.6	Oil shale
Calvin	41°50'N	85°52'W	USA	8.5	450 ± 10	Hydrocarbons
Carswell	58°27'N	109°30'W	Canada	39	115 ± 10	Uranium
Charlevoix	47°32'N	70°18'W	Canada	54	342 ± 15	Ilmenite
Chesapeake Bay	37°37'N	76°01'W	USA	80	35.5 ± 0.3	Groundwater
Cloud Creek	43°10.6'N	106°42.5'W	USA	7	190 ± 20	Hydrocarbons
Crooked Creek	37°50'N	91°23'W	USA	7	320 ± 80	Pb–ZnPb–ZnPb–Zn
Decaturville	37°54'N	92°43'W	USA	6	< 300	Pb–Zn
Dellen	61°48'N	16°48'E	Sweden	19	89.0 ± 2.7	Hydroelectric
Kara	69°06'N	64°09'E	Russia	65	70.3 ± 2.2	Impact diamonds
Kentland	40°45'N	87°24'W	USA	13	< 97	Pb–Zn
Lonar	19°58'N	76°31'E	India	1.8	0.05 ± 0.01	Trona
Manicouagan	51°23'N	68°42'W	Canada	100	214 ± 1	Hydroelectric
Marquez Dome	31°17'N	96°18'W	USA	13	58 ± 2	Hydrocarbons
Newporte	48°58'N	101°58'W	USA	3.2	< 500	Hydrocarbons
Obolon	49°35'N	32°55'E	Ukraine	20	169 ± 7	Oil shale
Popigai	71°39'N	111°11'E	Russia	100	35.7 ± 0.2	Impact diamonds
Puchezh-Katunki	56°58'N	43°43'E	Russia	40	167 ± 3	Impact diamonds
Red Wing Creek	47°36'N	103°33'W	USA	9	200 ± 25	Hydrocarbons
Ries	48°53'N	10°37'E	Germany	24	15.1 ± 0.1	Impact diamonds; bentonite; lignite; building stone
Rochechouart	45°50'N	00°56'E	France	23	201 ± 2	Building stone
Rotmistrovka	49°00'N	32°00'E	Ukraine	2.7	120 ± 10	Oil shale
Saint Martin	51°47'N	98°32'W	Canada	40	220 ± 32	Anhydrite; Gypsum
Serpent Mound	39°02'N	83°24'W	USA	8	< 320	Pb–Zn
Sierra Madera	30°36'N	102°55'	USA	13	< 100	Hydrocarbons
Siljan	61°02'N	14°52'E	Sweden	65	362 ± 1	Pb–Zn
Steen River	59°30'N	117°30'W	Canada	25	91 ± 7	Hydrocarbons
Sudbury	46°36'N	81°11'W	Canada	150–200	1850 ± 3	Ni, Cu, PGE; Cu–Pb–Zn; Impact diamonds
Ternovka	49°01'N	33°05'E	Ukraine	11	280 ± 10	Iron; uranium; impact diamonds
Tswaing	25°24'S	28°05'E	S. Africa	1.13	0.22 ± 0.05	Trona
Viewfield	49°35'N	103°04'W	Canada	2.5	190 ± 20	Hydrocarbons
Vredefort	27°00'N	27°30'E	S. Africa	250–300	2023 ± 4	Gold; uranium
Zapadnaya	49°44'N	29°00'E	Ukraine	3.2	165 ± 5	Impact diamonds

outer broad synclinorium of gently dipping Proterozoic sedimentary and volcanic rocks of the Transvaal Supergroup. Younger sandstone and shale of the Karoo Supergroup cover the southeastern portion of the structure (Fig. 10a). The most comprehensive and recent guide to the geology of Vredefort can be found in Gibson and Reimold (2008). The Vredefort impact event occurred at 2023 ± 4 Ma (Kamo et al. 1996). Based on the spatial distribution of impact-related deformation and structural features, Therriault et al. (1997) derived a self-consistent, empirical estimate of 225–300 km for the original apparent diameter of Vredefort. A similar size estimate was derived by Henkel and Reimold (1998) and Grieve et al. (2008). These estimates effectively equate the Vredefort impact structure to the entire Witwatersrand Basin in South Africa.

The Witwatersrand Basin is the world's largest goldfield, having supplied over 40% of the gold ever mined. Since gold was discovered there in 1886, it has produced 47 kt of gold (Robb and Robb 1998). In 1970, Witwatersrand gold accounted for 80% of world's gold supply. Production has declined since, with production for 2002 ~ 350 t, or ~ 13.5% of the global gold supply. Current production accounts for < 5% of the global supply, due to the high cost of 'deep' mining, although current reserve estimates are around 20 kt of gold. Approximately 150,000 t of uranium have been mined, gener-

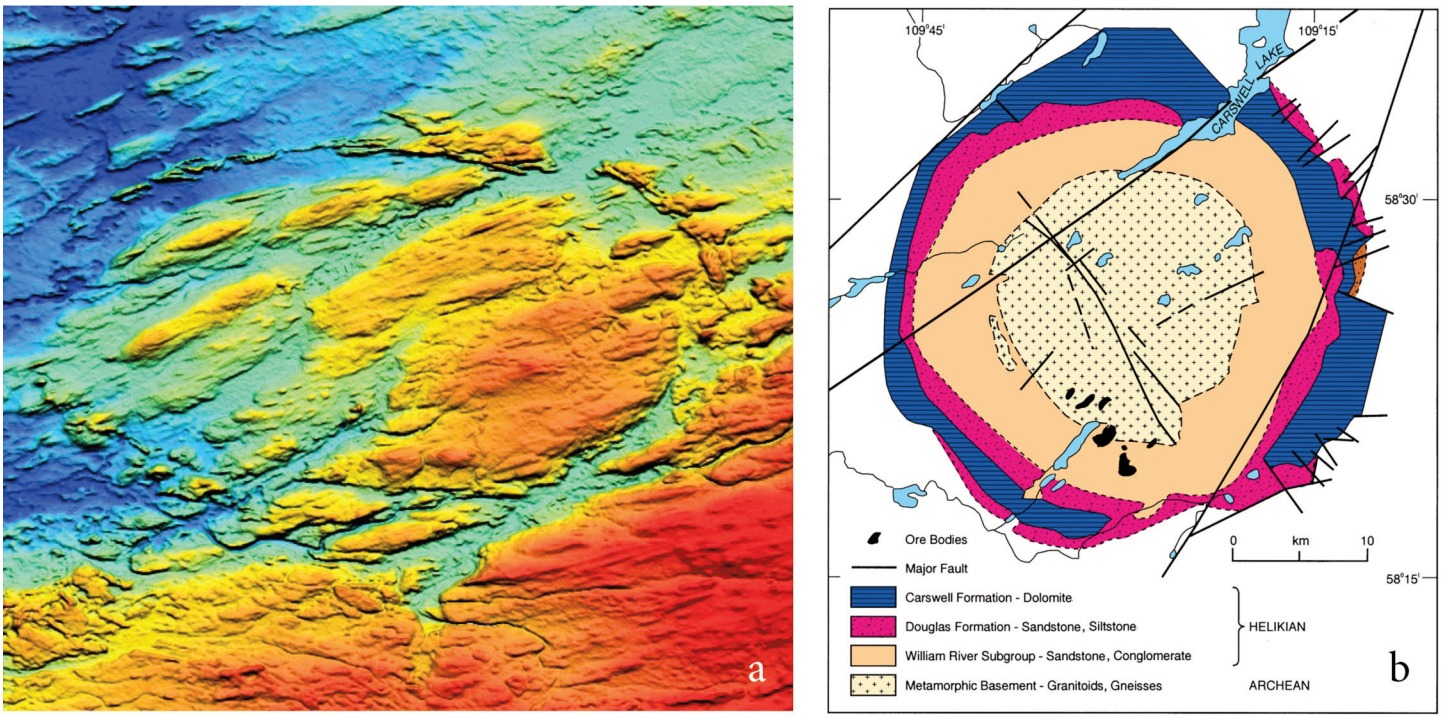

Figure 9. a) Colour image of topography of the complex Carswell structure, Canada, based on NASA SRTM data. Reds and yellows are high, blues and greens are low. Note conspicuous ridge at 39 km diameter, corresponding to the outcrop of the Carswell Formation and generally taken as the apparent diameter. Also visible are lineations in the central crystalline core due to the effects of glaciation. b) Simplified bedrock geologic map of the Carswell structure, showing uplifted crystalline core and down-faulted annulus of Carswell and Douglas Formations and the location of major uranium ore bodies.

ally as a by-product of gold mining, with estimated reserves of 475 kt (Reimold et al. 2005). Independent of impact studies, structural analyses have identified a series of concentric anticlinal and synclinal structures related to Vredefort (Fig. 10b). These Vredefort-related structures have led to the preservation of sedimentary rocks of the Witwatersrand Supergroup from erosion (McCarthy et al. 1990). The bulk of the gold has been mined from the upper succession of the Witwatersrand Supergroup known as the Central Rand Group.

General gold distribution is controlled by sedimentary attributes of the Central Rand. Pure detrital and hydrothermal models and combinations of the two have been proposed for the origin of the gold (e.g. Frimmel et al. 2005; Hayward et al. 2005; Meier et al. 2009), with clear detrital morphological features occurring with secondary, remobilized gold. This suggests that detrital gold was introduced into the basin but that some gold was subsequently remobilized by hydrothermal activity (e.g. Zhao et al. 2006). Two thermal or metamorphic events affected the rocks of the basin. A regional amphibolite facies metamorphism predates the Vredefort impact event. A later low-pressure (0.2–0.3 GPa), immediately post-impact event, however, produced peak temperatures of 350 ± 50°C in the Witwatersrand Supergroup to > 700°C in the centre of the crystalline core at Vredefort. This post-impact metamorphic-hydrothermal activity is directly attributed to the combination of post-shock heating and the structural uplift of originally relatively deep-seated parautochthonous rocks, during the Vredefort impact event (Gibson et al. 1998). Reimold et al. (1999) applied the term 'autometasomatism' to describe the alteration associated with the hydrothermal activity. This activity remobilized the gold (and uranium) within impact-related structures and fractures, which provided channels for fluid migration. A more detailed discussion of the effect of Vredefort-related hydrothermal activity can be found in Reimold et al. (2005). It is likely, however, that the Vredefort impact event played a larger role in the genesis of Witwatersrand Basin gold fields than simply preserving them from erosion by impact-related structural modification (Tucker et al. 2016).

Syngenetic Deposits

Syngenetic deposits originate as a direct result of impact processes. They owe their origin to the very high levels of impact energy deposition in the local upper crustal environment, resulting in such phenomena as phase changes and impact melting. In recent years, there has been greater recognition of the role for post-impact hydrothermal activity at impact structures (e.g. Abramov and Kring 2004; Ames et al. 2006). Post-impact hydrothermal deposits are a result of localized heating due to the impact process and, thus, considered as syngenetic deposits. The remobilization of some progenetic deposits by post-impact hydrothermal activity has blurred, in some cases, the separation between progenetic and syngenetic deposits. Syngenetic economic natural resources at impact structures include impact diamonds, Cu–Ni and platinum group sulphides and other metals (Table 1).

Impact Diamonds

The first indication of impact diamonds was the discovery in the 1960's of diamond with lonsdaleite, a high-pressure polymorph of carbon, in placer deposits (e.g. in the Ukraine),

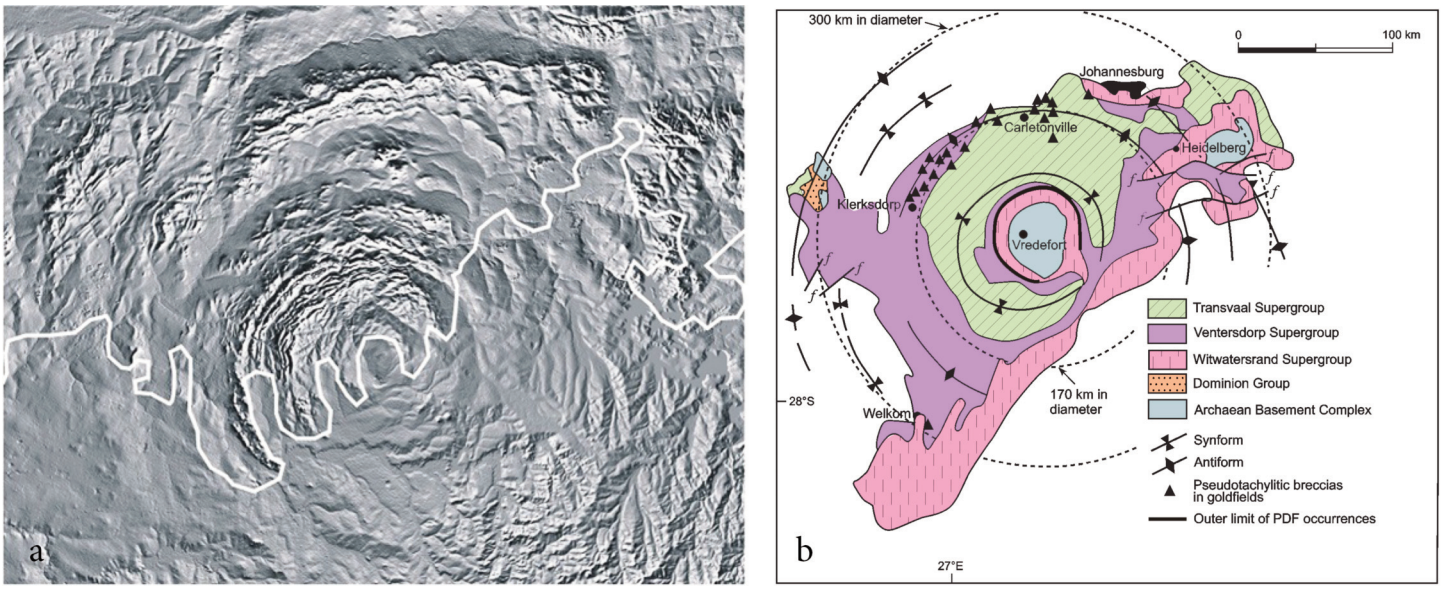

Figure 10. a) Greyscale image of topography of the complex Vredefort structure, South Africa, based on NASA SRTM. Image has been illuminated from the centre to emphasize the circumscribing anticlinal and synclinal structures. Such structures are not evident in SE quadrant, due to covering of post-impact Karoo sedimentary and volcanic rocks, 'northerly' outcrop limit of which is outlined by white line. b) Schematic geologic map of Vredefort structure, with post-impact Karoo rocks removed. Goldfields form the so-called 'golden arch,' passing through or close to Heidelberg, Johannesburg, Carletonville, Klerksdorp and Welkom.

although their source was unknown at the time. In the 1970's, diamond with lonsdaleite was discovered in the impact lithologies at the Popigai impact structure in Siberia, Russia. Since then, impact diamonds have been reported at a number of structures; e.g. Kara and Puchezh-Katunki in Russia, Lappajärvi in Finland, Ries in Germany, Sudbury in Canada, Ternovka and Zapadnaya in Ukraine and others. Impact diamonds originate when precursor carbonaceous materials (e.g. graphite, coal) are subjected to shock pressures greater than 35 GPa (Masaitis 1998). Diamonds from graphite occur as paramorphs and as microcrystalline aggregates. For example, at Popigai, these aggregates can reach 10 mm, but most are 0.2–5 mm in size (Masaitis 1998), and consist of cubic diamond and lonsdaleite. Diamonds are most common as inclusions in impact melt rocks and glass clasts in melt-bearing breccias. In impact melt rocks, diamonds occur in relatively minor amounts, with provisional average estimates in the order of 10 ppb; although, the cumulative volumes can be enormous. While still classified, the cumulative amount of impact diamonds occurring at Popigai makes it most likely the largest diamond deposit in the world. Diamonds produced by the shock transformation of graphite tend to be harder and more resistant to breaking than normal cubic diamonds. Impact diamonds, however, are not currently exploited commercially, due to the industrial production of synthetic diamonds.

Cu–Ni Sulphides and Platinum Group (PGE) Metals at Sudbury

The Sudbury structure, Ontario, Canada is the site of world-class Ni–Cu and PGE metal ores and is Canada's principal mining district. The pre-mining resources associated with the Sudbury Igneous Complex (SIC) are estimated at over 1.5×10^9 t of 1.2% Ni, 1.1% Cu and 1 $g.t^{-1}$ combined Pd + Pt (Farrow and Lightfoot 2002). There are also hydrothermal Zn–Pb deposits above the SIC (Ames and Farrow 2007). Nickel sulphides were first noted at Sudbury in 1856. It was not until they were 'rediscovered' during the building of the Trans-Canada railway in 1883, however, that they received attention, with the first production occurring in 1886 (Naldrett 2003). The cumulative total worth of metals produced from Sudbury is estimated at > US$300 billion (Ames and Farrow 2007).

The most prominent feature of the Sudbury structure is the ~ 30 × 60 km elliptical basin formed by the outcrop of the SIC, the interior of which is known as the Sudbury Basin (Fig. 11a, b). Neither the SIC nor the Sudbury Basin, however, is synonymous with the considerably larger Sudbury impact structure. The Sudbury impact structure includes the Sudbury Basin, the SIC and the surrounding brecciated basement rocks and covers a present area > 15,000 km^2. From the spatial distribution of shock metamorphic features (e.g. shatter cones) and other impact-related attributes, and by comparison with equivalent features at other large terrestrial impact structures (Chicxulub and Vredefort), Grieve et al. (2008) estimated that the original crater rim diameter was 150–200 km. Even larger original diameters have been suggested (e.g. Tuchscherer and Spray 2002; Naldrett 2003). With the post-impact tectonic deformation and the considerable erosion, estimated to be ~ 5–10 km, which has taken place at the Sudbury impact structure, it is difficult to constrain its original form. From its estimated original dimensions, it was most likely a peak-ring or a multiring basin (Stöffler et al. 1994; Grieve et al. 2008). Details of the geology of the Sudbury area can be found in Dressler (1984) and, most recently, in Ames et al. (2008).

The SIC is the remnant of the coherent impact melt sheet at the Sudbury structure (Grieve et al. 1991). It differs from most other terrestrial coherent impact melt sheets in that it is differentiated (due to its ~ 2.5 km thickness) and it is relatively, but not completely, clast free. For example, there are rare

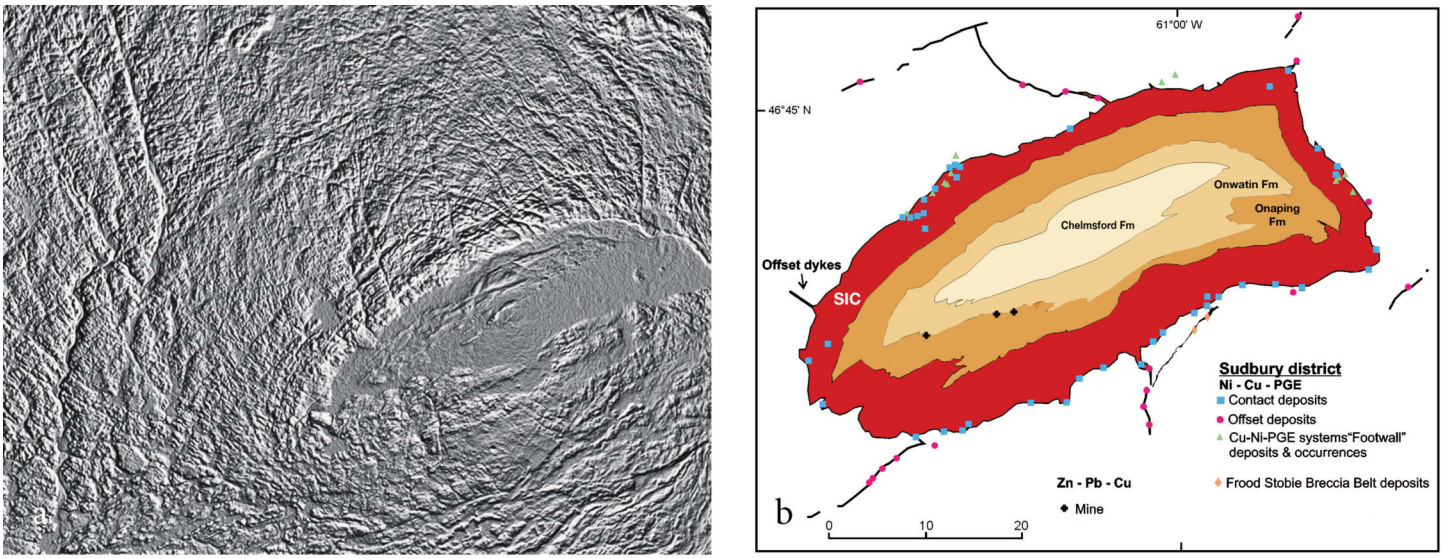

Figure 11. a) Greyscale image of topography of the complex Sudbury structure, Canada, based on NASA SRTM. Image has been illuminated from the centre. The most evident feature is the elliptical trace of the Sudbury Igneous Complex (SIC) (particularly in the north and east) and the interior Sudbury Basin. b) Simplified geologic map of ore occurrences at the Sudbury structure, relative to the SIC and overlying post-impact sedimentary rocks.

quartz clasts with partially annealed PDFs (Therriault et al. 2002). The details of the mineralogy and geochemistry support a cogenetic source for the sub-units of the so-called Main Mass of the SIC, produced by fractional crystallization of a single batch of silicate liquid (e.g. Lightfoot et al. 1997; Warner et al. 1998; Therriault et al. 2002). The conclusion that the SIC and its ores are crustal in composition is borne out by isotopic studies (e.g. Faggart et al. 1985; Walker et al. 1991; Dickin et al. 1992, 1996; Cohen et al. 2000). Osmium isotope studies of sulphides from several mines have confirmed their crustal origin from a binary mixture of Superior Province and Huronian metasedimentary target rocks (Morgan et al. 2002).

Recently, Farrow and Lightfoot (2002) and Ames and Farrow (2007) reviewed the nature of the ore deposits at Sudbury (Fig. 11b) and placed their formation in an integrated time-sequence model. They recognized: Ni–Cu–Co 'Contact' deposits associated with embayments at the base of the SIC and hosted by so-called Sublayer and Footwall Breccia; Ni–Cu–Pt–Pd–Au 'Offset' deposits associated with discontinuities and variations in thickness in the so-called Offset Dikes; and Cu–Pt–Pd–Au-rich 'Footwall' deposits that can occur in the underlying target rock, up to 1 km away from the SIC (Fig. 11). They also recognize a fourth deposit environment associated with pseudotachylitic, so-called, Sudbury Breccia. For example, the Frood-Stobie deposit, which contained some 15% of the entire known Sudbury resources and produced 600 × 10^6 t of ore, is hosted largely in Sudbury Breccia (Scott and Spray 2000).

The Contact deposits consist of massive sulphides and are volumetrically the largest deposit type, hosting approximately 50% of the known ore resources. The main economic Offset environments include the Copper Cliff and Worthington Offsets in the South Range, which, along with the Frood-Stobie, contain approximately 40% of the known ores at Sudbury. The Cu–PGE-rich Footwall deposits are volumetrically small (~ 10% of known ore) relative to the Contact deposits but are extremely valuable bodies, as they are relatively enriched in PGEs, in addition to copper. They represent a relatively new ore environment, which is hosted in the brecciated Footwall of the SIC and are best known in the North Range, where they occur as complex vein networks of sulphide and low sulphide, high precious metal disseminations (Ames and Farrow 2007). These Footwall deposits are the focus of much of the current exploration activity at Sudbury. There is increasing realization that hydrothermal remobilization played a role in the genesis of the Footwall deposits (e.g. Molnár et al. 2001; Hanley et al. 2005; Ames and Farrow 2007). This is consistent with the growing acknowledgement of post-impact hydrothermal activity, driven by the 'local' crustal thermal anomaly that results from large impact events (e.g. Abramov and Kring 2004).

The recent work at Sudbury can mostly be fitted into the framework of the formation of an approximately 150–200 km impact basin at 1.85 Ga. This resulted in massive (> 10^4 km^3) crustal melting producing a superheated melt of an unusual composition, which produced immiscible sulphides, during fractional crystallization. These sulphides settled gravitationally, resulting ultimately in the present Contact and Offset ore deposits. Complicating factors, but essential components of the evolutionary history of Sudbury, are the creation of a 'localized' but regional-scale impact-related hydrothermal system, which resulted in some ore fractionation and redistribution into the brecciated Footwall rocks, and the deformation by the Penokean orogeny that took place shortly after the impact. The Zn–Pb–Cu ores in the post-impact sedimentary rocks overlying the SIC are the result of the hydrothermal system fuelled by the heat of the SIC (Ames et al. 2006; Ames and Farrow 2007). This upper hydrothermal system involved sea water, as opposed to the Cl-rich brines that played a role in the origin of the Footwall deposits at the base of the SIC (Ames and Farrow 2007).

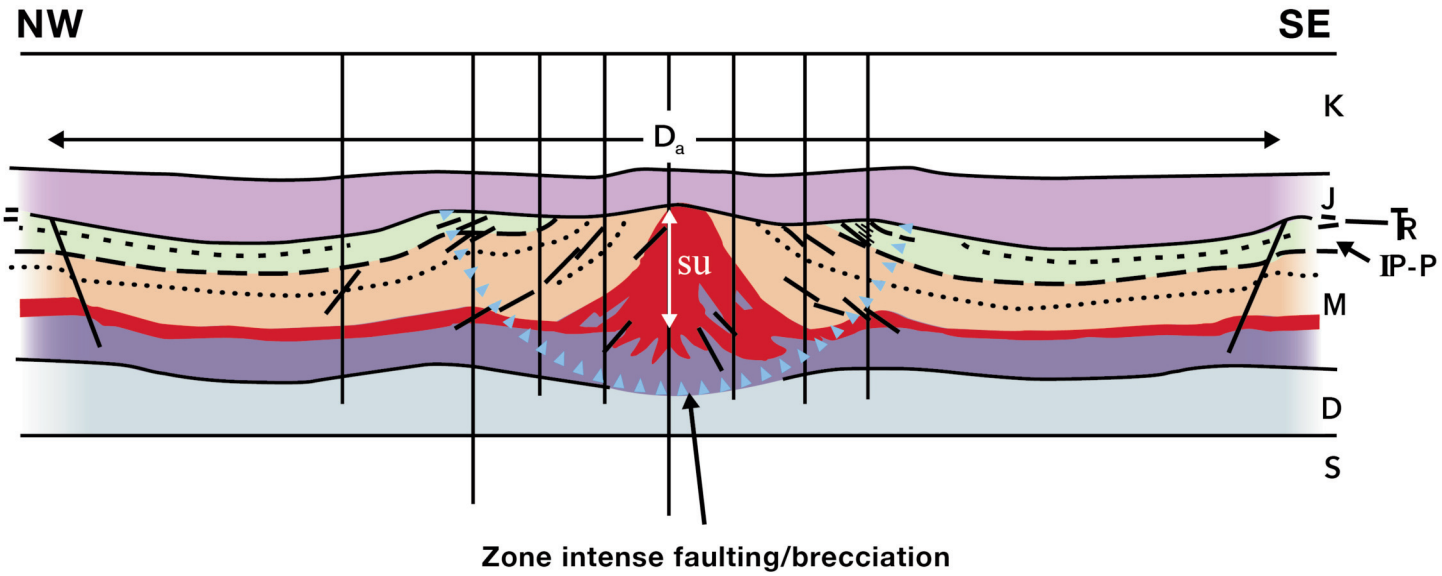

Figure 12. Schematic cross-section (no vertical exaggeration) of the complex Red Wing structure, USA. Strata: S, Silurian; D, Devonian; M, Carboniferous (Mississippian); IP-P, Permian; TR, Triassic; J, Jurassic; K, Cretaceous. Hydrocarbon production is from the duplicated, faulted and brecciated Mississippian (red) in the central structural uplift. Note difference in thickness of Mississippian in the central structural uplift, compared to annular trough and outside the structure.

Epigenetic Deposits

Epigenetic deposits result from impact producing isolated, enclosed topographic basins, with restricted sedimentation and/or the long-term flow of fluids into structural traps. Such deposits may originate almost immediately or over an extended period after the impact event and include reservoirs of liquid and gaseous hydrocarbons. There are also oil shales, various organic and chemical sedimentary rocks, as well as flows of fresh and mineralized waters (Table 1). For example, oil shales are known at Boltysh, Obolon and Rotmistrovka in the Ukraine. The most significant reserves are at Boltysh, where there is an estimated 4.5×10^9 t of oil shales, as the result of biological activity involving algae in this isolated topographic basin. A more complete listing of epigenetic deposits can be found in Reimold et al. (2005).

Hydrocarbon Accumulations

Hydrocarbons occur at a number of impact structures (Table 1). In North America, approximately 50% of the known impact structures in hydrocarbon-bearing sedimentary basins have commercial oil and/or gas fields. For example, the 25 km diameter Steen River structure in Alberta, Canada, has produced 3.5 million barrels of oil and 48.5 billion cubic feet of gas from wells on its rim, with an estimated 1.9 million barrels of oil and 4.5 billion cubic feet of gas as recoverable reserves. Oil and gas are produced from beneath the ~ 13 km diameter Marquez and Sierra Madera structures in Texas, USA (Donofrio 1998), which have a combined estimated reserve of 280 billion cubic feet of gas. Viewfield in Saskatchewan, Canada (Sawatzky 1977), which is a 2.5 km diameter simple bowl-shaped crater, produces some 600 barrels of oil and 250 million cubic feet of gas per day, with recoverable reserves estimated to be 2–4 million barrels of oil (Donofrio 1998). Some examples in which commercial hydrocarbons have accumulated under differing impact-related circumstances are given below.

Red Wing Creek

At the Red Wing Creek structure in North Dakota, USA, hydrocarbons are recovered from strata of the central uplift (Fig. 12). Red Wing Creek is estimated to be 200 ± 25 Ma old, but the source of the hydrocarbons is Carboniferous Mississippian strata, i.e. 360–320 Ma old. It is a complex impact structure, ~ 9 km in diameter, with a central peak in which strata have been uplifted by up to 1 km (Brenan et al. 1975). When the central uplift was drilled in 1972, approximately 820 m of Mississippian oil column, with considerable high-angle structural complexity and brecciation and a net pay of approximately 490 m, was discovered. Beyond the structure, dips are gentle and the oil column is ~ 30 m. In this case, the hydrocarbon resources are progenetic but were physically displaced in the formation of the impact structure, resulting in enhanced accumulations and permeability of reservoir rocks in the central structural uplift. Primary and secondary recoverable reserves are estimated at 60–70 million barrels of oil and 100 billion cubic feet of gas (Donofrio 1998). Virtually all the oil has been discovered within a diameter of 3 km, corresponding to the central uplift. Based on net pay and its limited aerial extent, Red Wing is the most prolific oil field in the USA, in terms of producing wells per km^2, with the wells having the highest cumulative productivity of all wells in North Dakota.

Ames

The Ames structure in Oklahoma, USA, is a complex impact structure ~ 14 km in diameter. It is buried by up to 3 km of Ordovician to Recent sedimentary rocks and sediments (Carpenter and Carlson 1992). The structure was discovered in the course of oil exploration in the area and is the principal subject

of a compilation of research papers in Johnson and Campbell (1997). The rim of the structure is defined by the structurally elevated Lower Ordovician Arbuckle dolomite. More than 600 m of Cambrian–Ordovician strata and some underlying basement rocks are missing in the centre of the structure due to impact. The entire structure is covered by the Middle Ordovician Oil Creek shale, which forms both the seal and source for hydrocarbons.

Initial oil and gas discoveries were made in 1990 from an approximately 500 m thick section of Lower Ordovician Arbuckle dolomite in the rim (Fig. 13). Wells drilled in the centre failed to encounter the Arbuckle dolomite and bottomed in granite breccias of the central uplift and, closer to the rim, in granite-dolomite breccias. These central wells produce over half the production from Ames and include the Gregory 1-20, which is the most productive oil well from a single pay zone in Oklahoma, flowing at the maximum regulated rate in Oklahoma and producing > 100,000 barrels of oil per year (Carpenter and Carlson 1992). Gregory 1-20 encountered an approximately 80 m section of granite breccias below the Oil Creek shale, with very effective porosity. A drill-stem test of the zone flowed at approximately 1300 barrels of oil per day, with a conservative estimate of primary recovery in excess of 5 million barrels from this single well. Conservative estimates of primary reserves at Ames suggest they exceed 25–50 million barrels of oil and 15–20 billion cubic feet of gas (Donofrio 1998). Hydrocarbon production is from the Arbuckle dolomite, the brecciated granite and granite-dolomite breccias and is largely due to impact-induced fracturing and brecciation, which has resulted in significant porosity and permeability. In the case of Ames, the impact not only produced the required reservoir rocks, but also the paleo-environment for the deposition of post-impact shales that provided the source of the oil and gas, upon subsequent burial and maturation. That is, the reservoir is syngenetic and the hydrocarbons are epigenetic.

There are similarities between the Ames crater shale and locally developed Ordovician shale in the Newporte structure in North Dakota, USA, an oil-producing (~ 120,000 barrels per year) 3.2 km diameter simple impact crater in Precambrian basement rocks of the Williston Basin. The Ames and Newporte discoveries have implications for oil and gas exploration in crystalline rock underlying hydrocarbon-bearing basins. Donofrio (1981) first proposed the existence of such hydrocarbon-bearing impact craters and that major oil and gas deposits could occur in brecciated basement rocks.

Campeche Bank

The Campeche Bank in the SE segment of the Gulf of Mexico is the most productive hydrocarbon-producing area in Mexico. The bulk of the hydrocarbons, from Jurassic source rocks (progenetic), are recovered from breccia deposits (syngenetic) at the Cretaceous–Paleogene (K–Pg) boundary. This area includes the world-class Cantarell oil field (Santiago-Acevedo 1980), which has produced over 11 billion barrels of oil and 3 trillion cubic feet of gas, between discovery in 1976 and 2006. Primary reserve estimates range as high as 30 billion

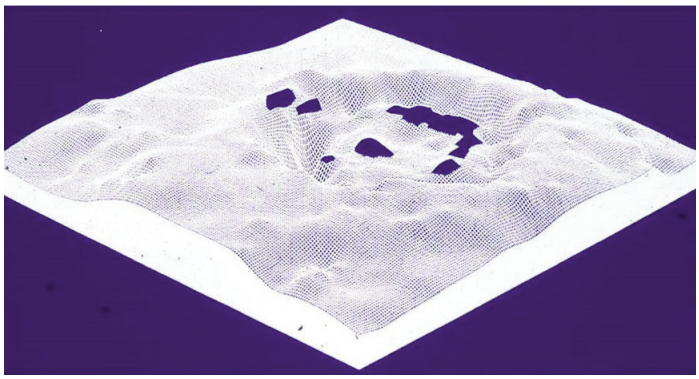

Figure 13. Three-dimensional mesh diagram of the topography on post-impact Slyvan shale at the complex Ames structure, USA. View is to NW at 25° elevation, with 20 times vertical exaggeration. Solid areas are hydrocarbon producing zones in the underlying Ames structure.

barrels of oil and 15 trillion cubic feet of gas. Production is from up to 300 m of K–Pg dolomitized limestone breccias, with a porosity of around 10%. The seal rocks are a bentonitic bed, with shocked materials, and are altered ejecta materials from the K–Pg impact structure Chicxulub, which lies some 350–600 km to the NE. Grajales-Nishimura et al. (2000) proposed the following sequence of events for the K–Pg lithologies. What were to become the main, hydrocarbon-bearing breccias resulted from the collapse of the offshore carbonate platform due to seismic energy from the Chicxulub impact. This was followed by the deposition of K–Pg ejecta through atmospheric transport. Subsequent dolomitization of the ejecta and Tertiary tectonics served to form the seal and trap, respectively, for migrating Jurassic hydrocarbons. The net result was the creation of oil fields that account for > 60% of Mexico's hydrocarbon production and have reserves in excess of the entire onshore and offshore traditional hydrocarbon reserves of the USA, including Alaska (Donofrio 1998). The Cantarell oil field is now in decline, with production falling from a peak of around 2 million barrels per day in 2003 to 770,000 barrels per day in 2009, when it was superseded by the adjacent Ku-Mallop-Zaap field as the most productive oil field in Mexico. Oil from the Campeche Bank accounts for the bulk of the > US$35 billion of hydrocarbons (oil at $50 a barrel) produced from North American impact structures per year.

In summary, economic deposits associated with terrestrial impact structures range from world-class to relatively localized occurrences. There is increasing evidence that post-impact hydrothermal systems at large impact structures are of importance, with respect to their potential to redistribute metals. Such hydrothermal systems can blur the clear distinction between purely progenetic, syngenetic and epigenetic ore deposits related to impact. Although Vredefort and Sudbury are world-class mining districts, hydrocarbon production dominates the annual monetary value of natural resource deposits at impact structures. Commercial hydrocarbon accumulations are generally located in the central structural uplift of complex structures and in the rim areas of both complex and simple structures. While spatially localized, such accumulations occur

https://doi.org/10.12789/geocanj.2017.44.113

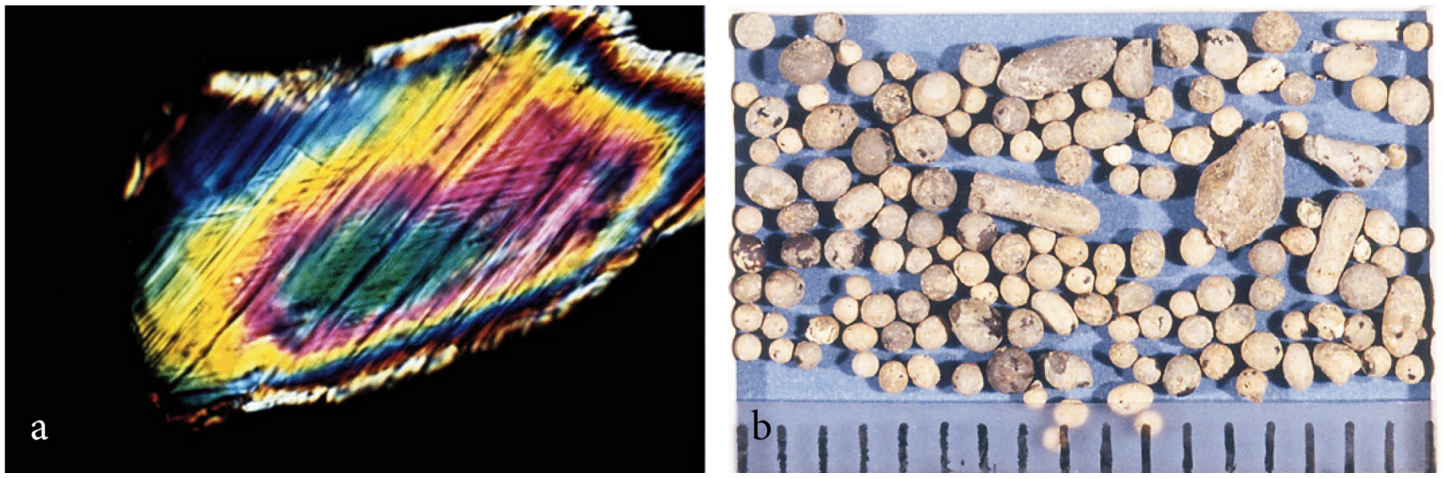

Figure 14. a) Shocked quartz displaying planar deformation features (PDFs) from the K–Pg boundary at Teapot Dome, USA. Length of grain is ~ 0.3 mm. Image from G. Izett, USGS. b) Impact spherules from the K–Pg boundary at Beloc, Haiti. Tick marks on scale are mm. Image from D.A. Kring, Lunar and Planetary Institute.

for a variety of reasons, including the physical redistribution of existing reservoir and seal rocks and brecciation to form reservoir rocks for migrating hydrocarbons. Many terrestrial impact structures remain to be discovered and, as targets for resource exploration, their relatively invariant morphological and structural properties, as a function of diameter, provide an aid to the development of efficient exploration strategies, particularly for hydrocarbons.

IMPACT AND THE PHANEROZOIC BIOSPHERE

The first suggestion that a large impact event may have resulted in the extinction of the dinosaurs at the end of the Cretaceous (K–Pg boundary) was by De Laubenfels (1956). No evidence, however, was presented beyond drawing analogies between the effects of the Tunguska atmospheric explosion in Siberia in 1908 and what would be the result of a much larger impact event. The first evidence that such an impact event had, in fact, occurred was the discovery of the geochemical signature, in the form of elevated PGE values, of meteoritic material in K–Pg boundary sedimentary rocks (e.g. Alvarez et al. 1980; Ganapathy 1980). This was followed by physical evidence through the identification of shocked quartz, with PDFs (Fig. 14; Bohor et al. 1984). The working hypothesis for the involvement of impact in defining the K–Pg boundary and as a cause of the associated mass extinction event was not without challenges (e.g. Officer et al. 1987). Much of the controversy was muted with the (re)discovery of the K–Pg impact site in the form of the buried Chicxulub impact structure in the Yucatan, Mexico (Fig. 15; Penfield and Camargo 1981; Hildebrand et al. 1991). Chicxulub itself was not without its debates, particularly centred on its size and form (e.g. Sharpton et al. 1996), which have largely been settled (~ 180 km in diameter, peak ring basin) through a series of offshore reflection seismic profiles (e.g. Morgan et al. 1997). The K–Pg boundary is now known from over 350 sites world-wide and a vast and diverse literature exists on its characteristics with respect to the Chicxulub impact. The most recent compilation and review of this literature making the case for a global correlation between Chicxulub, the impact evidence in K–Pg boundary deposits,

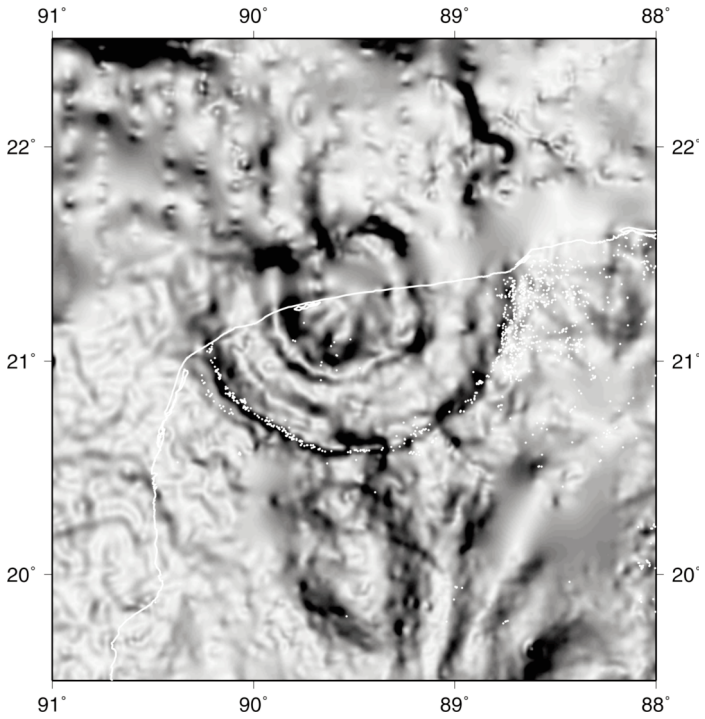

Figure 15. Greyscale image of horizontal gravity gradient over the buried K–Pg structure Chicxulub, Yucatan, Mexico. Solid white line defines the coast line with the Gulf of Mexico. Gravity image of the structure is better defined on-shore, due to spacing of gravity measurements. White dots are sink holes (cenotes). Groundwater flow is to the north and is deflected around the rim of the structure.

their variation in character with distance from Chicxulub (e.g. Fig. 14) and the attendant mass extinction event can be found in Schulte et al. (2010). It is not repeated here, in detail. Despite this weight of evidence, however, detractors of the impact working hypothesis remain (e.g. Keller et al. 2010).

The most outstanding questions centre on the details of the geology and structure of Chicxulub itself and on how this impact event led to severe global environmental degradation. With respect to the former, reflection seismic has clearly defined a topographic peak ring within the structure (e.g. Mor-

gan et al. 2011). From the point of view of impact mechanics, the exact formational mechanism of peak rings is a topic of debate. Currently, there are two major working hypotheses; one based on numerical models (e.g. Collins et al. 2002, 2008; Ivanov 2005), and the other a conceptual geological model based on planetary (Mercury and moon) observations and interpretations (e.g. Head 2010; Baker et al. 2011a, b). The most recent review of the nature and constraints on peak ring formation, as provided through imagery and altimetry from the Lunar Reconnaissance Orbiter, in comparison with recent numerical models, is somewhat equivocal as to supporting, or not, differing working hypotheses for the formation of peak rings (Baker et al. 2016). Baker et al. (2016) note specifically that "Unfortunately, *in situ* samples of peak rings have not been obtained from the Moon to aid in distinguishing between the scenarios described".

Equally unfortunately, the terrestrial impact record is not particularly forthcoming when it comes to the subject of peak rings. Peak rings occur only in large impact basins of which there are limited examples preserved on Earth. A combination of observations, interpretations and logical arguments suggests that the three largest known impact structures on Earth: Vredefort, Sudbury and Chicxulub, all had some form of peak ring (Grieve et al. 2008). Only Chicxulub, however, has a preserved topographic peak ring. The exact character of the peak ring at Chicxulub is currently being investigated through a recently completed joint IODP-ICDP drilling expedition (Morgan et al. 2015). The initial analysis and interpretation of this core is compatible with the working hypothesis of the collapse of an over-heightened central peak as the mechanism for peak ring formation, which is a feature of the numerical models (Morgan et al. 2016).

It is hoped that the analysis of this core will also provide some constraints on the nature of the impact-induced 'killing mechanism' for the Cretaceous biosphere. The initial kinetic energy of the body that resulted in the formation of Chicxulub is estimated to have been ~ 5×10^{23} J. To put this in context, the energy released was ~ 5×10^{3} times greater than the annual output of internal energy of the entire Earth of ~ 10^{20} J. While this is an immense amount of energy, most of it was contained at the impact site in the formation of the impact structure and in the melting and vaporization of the target rocks. There is evidence of catastrophic 'local' effects (seismic and tsunami events) and the air blast and wildfires from the impact event would have been, at least, sub-continental in scale (Grieve and Kring 2007). These, however, would not have resulted in the evidence for environmental degradation on a global scale at the K–Pg boundary. To be global, the effects on the Chicxulub impact event have to be coupled through the atmosphere.

In this regard, the initial working hypothesis was that the impact event ejected sufficient sub-micrometre dust into the stratosphere so that photosynthesis effectively ceased and the global food chain collapsed (Alvarez et al. 1980). Initial modelling of such dust loading estimated > 10^{17} g of sub-micrometre dust from the Chicxulub event, compared with 10^{16} g required to result in the cessation of photosynthesis (Toon et al. 1997). The problem with this working hypothesis is that, by analogy with Chicxulub, smaller impact events, such as the Manicouagan event in Quebec (100 km diameter, 214 ± 1 Ma), would have produced 10^{16} g of stratospheric sub-micrometre dust but they did not result in a global mass extinction event (Grieve and Kring 2007). To compound difficulties with the initial working hypothesis, modelling of the Chicxulub event and its interaction with the atmosphere indicated that, although the impact-related fireball that reached above the Earth's atmosphere contained > 10^{18} g of material, most of this material was initially in the form of vapour and re-entered the Earth's atmosphere as condensation droplets in the hundreds of micrometres size range (e.g. Toon et al. 1997; Pierazzo et al. 1998). In addition, more recent analysis estimates that the total mass of clastic debris in the fireball and available for global distribution through the atmosphere is < 10^{16} g and of that < 10^{14} g is sub-micrometre in size (Pope 2002), i.e. well below the atmospheric dust loading required for the cessation of photosynthesis.

Soot has been discovered in the K–Pg boundary layer and the occurrence of global wildfires has been proposed as one of the major deleterious effects of the Chicxulub impact (e.g. Woolbach et al. 1990). The total mass of combusted carbon is estimated to be close to 10^{17} g, which is actually greater than expected from the global burning of all vegetation at the time of the K–Pg event (Woolbach et al. 1990). It has been suggested that in addition to setting vegetation alight, the impact event and what followed resulted in the combustion of all organic material at the impact site, as well as oil seeps, coal beds, etc. There are two major ignition sources in an impact event the size of Chicxulub: the impact fireball of hot melt and vapour and the heating of high-velocity, impact ejecta re-entering the Earth's atmosphere. The impact fireball, however, will only ignite fires close to the impact site. Scaling from much smaller events, such as Tunguska and nuclear weapon tests, have considerable uncertainty but place some limits on the ability of the fireball to ignite vegetation, with estimates ranging from radial distances from the impact site of ~ 1250 km (Toon et al. 1997) to as much as ~ 3000 km (Shuvalov and Artemieva 2002).

Only thermal radiation from re-entering ejecta has the potential to produce wildfires on a global scale at the K–Pg boundary. Initial models of the thermal pulse associated with the re-entry of ejecta have suggested thermal radiation of > 10 $kW.m^{-2}$ over some 20 minutes (e.g. Melosh et al. 1990), sufficient to ignite global wildfires. Subsequent, more complex models, acknowledged that not all the thermal radiation from re-entering ejecta reached the Earth's surface and that there was a component of self-shielding with respect to the radiation from later arriving ejecta, which could reduce the thermal pulse to 5 $kW.m^{-2}$ and only for several minutes. This would be sufficient to ignite tinder but not living vegetation (Goldin and Melosh 2009). It has been argued, however, that such a scenario would lead to the subsequent ignition of global wildfires (e.g. Robertson et al. 2013). It has also been noted that the global distribution of re-entering ejecta will not be uniform, as assumed in some model calculations, and will be affected by such parameters as the impact angle and direction, and the

https://doi.org/10.12789/geocanj.2017.44.113

Figure 16. Scenario for the evolution of the degradational effects on the environment by the K–Pg impact event. Modified from an original diagram by D.A. Kring, Lunar and Planetary Institute.

Earth's rotation. Also, ejecta re-entry times will span a few days after the impact and will not be uniform over this time interval (e.g. Kring and Durda 2002). This more complex scenario is acknowledged in some recent modelling (e.g. Morgan et al. 2013), with the general conclusion that the thermal radiation from the Chicxulub impact will not be distributed uniformly over the Earth's surface and wildfires directly from the impact will not be global in extent. Nevertheless, the thermal pulse will lead to desiccation of vegetation and the effects of global cooling and darkness will cause widespread die off in vegetation and leave it extremely susceptible to fires ignited by such things as lightning strikes, i.e. the global soot at the K–Pg boundary may be the result of both impact-related and post-impact wildfires.

One feature of the Chicxulub impact site that may have been critical with respect to the impact resulting in a global mass extinction event is that it contained anhydrite in the target rocks. Although estimates vary by orders of magnitude, the amount of sulphur released by the impact was ~ 10^{16}–10^{18} g (e.g. Pope et al. 1997; Kring 2007). While the small portion of the sulphur aerosols contained in the atmosphere would have likely combined with water vapour to produce acid rain, this would not have been sufficient to acidify the oceans, although it may have had more local effects in shallow environments and continental watersheds. Sulphur aerosols are much more efficient in reducing solar radiation reaching the Earth's surface than dust and are the main cause of such reductions and cooling due to volcanic eruptions. For example, some 10^{13} g of sulphur was released into the lower stratosphere during the 1991 Mt. Pinatubo eruption, resulting in a cooling of the surface of ~ 0.5°C for several years (Ward 2009). By comparison, the K–Pg impact is considered to have produced 3–5 orders of magnitude more sulphur aerosols. A number of other chemically active gases and deleterious atmospheric changes (e.g. oxides of nitrogen due to shock and later ejecta re-entry heating of the atmosphere) would have been produced by the K–Pg impact event (e.g. Kring 2004).

At this time, there is no definitive, single causative impact-related agent for the K–Pg mass extinction event and it may have been a combination of effects (dust and sulphur aerosol loadings, massive wildfires, atmospheric changes and global cooling (Fig. 16; Pope et al. 1994, 1997)). As noted, it is hoped that the results of the recently completed joint IODP-ICDP drilling project within Chicxulub will provide further resolution and constraints (e.g. Morgan et al. 2015; 2016). Based on modelling and logical inference of the results of the Chicxulub impact, the post-K–Pg impact world, however, must have been a 'hellish' place of cold, darkness, choking fumes and acid rain; all leading to the global collapse of both the marine and terrestrial food webs. Analogies have been made with the results of a catastrophic 'nuclear winter' (e.g. Toon et al. 1997). Until recently, unequivocal evidence for the working hypothesis of a K–Pg 'impact winter' has been lacking, due largely to the absence of climatic records of sufficient temporal resolution. The recent results of high resolution organic TEX_{86} paleothermometry on three cores spanning the K–Pg boundary in

New Jersey, USA, however, indicate a sharp drop in temperature of ~ 3°C, coinciding exactly with the K–Pg boundary (Vellekoop et al. 2016).

Although there have been controversial claims of other impact-related extinctions in the terrestrial record (e.g. the temporal relation between the so-called Bedout High and the Permian–Triassic mass extinction event (Becker et al. 2001, 2004)), no evidence such as that from Chicxulub and the K–Pg boundary sedimentary rocks has been forthcoming. Impact events on the scale of Chicxulub, however, are estimated to occur on Earth on time-scales of ~ 100 Ma (Toon et al. 1997). Given that impact is a process governed by physics, impacts of similar scale on a given planetary body will produce similar results. The one variable that has the potential to modify this is changes in the type of target material. This has only minor effects on the cratering process *per se* but may well be significant with respect to the effects of the impact on changes to the atmosphere. Given that Chicxulub appears unique with respect to its effect on the Phanerozoic biosphere, it suggests that sulphate-bearing lithologies in the Chicxulub target may be the significant variable with respect to the effects of this particular large-scale impact on the terrestrial atmosphere and, thus, biosphere.

It has been suggested that impacts smaller than Chicxulub will produce severe effects to the 'local' biosphere and may be responsible for some of the sudden, short-term climatic disruptions, as mirrored by stable isotope excursions in the stratigraphic record (Grieve 1997). For example, a 25 mm thick ejecta layer dated at 214 ± 2.5 Ma and believed to be from Manicouagan (214 ± 1 Ma) has been reported from near Bristol, UK (Walkden et al. 2002). The surface blast wave from an event such as Manicouagan would have wind speeds of over 1000 $km.s^{-1}$ near the impact site and be sufficient to kill and injure exposed plant and animal life out to a radius of ~ 550 km (Grieve and Kring 2007). A late Eocene carbon and oxygen isotope anomaly has been ascribed to the almost simultaneous impacts that formed the Chesapeake Bay (40 km diameter, 35.5 ± 0.3 Ma) and Popigai (100 km diameter, 35.7 ± 0.2 Ma) impact structures (Vonhof et al. 2000). A ^{12}C anomaly and, most recently, what are interpreted to be impact-related spherules (Fig. 17) and shocked quartz have been discovered at the Paleocene–Eocene boundary and a case made for an impact trigger for the Paleocene–Eocene Thermal Maximum (PETM) 56 Ma ago (Kent et al. 2003; Schaller et al. 2016).

IMPACT AND THE EARLY EARTH

Precambrian

Although many terrestrial impact structures occur on Precambrian Shield and cratonic areas of the crust, due to their intrinsically low erosion rates and greater deformational stability, the record of Precambrian-aged structures is relatively sparse. This is due to their formational-age and is reflected in the previously noted fact that the known terrestrial impact structures are a preservation sample of an originally more numerous population. The Precambrian record does include two of the largest known structures; Sudbury and Vredefort (Vredefort being the oldest and largest with an age of ~ 2.02 Ga and an estimated original diameter of ~ 300 km). The dominant record of impact in the Precambrian is in the form of spherule beds, which are considered to have an impact origin, in supracrustal successions between ~ 3.47 and ~ 2.49 Ga in age (Lowe et al. 2014). These beds occur in South Africa and Australia and range from ~ 1 cm to a few 10's of metres in thickness. Various lines of evidence have been presented to support an impact origin, including near chondritic platinum group element ratios, extra-terrestrial chromium isotopic compositions and the presence of nickel-rich chromite (e.g. Kyte et al. 2003; Simonson et al. 2009; Lowe et al. 2014). At least 18 such spherule beds are known, with the latest discovery being an ~ 3.46 Ga example in Western Australia (Glickson et al. 2016).

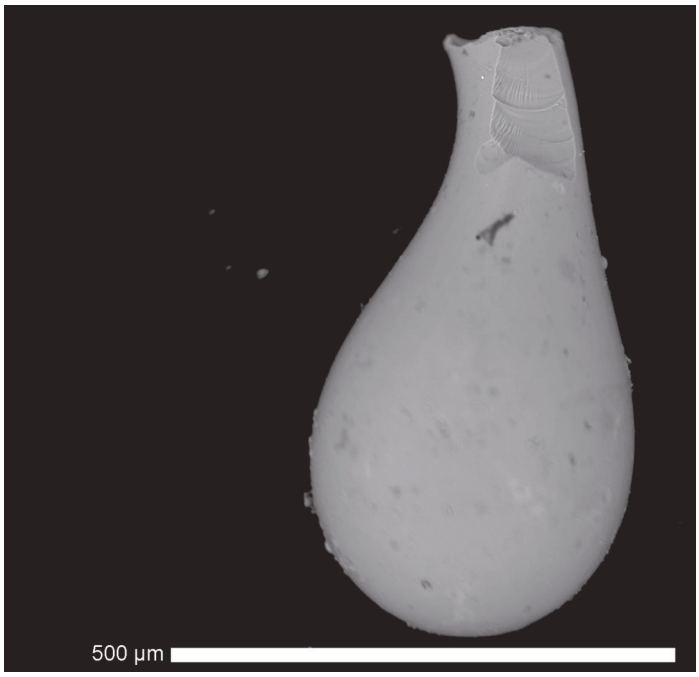

Figure 17. Impact spherule from the Paleocene–Eocene–Thermal Maximum in Milliville drill hole (ODP, Leg 174AX). Image from M. Schaller, Rensselaer Polytechnical Institute.

Impact-related spherule beds are known from the Phanerozoic, e.g. tektites and micro-tektites (e.g. Simonson and Glass 2004) and from the preserved ejecta of such impact structures as Chicxulub and Sudbury (e.g. Addison et al. 2005). These spherules, however, are generally accompanied by evidence of sub-solidus shock effects, such as quartz with planar deformation features. In the case of these Precambrian spherule beds, there has been only one case of reported sub-solidus shock in the form of a single shocked quartz grain (Rasmussen and Koeberl 2004). The apparent dearth of sub-solidus shocked material could be attributed to the age of these beds, with such features as planar deformation features having completely annealed out over time. Most recently, however, the high pressure polymorph TiO_2-II, which is known to occur in impact deposits (e.g. Jackson et al. 2006), has been reported from four Neoarchean spherule beds (Smith et al. 2016).

Questions, however, remain. In particular, why are there so many apparently impact-related spherule beds over a relatively limited time period, compared to the remainder of the terres-

trial sedimentary record? This could be simply an aberration with respect to preservation of the record. Also, it is generally assumed that such beds are the product of large impact events (e.g. Glickson et al. 2016), with analogies with Chicxulub and its ejecta the most common. The lunar impact record suggests that the impact-rate in the Earth-moon system at this time was not much higher than in the Phanerozoic (Fig. 18; Stöffler et al. 2006). A minimum of 18 such events, however, in an ~ 1 Ga time-period suggests that possibly impacts smaller than Chicxulub could produce such spherule beds.

Hadean

It is generally believed that the terrestrial planets formed in a similar manner through the rapid accretion of planetismals and planetary embryos over a relatively short period of a few tens of millions of years (e.g. Chambers 2004). This rapid accretion and the conversion of accretional kinetic energy into heat resulted in the formation of magma oceans, leading to the primary differentiation of the terrestrial planets and the formation of their initial crusts. From then, further evolution of the terrestrial planets diverged, depending on their size (thermal regime, planetary gravity) and the presence or absence of water. Another commonality is that, following the formation of their initial crusts, they continued to be subjected to an intense impact regime over the time period of what is referred to as the Hadean (~ 4.5–3.9 Ga), in the case of the Earth. The evidence for such an early period of intense bombardment is most compelling on the smaller and less evolved terrestrial planets, such as the moon and Mercury, in the form of a multitude of impact craters, including multiring basins, some with diameters in excess of 1000 km. Reasoned speculation and theoretical modelling considerations on the effects of this bombardment on the Hadean Earth have included the sterilization of the Earth's surface and its role in delivering and inhibiting the development and evolution of life (e.g. Thomas et al. 1997), the erosion of the primordial atmosphere (e.g. Melosh and Vickery 1989) and the boiling-off of portions, if not all, of the primordial hydrosphere (e.g. Zahnle and Sleep 1997).

In terms of the effects of such an early bombardment on terrestrial crustal evolution, many works explicitly acknowledge that such a bombardment took place but largely ignore any effects on crustal evolution (e.g. Harrison 2009). Early models of the effects of such a bombardment on the early Earth relied heavily on analogies with what is inferred with respect to the effects of such a bombardment on lunar crustal evolution, with allowances for a different thermal regime, higher planetary gravity and the presence of water (e.g. Green 1972; Frey 1980; Grieve 1980). At the time, however, a fundamental property of impact processes, which has been termed "differential scaling" (Grieve and Cintala 1992), was not recognized. As a result of this property, strict analogies between lunar and terrestrial impacts of similar size, particularly, with respect to the volumes of impact melt generated are not valid and very large lunar impacts, such as those that produced the multiring basins, are poor analogies for similar-sized impacts on the Hadean Earth.

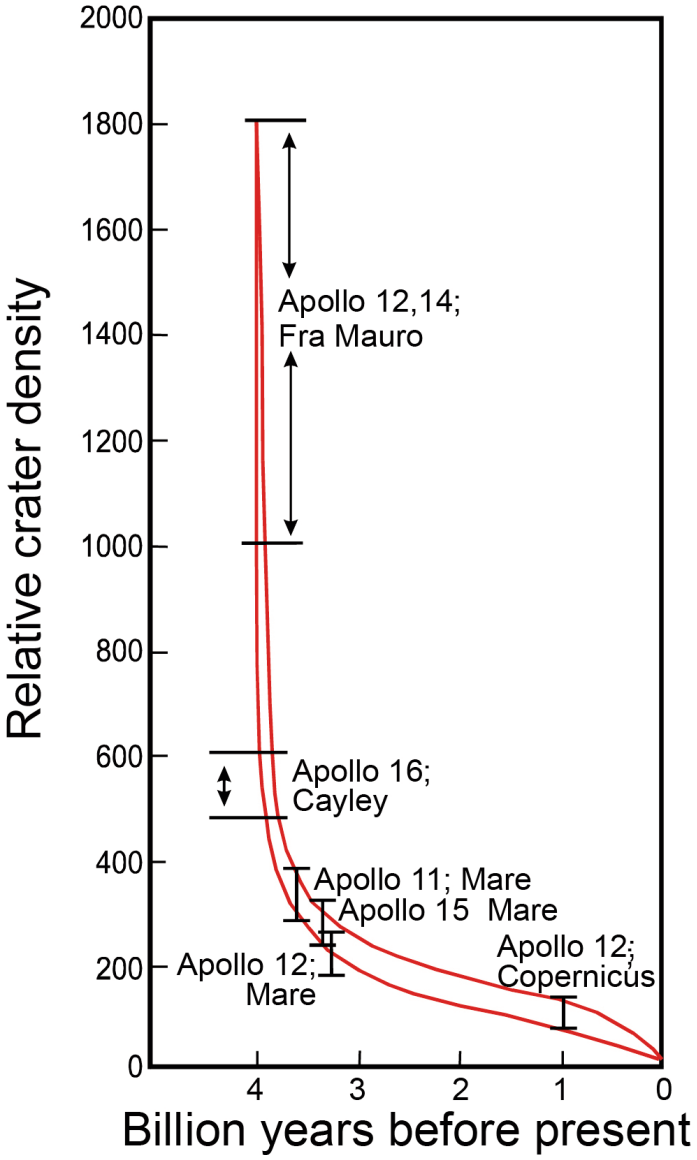

Figure 18. Variation in relative crater density for craters > 4 km diameter on the moon, with age of counting surface. Envelope of curves can be taken as a proxy for the variation in the cratering rate with time in the Earth-moon system. Note the steep rise in the cratering rate for ages > 3.8 Ga. The rate for ages < 3.5 Ga is essentially constant.

Differential scaling refers to the fact that planetary gravity is a primary variable in determining the efficiency of a given impact to form a crater of a given size. As it is a force that inhibits crater growth and includes a time term, cratering efficiency is reduced on higher gravity planetary bodies and in larger, compared to smaller, impacts. Thus, the effects of gravity are most pronounced in comparing large impact structures between bodies such as the Earth and moon. Gravity, however, is not a primary variable in the magnitude and geometry of the shock wave in the target and, thus, the volume of impact melt produced in a given impact, although planetary gravity affects impact velocity, with higher velocities resulting in more melt. In the case of the Earth, the volume of impact melt produced in an impact that would result in a several hundred kilometre

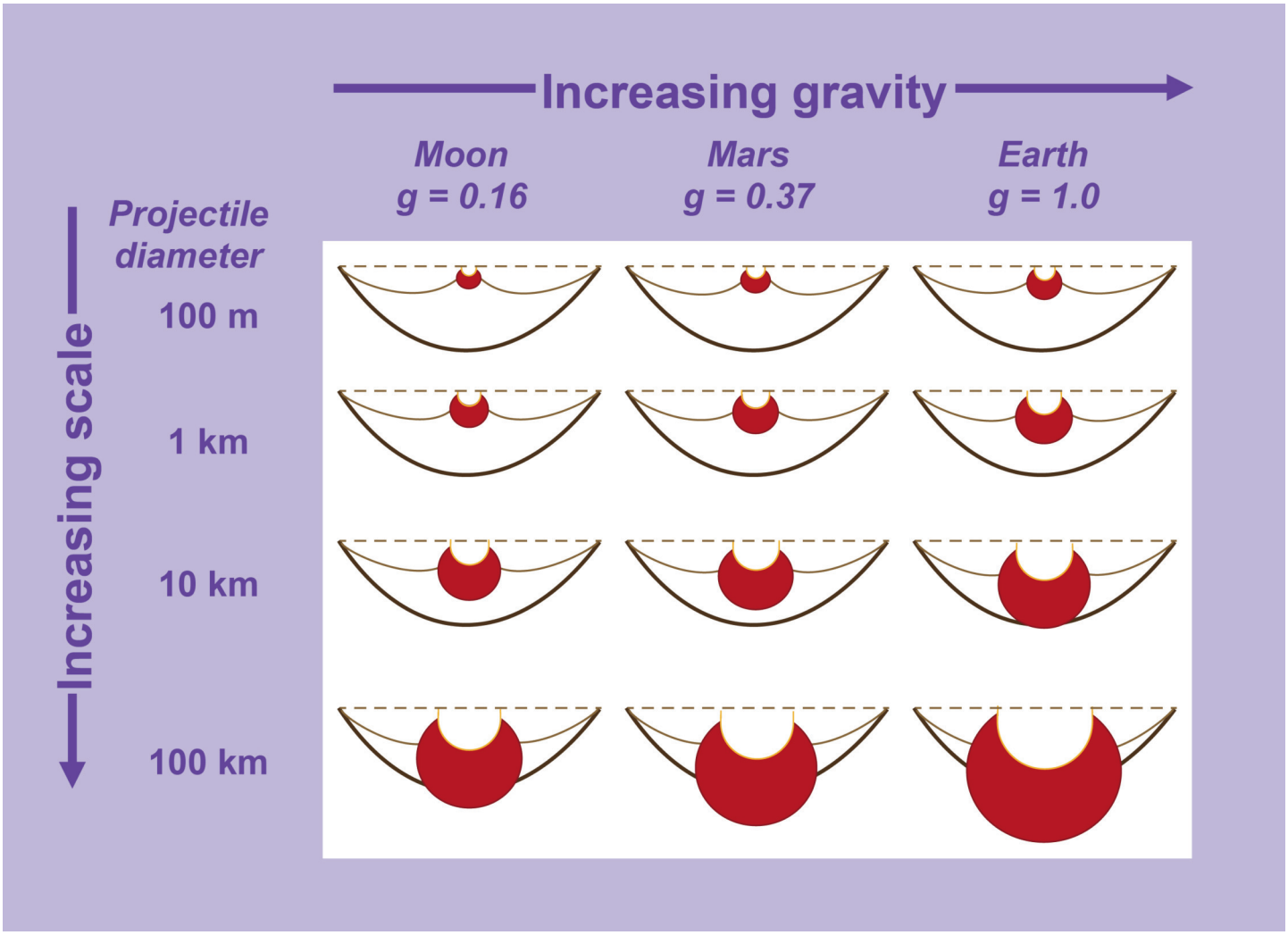

Figure 19. Schematic cross-section representation, scaled to transient cavity size, of the concept of differential scaling. Indicated are melt (red), transient cavity (solid) and ejected (dashed) areas, with increasing gravity (g), relative to the Earth (left to right) and increasing event size (top to bottom), all other impact parameters being fixed for the respective planetary bodies.

diameter crater on the moon exceeds that of the volume of the transient cavity produced by the cratering-flow field (Fig. 19). Thus, in terms of large impact events occurring on the Hadean Earth, the net result would not be final craterforms resembling their lunar counterparts produced by equivalent magnitude impacts. As melt has no strength, the resultant craterform would be extremely shallow, at best, and, most likely, conform more to a massive melt pool than recognizable craterforms.

The depths of these melt pools would have been variable and in the range of many kilometres to many tens of kilometres. What seems clear is that the surface and crust of the Hadean Earth would have had extensive and voluminous impact-produced melt pools of mafic composition, assuming an initial basaltic crust (Fig. 20). Given the appropriate cooling times, bodies of basaltic melt > 300 m thick differentiate in the terrestrial environment, with the potential degree of differentiation being a function of the thickness of the melt body (Jaupart and Tait 1995). It is, therefore, expected that these thick, closed-system melt pools would have differentiated into an ultramafic-mafic base and a more felsic top, much in the same manner as the ~ 2.5 km thick impact melt sheet, now manifested as the Sudbury Igneous Complex, at the originally ~ 150–200 km diameter Sudbury impact structure, Canada (Therriault et al. 2002). The results of individual impacts on the Hadean Earth would have been impressive. For example, a terrestrial impact event with the magnitude of the one that resulted in the Orientale basin on the moon would have generated in excess of 10^7 km^3 of impact melt. If only 10% of the initial melt volume took the form of felsic differentiates, they would have been comparable in volume to the Columbia River basalts.

The impact rate in the Hadean can be estimated from the lunar record of impacts for the same time period (Fig. 18). As the Earth has a larger gravitational cross-section than the moon, the impact rate will have been higher. How much higher, depends on the approach velocity of the impacting bodies, with slower approach velocities, which are generally considered

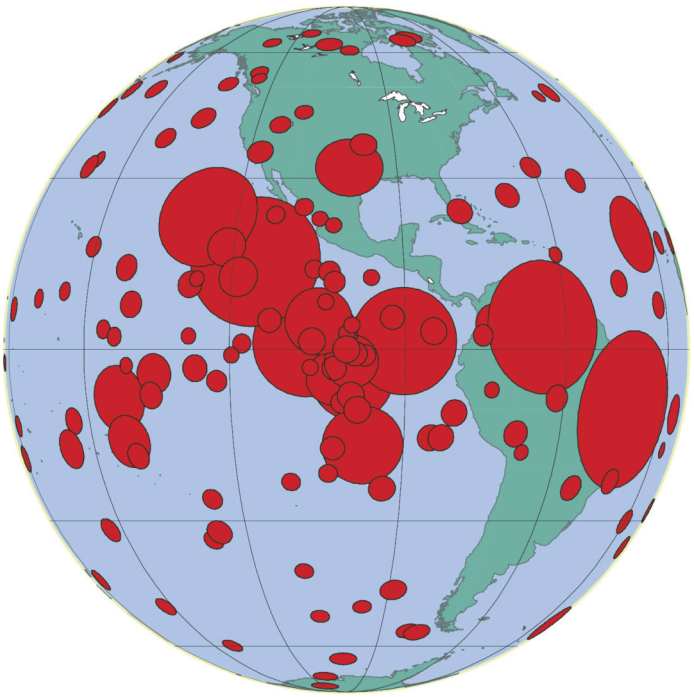

Figure 20. Cartoon of the number of impact melt pools (approximated by transient cavity diameters), where melt volumes exceed transient cavity volumes on the Hadean Earth. This is a minimum number, as the impact velocity was constrained to 22.4 km.s^{-1} (Table 2), close to the present-day average asteroidal impact velocity. Number of melt pools was estimated based on the lunar cratering record, scaled to terrestrial conditions (Grieve et al. 2006). Locations of melt pools were based on random numbers and current land masses are shown for scale.

to be the case in early solar system history, increasing the gravitational cross-section ratio (Table 2). With the lunar record as a proxy, such cumulative effects as the total amount of impact melting (as high as ~ 10^{12} km^3) can be estimated (Table 2). Such a range of cumulative effects can be found in Grieve et al. (2006). In essence, it suggests a Hadean Earth with a surface dominated by melt-pools, some of which were sub-continental in scale. Most recently more sophisticated modelling, using Monte Carlo simulations (5000 times) to calculate the impact flux and hydrocode simulations to calculate impact melting, reached similar conclusions (Marchi et al. 2014).

There are few rocks older than 4.0 Ga and the lithological nature of the Hadean depends on the interpretation of Hadean detrital zircons. The Ti-in-zircon crystallization temperature of these zircons is relatively low (~ 685°C) and felsic mineral inclusions have suggested crystallization from anatectic granitic melts (e.g. Cavoise et al. 2004; Watson and Harrison 2005) and by implication some form of plate tectonic processes operating in the Hadean (e.g. Hopkins et al. 2008). Grieve et al. (2006) suggested that, by analogy with the Sudbury Igneous Complex, such zircons could have also been produced in the more felsic components of differentiated impact melt sheets. Direct tests on zircons from the Sudbury Igneous Complex appeared to contradict this, in terms of crystallization temperatures for its zircons that were too high (Wielicki et al. 2012). Most recently, however, measurements on a more complete suite of samples from the Sudbury Igneous Complex, and using ion microprobe analyses, have indicated zircon crystallization temperatures overlapping that of Hadean zircons (Kenney et al. 2016). These results serve to revive the hypothesis that Hadean zircons could result from differentiated impact melt sheets, although they do not preclude an origin by more conventional plate tectonic-like processes. In their simulation of the impact history of the Hadean Earth, Marchi et al. (2014) argue that the peak in known Hadean zircon ages at 4.2–4.1 Ga coincides with the time, and is the result of, the so-called "Late Heavy Bombardment" in the Earth-moon system.

The most important impact in a planet's evolutionary history is the largest. The origin of the Earth's moon by such working hypotheses as capture, co-accretion and fusion all have severe difficulties, based on the size and composition of the moon and the angular momentum of the Earth-moon system (e.g. Hartmann et al. 1986). First suggested by Hartmann and Davis (1975), an alternate working hypothesis is that the moon is the result of the impact of a Mars-sized object, now named Theia (mother of the Greek moon goddess Selene) with the proto-Earth after core formation. This giant impact hypothesis was attractive in that it accounted for the unusual nature of the Earth-moon system compared to other planets and their satellites and was consistent with the origin of the moon not by an evolutionary but rather by a stochastic process in planetary dynamics. In computer simulations, a relatively low velocity oblique impact resulted in the formation of an iron-depleted accretionary disc around the proto-Earth from which an iron-poor moon formed and culminated in an Earth-moon system with the appropriate angular momentum (e.g. Canup and Asphaug 2001).

In these simulations, the material in the accretionary disc was largely from Theia's mantle. One of the main results of the analyses of lunar materials, however, is a remarkable simi-

Table 2. Relative asteroidal impact velocities and corresponding gravitational cross-sections for lunar and terrestrial impacts and culumulative impact melt produced on the Hadean Earth, in which melt volumes exceed transient cavity volumes (see text for details).

Impact velocity, moon, km.s^{-1}	Impact velocity, Earth, km.s^{-1}	Gravitational cross-section, moon, km^2	Gravitational cross-section, Earth, km^2	Ratio cross-section areas, Earth/moon	Cumulative impact melt volume, km^3
7.5	14.9	1.34×10^7	1.29×10^9	96.14	1.31×10^{12}
10	17.4	1.09×10^7	5.41×10^8	49.76	3.25×10^{11}
15	22.4	9.91×10^6	2.54×10^6	25.76	7.87×10^{10}

larity in composition with the Earth, particularly with respect to some isotopic ratios (e.g. Wiechert et al. 2001; Zhang et al. 2012). This requires that Theia's mantle was similar in composition to that of the Earth and, thus, Theia originated from a position in the solar system similar to that of the Earth. This is an unlikely scenario, given simulations of the formation of the terrestrial planets (e.g. Chambers 2001). More recent computer simulations, however, of the moon's origin by impact appear to have addressed the compositional similarity through high speed impact into a fast spinning proto-Earth or impacts with similar-sized bodies in that the resultant accretionary disc, from which the moon formed, is largely Earth mantle materials (e.g. Ćuk and Stewart 2012; Canup 2012).

Recent work on Pb isotopes suggests a major loss of volatile Pb relative to refractory U at 4.43–4.42 Ga on Earth and provides an age constraint on the timing of the moon-forming event by Connelly and Bizzarro (2016). They estimate a loss of ~ 98% of terrestrial Pb relative to solar system bulk composition by the moon-forming impact due to volatility. If Pb was lost during the moon-forming event, then more volatile materials, such as water, were also lost. This is in keeping with models that indicate the present inventory of terrestrial volatiles is from post moon-forming accreting chondritic materials (e.g. Albarede et al. 2013).

The moon (and its postulated effects) is a prominent feature of human culture and lore. Without a moon-forming impact event, however, the major effect of the lack of such a massive satellite on the Earth would have been the lack of lunar tides. With only solar tides, the extent of tidal zones to the world's oceans and seas would be reduced by ~ 55%. As such tidal zones represent the transition between the marine and terrestrial environments and biospheres, it can be speculated that such a reduction in their extent could well have affected the path and speed of terrestrial biosphere evolution.

IMPACTS AND THE FUTURE EARTH

The future impact of a sizeable extraterrestrial body on the Earth is inevitable. Relatively small events, such as the one that resulted in the famous ~ 1.2 km diameter Barringer or Meteor crater in Arizona, USA, some 50,000 years ago, and even those involving objects too small or weak to reach the ground, such as the 1908 Tunguska event in Siberia, Russia, have the capacity to have severe social and economic consequences, depending on the location of the event (e.g. Dore 2007). The most recent event was the February, 2013, air blast from the passage of an ~ 20 metre object at ~ 30–50 km altitude over the city of Chelyabinsk in the Urals, Russia (e.g. Brown et al. 2013). The shock wave damaged buildings and resulted in injuries to over 7,000 people, although there were no reported fatalities. Toon et al. (1997) found that impact events occurring on frequencies less than ~ 50,000 years produce blast damage, earthquakes, and fires over areas (10^4–10^5 km^2) that are similar in size to those affected by recent disasters. Readers wishing to know the potential effects at a specified distance of a specified impact event are referred to http://impact.ese.ic.ac.uk/ImpactEffects/. An ICSU-sponsored series of works dealing with the impact hazard and its effects (social, economic, potential deaths, etc.) can be found in Bobrowsky and Rickman (2007).

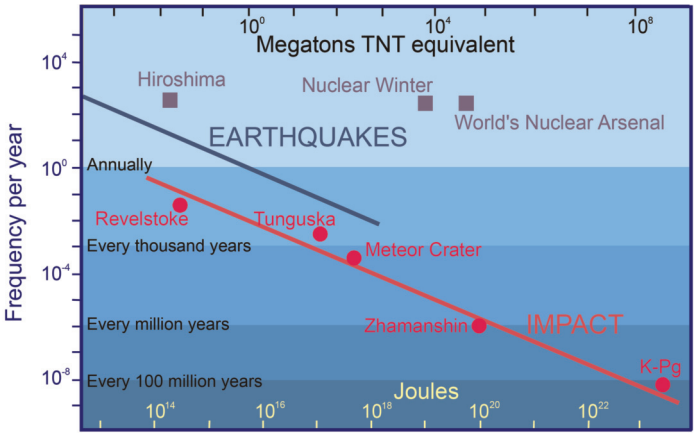

Figure 21. Logarithmic plot of frequency versus energy (J and TNT equivalent) of terrestrial impact events compared to earthquakes. Earthquakes are more frequent than impacts but have an upper limit to the energies involved. The energies and frequencies of some specific terrestrial impact events are indicated, as are the nuclear energies of the Hiroshima atomic bomb and those believed to be sufficient to result in a 'nuclear winter' and contained in the world's nuclear arsenal.

The threshold for disrupting human civilization is much less than that needed for a significant extinction event, such as at the K–Pg boundary. To affect global society, impacts have to be energetic enough to produce dust-loadings and other chemical changes in the atmosphere that result in short-term climatic changes, particularly cooling (MacCracken 2007). Since 75% of the Earth's surface is covered by water, impact-induced tsunamis may be a greater potential threat (e.g. Hills et al. 1994; Chapman 2004). The magnitude, however, of such a threat is somewhat controversial and uncertain, as it is most likely that the envisioned massive waves would collapse under their own weight, resulting in turbulence and the dissipation of the bulk of their energy relatively close to the impact point (e.g. Melosh 2007). Global consequences, however, of impacts into water may occur on time-scales of 300,000 years, when the impacts distribute water vapour and destroy ozone in the atmosphere (Birks et al. 2007), with larger impact events creating disasters beyond anything recorded in human history. Other natural disasters (e.g. hurricanes, earthquakes) occur more frequently than impact events (Chapman 2004). Impact events, however, can release vast amounts of energy (Fig. 21) and have the capacity of creating disasters of far greater magnitude than any other natural process. They are low probability but high consequence events, which can affect much larger regions, produce several environmental perturbations simultaneously and have essentially no upper limit to their energy release and, thus, severity.

SUMMARY REMARKS

Perhaps due to the wide range of highly active endogenic geologic processes on the Earth, the earth sciences were slow to recognize the evidence for the occurrence of impact events on Earth. The first terrestrial impact site (Barringer) was documented ~ 100 years ago, but its impact origin at the time was highly controversial. Focused exploration efforts on terrestrial

impact structures as geologic features, and lunar analogues, did not occur until the immediate pre-Apollo era. Today, the basic physical and chemical characteristics of terrestrial impact structures and how they vary in form with diameter have been documented. The characteristics clearly delineate them from other terrestrial geologic structures. Nevertheless, the number of known impact structures and records of impact in the stratigraphic record is small (~ 200) and it would be premature to state that the current sample is complete or that impact processes have truly entered into the mainstream knowledge base of the earth science community.

At present, some sixteen impact structures are known with diameters > 20 km and ages less than 100 Ma on the Earth's land surface. These had impact energies in excess of ~ 10^6 MT TNT equivalent (~ 4×10^{21} J) and were dramatic events that had potentially catastrophic regional environmental effects and moderate to severe continental and global effects. To put the potential of impact to affect catastrophic change in a more realistic perspective, the average impact cratering rate during the last 100 Ma is estimated to be $5.6 \pm 2.8 \times 10^{-15}$ km^{-2}.a^{-1} for events that produce > 20 km diameter craters (Grieve 1984). This translates to ~ 85 impact events of such magnitude that actually occurred on the Earth's land surface in the last 100 Ma, i.e. the known sample is ~ 20% of the actual number of events that occurred. The largest, the end-Cretaceous Chicxulub impact, extinguished ~ 75% of species living at the time. This mass extinction provided evolutionary opportunities and surviving members of the extinction underwent massive adaptive radiations into the emptied ecological niches. Such ushered in the rise of mammals, which ultimately led to the evolution of humans. Chicxulub, and other impacts, have begun to demonstrate the regional to global environmental effects of impacts and evaluating their environmental and biologic effects is a critical step in the assessment of the hazards from future impact events Although such large impact events are regionally and/or globally important, smaller impact events can not be ignored on an Earth that has an ever-increasing population. Even Barringer-sized events have the potential to destroy a modern city. It is estimated that 1 km diameter cratering events occur every few thousand years (Neukum and Ivanov 1994). Impact airbursts, like Tunguska, which are also capable of considerable destruction, occur more frequently, perhaps every few hundred years. It is inevitable that human civilization, if it survives itself long enough, will be exposed to an impact-induced environmental crisis of potentially extreme proportions.

As the Chicxulub event and the subsequent biological evolutionary trends favouring mammals indicate, impact events are not entirely a negative phenomenon with respect to the current human condition. In addition, they represent unusual geological events and, as such, they have resulted in local anomalous geological environments, some of which have produced significant economic deposits. About 20% of known terrestrial impact structures have some form of economic deposit associated with them, and about half of these are currently exploited or have been exploited in the recent past. The deposits range from local and uneconomic (e.g. reserves of 3 $\times 10^5$ t of hydrothermal Pb–Zn ores at Siljan, Sweden) to world-class (e.g. 1.5×10^9 t Ni–Cu–PGE ores at Sudbury) and also include significant (and sometimes unusual) hydrocarbon deposits.

With respect to crustal evolution, all the terrestrial planets were subject to a period of intense bombardment following their formation. What the result of this bombardment was for the Hadean can only be the subject of reasoned speculation. The argument advanced, here, is that such a period of bombardment would not result in the 100's–1000's km diameter multiring basins, as observed on the moon, but rather in immense pools of impact melt, due to the effect of the high planetary gravity on Earth and its effect in the phenomenon termed 'differential scaling.' Such silicate melt bodies, whether produced by igneous or impact processes, have the potential to differentiate. This is observed at the largest currently known impact melt sheet on Earth, the Sudbury Igneous Complex. The only known surviving products of the early Earth are Hadean-age detrital zircons in younger lithologies. Recent analyses indicate that the crystallization temperatures of zircons from the Sudbury Igneous Complex span the range of those in these Hadean zircons, effectively removing an objection to the hypothesis that Hadean zircons could be impact melt products. This reopens the door to the hypothesis that impact melt formation and differentiation was a mechanism to produce the earliest felsic lithologies of the Earth's crust. It does not, however, preclude other processes but suggests that the potential effects of this intense bombardment on early Earth's history can not be simply ignored.

Amongst the terrestrial planets, the Earth's moon is unique, particularly in terms of its size relative to the Earth. Although it may have a counterpart in the size relation between Pluto and its satellite Charon, this suggests a non-evolutionary, stochastic process may have been involved in its origin. The giant impact hypothesis on the proto-Earth at > 4.4 Ga is currently the favoured working model. Recent computer simulations indicate that it is possible to account for the isotopic similarities between the Earth and the moon, which was a major stumbling block in accepting some of the earlier modelling of such a moon-forming impact. Although sometimes forgotten in today's computational environment, however, the 'fact' that some phenomenon can be modelled and apparently satisfy the known evidence does not elevate the model, itself, to empirical evidence for that process. Nevertheless, it does appear to be a more satisfying working hypothesis than those previously advanced to account for the origin of the moon.

Although not detailed here, but with moon-forming impact as a context, it can be argued that impact is the most fundamental of the physical processes in Earth's history, as it was the process whereby the terrestrial planets, themselves, were formed and, in the case of the Earth, received its volatile budget. Finally, it can also be argued that the formation of the moon, the K–Pg mass extinction and the creation of exploitable natural resources by large-scale impact on Earth have all been positives towards the current evolution of humanity. Ultimately, however, the impact hazard must also be recognized as a reality and as a negative in the long-term extended future of humanity.

ACKNOWLEDGEMENTS

Much of my efforts to understand impact processes and their effects were undertaken in collaboration and in co-authorship with international colleagues, to whom I will always be grateful. In particular, I would like to acknowledge J. Garvin and M. Cintala (NASA), J. Head (Brown U.), J. Morgan (Imperial College), U. Riller (U. Hamburg), D. Stöffler (Humboldt U.), V. Masaitis (Karpinsky Institute), G. Osinski (Western U.) and A. Therriault and B. Robertson (GSC) for their stimulating intellectual interactions over the years. Thanks also go to M. Grieve for his efforts in providing the graphics and to A. Therriault for critical reading of this contribution. Formal reviews by F. Hörz and an anonymous reviewer are greatly appreciated.

REFERENCES

Abramov, O., and Kring, D.A., 2004, Numerical modeling of an impact-induced hydrothermal system at the Sudbury crater: Journal of Geophysical Research, v. 109, E10007, https://doi.org/10.1029/2003JE02213.

Addison, W.D., Brumpton, G.R., Vallini, D.A., McNaughton, N.J., Davis, D.W., Kissin, S.A., Fralick, P.W., and Hammond, A.L., 2005, Discovery of distal ejecta from the 1850 Ma Sudbury impact event: Geology, v. 33, p. 193–196, https://doi.org/10.1130/G21048.1.

Albarede, F., Ballhaus, C., Blichert-Toft, J., Lee, C-T., Marty, B., Moynier, F., and Qing-Zhu, Y., 2013, Asteroidal impacts and the origin of terrestrial and lunar volatiles: Icarus, v. 222, p. 44–52, https://doi.org/10.1016/j.icarus.2012.10.026.

Alvarez, L.W., Alvarez, W., Asaro, F., and Michel, H.V., 1980, Extraterrestrial cause for the Cretaceous–Tertiary extinction: Science, v. 208, p. 1095–1108, https://doi.org/10.1126/science.208.4448.1095.

Ames, D.E., and Farrow, C.E.G., 2007, Metallogeny of the Sudbury mining camp, *in* Goodfellow, W.D., *ed.*, Mineral Deposits of Canada: Mineral Deposits Division, Special Publication 5, Geological Association of Canada, St. John's, NL, p. 329–350.

Ames, D.E., Jonasson, I.R., Gibson, H.L., and Pope, K.O., 2006, Impact-generated hydrothermal system — Constraints from the large Paleoproterozoic Sudbury crater, Canada, *in* Cockell, C., Koeberl, C., and Gilmour, I., *eds.*, Biological Processes Associated with Impact Events: Springer-Verlag, Berlin, p. 55–100, https://doi.org/10.1007/3-540-25736-5_4.

Ames, D.E., Davidson, A., and Wodicka, N., 2008, Geology of the giant Sudbury polymetallic mining camp, Ontario, Canada: Economic Geology, v. 103, p. 1057–1077, https://doi.org/10.2113/gsecongeo.103.5.1057.

Baker, D.M.H., Head, J.W., Schon, S.C., Ernst, C.M., Prockter, L.M., Murchie, S.L., Denevi, B.W., Solomon, S.C., and Strom, R.G., 2011a, The transition from complex crater to peak-ring basin on Mercury: New observation from MESSENGER flyby data and constraints on basin-formation models: Planetary and Space Science, v. 59, p. 1932–1948, https://doi.org/10.1016/j.pss.2011.05.010.

Baker, D.M.H., Head, J.W., Fasset, C.I., Kadish, S.J., Smith, D.E., Zuber, M.T., and Neumann, G.A., 2011b, The transition from complex crater to peak-ring basin on the Moon: New observations from Lunar Orbiter Laser Altimeter (LOLA) instrument: Icarus, v. 214, p. 377–393, https://doi.org/10.1016/j.icarus.2011.05.030.

Baker, D.M.H., Head, J.W., Collins, G.S., and Potter, R.W.K., 2016, The formation of peak-ring basins: Working hypotheses and path forward in using observations to constrain models of impact-basin formation: Icarus, v. 273, p. 146–163, https://doi.org/10.1016/j.icarus.2015.11.033.

Barringer, D.M., 1905, Coon Mountain and its crater: Proceedings Academy of Natural Sciences of Philadelphia, v. 57, p. 861–886, http://www.jstor.org/stable/4063062.

Baudemont, D., and Fedorowich, J., 1996, Structural control of uranium mineralization at the Dominique-Peter deposit, Saskatchewan, Canada: Economic Geology, v. 91, p. 855–874, https://doi.org/10.2113/gsecongeo.91.5.855.

Becker, L., Poreda, R.J., Hunt, A.G., Bunch, T.E., and Rampino, M., 2001, Impact event at the Permian–Triassic boundary: Evidence from extraterrestrial noble gases in fullerenes: Science, v. 291, p. 1530–1533, https://doi.org/10.1126/science.1057243.

Becker, L., Poreda, R.J., Basu, A.R., Pope, K.O., Harrison, T.M., Nicholson, C., and Lasky, R., 2004, Bedout: A possible end-Permian impact crater offshore of northwestern Australia: Science, v. 304, p. 1469–1476, https://doi.org/10.1126/science.1093925.

Birks, J.W., Crutzen, P.J., and Roble, R.G., 2007, Frequent ozone depletion resulting from impacts of asteroids and comets, *in* Bobrowsky, P., and Rickman, H., *eds.*, Comet/Asteroid Impacts and Human Society: Springer, New York, p. 225–245, https://doi.org/10.1007/978-3-540-32711-0_13.

Bobrowsky, P., and Rickman, H., *editors*, 2007, Comet/Asteroid Impacts and Human Society: Springer, New York, 546 p.

Bohor, B.F., Foord, E.E., Modreski, P.J., and Triplehorn, D.M., 1984, Mineralogical evidence for an impact at the Cretaceous–Tertiary Boundary: Science, v. 224, p. 867–869, https://doi.org/10.1126/science.224.4651.867.

Brenan, R.L., Peterson, B.I., and Smith, H.J., 1975, The origin of Red Wing Creek Structure, McKenzie County, North Dakota: Wyoming Geological Association Earth Science Bulletin, v. 8, p. 1–41.

Brown, P.G., and 32 others, 2013, A 500-kiloton airburst over Chelyabinsk and an enhanced hazard from small impactors: Nature, v. 503, p. 238–241, https://doi.org/10.1038/nature12741.

Canup, R.M., 2012, Forming a Moon with an Earth-like composition via a giant impact: Science, v. 338, p. 1052–1055, https://doi.org/10.1126/science.1226073.

Canup, R.M., and Asphaug, E., 2001, Origin of the Moon in a giant impact near the end of the Earth's formation: Nature, v. 412, p. 708–712, https://doi.org/10.1038/35089010.

Carpenter, B.N., and Carlson, R., 1992, The Ames impact crater: Oklahoma Geological Survey, v. 52, p. 208–223.

Cavoise., A.J., Wilde, S.A., Liu, D., Weiblen, P.W., and Valley, J.W., 2004, Internal zoning and U–Th–Pb chemistry of Jack Hills zircons: A mineral record of Archean to Mesoproterozoic (4348–1576 Ma) magmatism: Precambrian Research, v. 135, p. 251–279, https://doi.org/10.1016/j.precamres.2004.09.001.

Chambers, J.E., 2001, Making more terrestrial planets: Icarus, v. 152, p. 205–224, https://doi.org/10.1006/icar.2001.6639.

Chambers, J.E., 2004, Planetary accretion in the inner Solar System: Earth and Planetary Science Letters, v. 223, p. 241–252, https://doi.org/10.1016/j.epsl.2004.04.031.

Chao, E.C.T., Shoemaker, E.M., and Madsen, B.M., 1960, First natural occurrence of coesite: Science, v. 132, p. 220–222, https://doi.org/10.1126/science.132.3421.220.

Chapman, C.R., 2004, The hazard of near-Earth asteroid impacts on Earth: Earth and Planetary Science Letters, v. 222, p. 1–15, https://doi.org/10.1016/j.epsl.2004.03.004.

Cohen, A.S., Burnham, O.M., Hawkesworth, C.J., and Lightfoot, P.C., 2000, Pre-emplacement Re–Os ages for ultramafic inclusions in the sublayer of the Sudbury igneous complex: Chemical Geology, v. 165, p. 37–46, http://dx.doi.org/10.1016/S0009-2451(99)00162-x.

Collins, G.S., Melosh, H.J., Morgan, J.V., and Warner, M.R, 2002, Hydrocode simulations of Chicxulub crater collapse and peak-ring formation: Icarus, v. 157, p. 24–33, https://doi.org/10.1006/Icar.2002.6822.

Collins, G.S., Morgan, J., Barton, P., Christeson, G.L., Gulick, S., Urrutia, J., Warner, M., and Wünnemann, K., 2008, Dynamic modeling suggests terrace zone asymmetry in the Chicxulub crater is caused by target heterogeneity: Earth and Planetary Science Letters, v. 270, p. 221–230, https://doi.org/10.1016/j.epsl.2008.03.032.

Connelly, J.N., and Bizzarro, M., 2016, Lead isotope evidence for a young formation age of the Earth–Moon system: Earth and Planetary Science Letters, v. 452, p. 36–43, https://doi.org/10.1016/j.epsl.2016.07.010.

Ćuk, M., and Stewart, S.T., 2012, Making the Moon from a fast-spinning Earth: A giant impact followed by resonant despinning: Science, v. 338, p. 1047–1052, https://doi.org/10.1126/science.1225542.

De Laubenfels, M.W., 1956, Dinosaur extinction: One more hypothesis: Journal of Paleontology, v. 30, p. 207–212, http://www.jstor.org/stable/1300393.

Dickin, A.P., Richardson, J.M., Crocket, J.H., McNutt, R.H., and Peredery, W.V., 1992, Osmium isotope evidence for a crustal origin of platinum group elements in the Sudbury nickel ore, Ontario, Canada: Geochimica et Cosmochimica Acta, v. 56, p. 3531–3537, https://doi.org/10.1016/0016-7037(92)90396-Z.

Dickin, A.P., Artan, M.A., and Crocket, J.H., 1996, Isotopic evidence for distinct crustal sources of North and South Range ores, Sudbury Igneous Complex: Geochimica et Cosmochimica Acta, v. 60, p. 1605–1613, https://doi.org/10.1016/0016-7037(96)00044-0.

Donofrio, R.R., 1981, Impact craters: Implications for basement hydrocarbon production: Journal of Petroleum Geology, v. 3, p. 279–302, https://doi.org/10.1111/j.1747-5457.1981.tb00931.x.

Donofrio, R.R., 1998, North American impact structures hold giant field potential: Oil and Gas Journal, v. 96, p. 69–83.

Dore, M.H.I., 2007, The economic consequences of disasters due to asteroid and comet impacts, small and large, *in* Bobrowsky, P., and Rickman, H., *eds.*, Comet/Asteroid Impacts and Human Society: Springer, New York, p. 479–493, https://doi.org/10.1007/978-3-540-32711-0_29.

Dressler, B.O., 1984, General geology of the Sudbury area, *in* Pye, E.G., Naldrett, A.J., and Giblin, P.E., *eds.*, The Geology and Ore Deposits of the Sudbury Structure: Ontario Geological Survey Special Paper 1, Toronto, p. 57–82.

Faggart Jr., B.E., Basu, A.R., and Tatsumoto, M., 1985, Origin of the Sudbury Complex by meteoritic impact: Neodymium isotopic evidence: Science, v. 230, p.

436–439, https://doi.org/10.1126/science.230.4724.436.
Farrow, C.E.G., and Lightfoot, P.C., 2002, Sudbury PGE revisited: Toward an integrated model, *in* Cabri, L.I., *ed.*, The Geology, Geochemistry, Mineralogy and Beneficiation of Platinum-Group Elements: Canadian Institute of Mining and Metallurgy, Special Volume 54, Montreal, p. 273–297.
French, B.M., and Short, N.M., *editors*, 1968, Shock Metamorphism of Natural Materials: Mono Book Corp., Baltimore, 644 p.
Frey, H., 1980, Crustal evolution of the early Earth: The role of major impacts: Precambrian Research, v. 10, p. 195–216, https://doi.org/10.1016/0301-9268(80)90012-1.
Frimmel, H.E., Groves, D.I., Kirk, J., Ruiz, J., Chesley, J., and Minter, W.E.L., 2005, The formation and preservation of the Witwatersrand goldfields, the world's largest gold province: Economic Geology, v. 100, p. 769–798.
Ganapathy, R., 1980, A major meteorite impact event on the Earth 65 million years ago: Evidence from the Cretaceous–Tertiary boundary clay: Science, v. 209, p. 921–923, https://doi.org/10.1126/science.209.4459.921.
Gibson, R.L., and Reimold, W.U., 2008, Geology of the Vredefort Impact Structures: A Guide to Sites of Interest: South African Council for Geoscience, Memoir 97, Pretoria, 181 p.
Gibson, R.L., Reimold, W.U., and Stevens, G., 1998, Thermal-metamorphic signature of an impact event in the Vredefort dome, South Africa: Geology, v. 26, p. 787–790, https://doi.org/10.1130/0091-7613(1998)026<0787:TMSOAI>2.3.CO;2.
Glickson, A., Hickman, A., Evans, N.J., Kirkland, C.L., Park, J.-W., Rapp, R., and Romano, S., 2016, A new ~3.46 Ga asteroid impact ejecta unit at Marble Bar, Pilbara craton, Western Australia: A petrologic, microprobe and laser ablation ICPMS study: Precambrian Research, v. 279, p. 103–122, https://doi.org/10.1016/j.precamres.2016.04.003.
Goldin, T.J., and Melosh, H.J., 2009, Self-shielding of thermal radiation by Chicxulub impact ejecta: Firestorm or fizzle?: Geology, v. 37, p. 1135–1138, https://doi.org/10.1130/G30433A.1.
Grajales-Nishimura, J.M., Cedillo-Pardo, E., Rosales-Domíniguez, C., Morán-Zenteno, D.J., Alvarez, W., Claeys, P., Ruíz-Morales, J., García-Hernández, J., Padilla-Avila, P., and Sánchez-Ríos, A., 2000, Chicxulub impact: The origin of reservoir and seal facies in the southeastern Mexico oil fields: Geology, v. 28, p. 307–310, https://doi.org/10.1130/0091-7613(2000)28<307:CITOOR>2.0.CO;2.
Green, D.H., 1972, Archean greenstone belts may include terrestrial equivalents of lunar maria?: Earth and Planetary Science Letters, v. 15, p. 263–270, https://doi.org/10.1016/0012-821X(72)90172-0.
Grieve, R.A.F., 1980, Impact bombardment and its role in proto-continental growth on the early Earth: Precambrian Research, v. 10, p. 217–247, https://doi.org/10.1016/0301-9268(80)90013-3.
Grieve, R.A.F., 1984, The impact cratering rate in recent time: Journal of Geophysical Research, v. 89, p. B403–B408, https://doi.org/10.1029/JB089iS02p0B403.
Grieve, R.A.F., 1997, Extraterrestrial impact events: The record in the rocks and the stratigraphic column: Palaeogeography, Palaeclimatology, Palaeoecology, v. 132, p. 5–23, https://doi.org/10.1016/S0031-0182(97)00058-8.
Grieve, R.A.F., 2012, Economic deposits at terrestrial impact structures, *in* Osinski, G.R., and Pierazzo, E., *eds.*, Impact Cratering: Processes and Products: John Wiley & Sons, Ltd, Chichester, UK, p. 177–193, https://doi.org/10.1002/9781118447307.ch12.
Grieve, R.A.F., and Cintala, M.J., 1992, An analysis of differential impact melt-crater scaling and implications for the terrestrial impact record: Meteoritics, v. 27, p. 526–538, https://doi.org/10.1111/j.1945-5100.1992.tb01074.x.
Grieve, R.A.F., and Kring, D.A., 2007, The geologic record of destructive impact events on Earth, *in* Bobrowsky, P., and Rickman, H., *eds.*, Comet/Asteroid Impacts and Human Society: Springer, New York, p. 3–24, https://doi.org/10.1007/978-3-540-32711-0_1.
Grieve, R.A.F., and Masaitis, V.L., 1994, The economic potential of terrestrial impact craters: International Geology Review, v. 36, p. 105–151, https://doi.org/10.1080/00206819409465452.
Grieve, R.A.F., Stöffler, D., and Deutsch, A., 1991, The Sudbury structure: Controversial or misunderstood?: Journal of Geophysical Research, v. 96, p. 22753–22764, https://doi.org/10.1029/91JE02513.
Grieve, R.A.F., Cintala, M.J., and Therriault, A.M., 2006, Large-scale impacts and the evolution of the Earth's crust: The early years, *in* Reimold, W.U., and Gibson, R.L., *eds.*, Processes on the Early Earth: Geological Society of America Special Papers, v. 405, p. 23–31, https://doi.org/10.1130/2006.2405(02).
Grieve, R.A.F., Reimold, W.U., Morgan, J., Riller, U., and Pilkington, M., 2008, Observations and interpretations at Vredefort, Sudbury and Chicxulub: Towards an empirical model of terrestrial impact basin formation: Meteoritics and Planetary Science, v. 43, p. 855–882, https://doi.org/10.1111/j.1945-5100.2008.tb01086.x.
Hanley, J.J., Mungall, J.E., Pettke, T., Spooner, E.T.C., and Bray, C.J., 2005, Ore metal redistribution by hydrocarbon-brine and hydrocarbon-halide melt phases, North Range footwall of the Sudbury Igneous Complex, Ontario, Canada: Mineralium Deposita, v. 40, p. 237–256, https://doi.org/10.1007/s00126-005-0004-z.
Harrison, T.M., 2009, The Hadean crust: Evidence from > 4 Ga zircons: Annual Review of Earth and Planetary Sciences, v. 37, p. 479–505, https://doi.org/10.1146/annurev.earth.031208.100151.
Hartmann, W.K., and Davis, D.R., 1975, Satellite-sized planetesimals and lunar origin: Icarus, v. 24, p. 504–515, https://doi.org/10.1016/0019-1035(75)90070-6.
Hartmann, W.K., Phillips, R.J., and Taylor, G.J., *editors*, 1986, Origin of the Moon: Lunar and Planetary Institute, Houston, 797 p.
Hayward, C.L., Reimold, W.U., Gibson, R.L., and Robb, L.J., 2005, Gold mineralization within the Witwatersrand Basin, South Africa: Evidence for a modified placer origin, and the role of the Vredefort impact event, *in* McDonald, I.M., Boyce, A.J., Butler, I.B., Herrington, R.J., and Polya, D.A., *eds.*, Mineral Deposits and Earth Evolution: Geological Society, London, Special Publications, v. 248, p. 31–58, http://dx.doi.org/10.1114/GSL.SP.2005.2.48.01.02.
Head, J.W., 2010, Transition from complex craters to multi-ringed basins on terrestrial planetary bodies: Scale-dependent role of expanding melt cavity and progressive interaction with the displaced zone: Geophysical Research Letters, v. 37, L02203, https://doi.org/10.1029/2009GL041790.
Henkel, H., and Reimold, W.U., 1998, Integrated geophysical modelling of a giant, complex impact structure: Anatomy of the Vredefort Structure, South Africa: Tectonophysics, v. 287, p. 1–20, https://doi.org/10.1016/S0040-1951(98)80058-9.
Hildebrand, A.R., Penfield, G.T., Kring D.A., Pilkington, M., Camargo, Z.A., Jacobsen, S.B., and Boynton, W.V., 1991, Chicxulub Crater: A possible Cretaceous/Tertiary boundary impact crater on the Yucatán Peninsula, Mexico: Geology, v. 19, p. 867–871, https://doi.org/10.1130/0091-7613(1991)019<0867:CCAPCT>2.3.CO;2.
Hills, J.G., Nemchinov, I.V., Popov, S.P., and Teterev, A.V., 1994, Tsunami generated by small impacts, *in* Geherls, T., *ed.*, Hazards from comets and asteroids: University Arizona Press, Tucson, p. 779–789.
Hopkins, M., Harrison, T.M., and Manning, C.E., 2008, Low heat flow inferred from > 4 Gyr zircons suggests Hadean plate boundary interactions: Nature, v. 456, p. 493–496, https://doi.org/10.1038/nature07465.
Ivanov, B.A., 2005, Numerical modeling of the largest terrestrial meteorite craters: Solar System Research, v. 39, p. 381–409, https://doi.org/10.1007/s11208-005-0051-0.
Jackson, J.C., Horton, J.W., Chou, I.-M., and Belkin, H.E., 2006, A shock-induced polymorph of anatase and rutile from the Chesapeake Bay impact structure, Virginia, U.S.A.: American Mineralogist, v. 91, p. 604–608, https://doi.org/10.2138/am.2006.2061.
Jaupart, C., and Tait, S., 1995, Dynamics of differentiation in magma reservoirs: Journal of Geophysical Research, v. 100, p. 17615–17636, https://doi.org/10.1029/95JB01239.
Jefferson, C.W., and Delaney, G., *editors*, 2007, EXTECH IV: Geology and uranium exploration technology of the Proterozoic Athabasca Basin, Saskatchewan and Alberta: Geological Association of Canada, Mineral Deposits Division, Special Publication 4, St. John's, NL, 645 p.
Johnson, K.S., and Campbell, J.A., *editors*, 1997, Ames Structure in Northwest Oklahoma and Similar Features: Origin and Petroleum Production: Oklahoma Geological Survey, Circular 100, Norman, 396 p.
Kamo, S.L., Reimold, W.U., Krogh, T.E., and Colliston, W.P., 1996, A 2.023 Ga age for the Vredefort impact event and a first report of shock metamorphosed zircons in pseudotachylitic breccias and granophyre: Earth and Planetary Science Letters, v. 144, p. 369–387, https://doi.org/10.1016/S0012-821X(96)00180-X.
Keller, G., Adatte, T., Pardo, A., Bajpai, S., Khosla, A., and Samant, B., 2010, Cretaceous Extinctions: Evidence overlooked: Science, v. 328, p. 974–975, https://doi.org/10.1126/science.328.5981.974-a.
Kenney, G.G., Whitehouse, M.J., and Kamber, B.S., 2016, Differentiated impact melt sheets may be a potential source of Hadean detrital zircon: Geology, v. 44, p. 435–438, https://doi.org/10.1130/G37898.1.
Kent, D.V., Creamer, B.S., Lanci, L., Wang, D., Wright, J.D., and Van der Voo, R., 2003, A case for a comet impact trigger for the Paleocene/Eocene thermal maximum and carbon isotope excursion: Earth and Planetary Science Letters, v. 211, p. 13–26, https://doi.org/10.1016/S0012-821X(03)00188-2.
Kring, D.A., 2004, Environmental consequences of impact cratering events as a function of ambient conditions on Earth: Astrobiology, v. 3, p. 133–152, https://doi.org/10.1089/153110703321632471.
Kring, D.A., 2007, The Chicxulub impact event and its environmental consequences at the Cretaceous–Tertiary boundary: Palaeogeography, Palaeclimatology,

Palaeoecology, v. 255, p. 4–21, https://doi.org/10.1016/j.palaeo.2007.02.037.
Kring, D.A., and Durda, D.D., 2002, Trajectories and distribution of material ejected from the Chicxulub impact crater: Implications for post-impact wildfires: Journal of Geophysical Research, v. 107, p. 6-1–6-22, https://doi.org/10.1029/2001JE001532.
Kyte, F.T., Shukolyukov, A., Lugmair, G.W., Lowe, D.R., and Byerly, G.R., 2003, Early Archean spherule beds: Chromium isotopes confirm origin through multiple impacts of projectiles of carbonaceous chondrite type: Geology, v. 31, p. 283–286, https://doi.org/10.1130/0091-7613(2003)031<0283:EASBCI>2.0.CO;2.
Lainé, R., Alonso, D., and Svab, M., *editors*, 1985, The Carswell Structure Uranium Deposits, Saskatchewan: Geological Association of Canada, Special Paper 29, St. John's, NL, 230 p.
Lightfoot, P.C., Keays, R.R., Morrison, G.G., Bite, A., and Farrel, K.P., 1997, Geochemical relationships in the Sudbury Igneous Complex: Origin of the main mass and offset dikes: Economic Geology, v. 92, p. 289–307, https://doi.org/10.2113/gsecongeo.92.3.289.
Lowe, D.R., Byerly, G.R., and Kyte, F.T., 2014, Recently discovered 3.42–3.23 Ga impact layers, Barberton Belt, South Africa: 3.8 Ga detrital zircons, Archean impact history, and tectonic implications: Geology, v. 42, p. 747–750, https://doi.org/10.1130/G35743.1.
MacCracken, M.C., 2007, The climatic effects of asteroid and comet impacts: Consequences for an increasingly interconnected society, *in* Bobrowsky, P., and Rickman, H., *eds.*, Comet/Asteroid Impacts and Human Society: Springer, New York, p. 277–289, https://doi.org/10.1007/978-3-540-32711-0_16.
Marchi, S., Bottke, W.F., Elkins-Tanton, L.T., Bierhaus, M., Wuennemann, K., Morbidelli, A., and Kring, D.A., 2014, Widespread mixing and burial of Earth's Hadean crust by asteroid impacts: Nature, v. 511, p. 578–582, https://doi.org/10.1038/nature13539.
Masaitis, V.L., 1998, Popigai crater: Origin and distribution of diamond-bearing impactites: Meteoritics and Planetary Science, v. 33, p. 349–359, https://doi.org/10.1111/j.1945-5100.1998.tb01639.x.
McCarthy, T.S., Stanistreet, I.G., and Robb, L.J., 1990, Geological studies related to the origin of the Witwatersrand Basin and its mineralization: An introduction and a strategy for research and exploration: South African Journal of Geology, v. 93, p. 1–4.
Meier, D.L., Heinrich, C.A., and Watts, M.A., 2009, Mafic dikes displacing Witwatersrand gold reefs: Evidence against metamorphic-hydrothermal ore formation: Geology, v. 37, p. 607–610, https://doi.org/10.1130/G25657A.1.
Melosh, H.J., 1989, Impact Cratering: A Geologic Process: Oxford University Press, New York, 245 p.
Melosh, H.J., 2007, Physical effects of comet and asteroid impacts: Beyond the crater rim, *in* Bobrowsky, P., and Rickman, H., *eds.*, Comet/Asteroid Impacts and Human Society: Springer, New York, p. 211–224, https://doi.org/10.1007/978-3-540-32711-0_12.
Melosh, H.J., and Vickery, A.M., 1989, Impact erosion of the primordial atmosphere of Mars: Nature, v. 338, p. 487–489, https://doi.org/10.1038/338487a0.
Melosh, H.J., Schneider, N.M., Zahnle, K.J., and Latham, D., 1990, Ignition of global wildfires at the Cretaceous/Tertiary boundary: Nature, v. 343, p. 251–254, https://doi.org/10.1038/343251a0.
Molnár, F., Watkinson, D.H., and Jones, P.C., 2001, Multiple hydrothermal processes in footwall units of the North Range, Sudbury Igneous Complex, Canada, and implications for the genesis of vein-type Cu–Ni–PGE deposits: Economic Geology, v. 96, p. 1645–1670, https://doi.org/10.2113/gsecongeo.96.7.1645.
Morgan, J., Warner, M., and the Chicxulub Working Group, 1997, Size and morphology of the Chicxulub impact crater: Nature, v. 390, p. 472–476, https://doi.org/10.1038/37291.
Morgan, J.V., Warner, M.R., Collins, G.S., Grieve, R.A.F., Christeson, G.L., Gulick, S.P.S., and Barton, P.J., 2011, Full waveform tomographic images of the peak ring at the Chicxulub impact crater: Journal of Geophysical Research, v. 116, B06303, https://doi.org/10.1029/2010JB008015.
Morgan, J.V., Artemieva, N., and Goldin, T., 2013, Revisiting wildfires at the K–Pg boundary: Journal of Geophysical Research, v. 118, p. 1508–1520, https://doi.org/10.1002/2013JG002428.
Morgan, J.V., Gulick, S.P.S., Urrutia-Fucugauchi, J., Collins, G.S., Perz-Cruz, L., and Rebolledo-Vieyra, M., 2015, IODP-ICDP expedition 364: Drilling the K–Pg impact structure (Abstract): Lunar and Planetary Science Conference 46, #1747.
Morgan, J.V., and 38 others, 2016, The formation of peak rings in large impact craters: Science, v. 354, p. 878–882, https://doi.org/10.1126/science.aah6561.
Morgan, J.W., Walker, R.J., Horan, M.F., Beary, E.S., and Naldrett, A.J., 2002, ^{190}Pt–^{186}Os and ^{187}Re–^{187}Os systematics of the Sudbury Igneous Complex, Ontario: Geochimica et Cosmochimica Acta, v. 66, p. 273–290, https://doi.org/10.1016/S0016-7037(01)00768-2.
Naldrett, A.J., 2003, From impact to riches: Evolution of geological understanding as seen at Sudbury: GSA Today, v. 13, p. 4–9.
Neukum, G., and Ivanov, B.A., 1994, Crater size distributions and impact probabilities on Earth from lunar, terrestrial-planet and asteroidal cratering data, *in* Geherels, T., *ed.*, Hazards due to Comets and Asteroids: University of Arizona Press, Tucson, p. 359–416.
Officer, C.B., Hallam, A., Drake, C.L., and Devine, J.D., 1987, Late Cretaceous and paroxysmal Cretaceous/Tertiary extinctions: Nature, v. 326, p. 143–149, https://doi.org/10.1038/326143a0.
Osinski, G.R., and Kring, D.A., *editors*, 2015, Large Meteorite Impacts and Planetary Evolution V: Geological Society of America Special Papers, v. 518, 227 p., https://doi.org/10.1130/9780813725185.
Osinski, G.R., and Pierazzo, E., *editors*, 2012, Impact Cratering: Processes and Products: John Wiley & Sons, Ltd, Chichester, UK, 336 p., https://doi.org/10.1002/9781118447307.
Penfield, G.T., and Camargo, A.Z., 1981, Definition of a major igneous zone in the central Yucatan platform with aeromagnetic and gravity (Abstract): Society of Exploration Geophysists, 51st Annual International Meeting, Houston.
Pierazzo, E., Kring, D.A., and Melosh, H.J., 1998, Hydrocode simulation of the Chicxulub impact event and the production of climatically active gases: Journal of Geophysical Research, v. 103, p. 28607–28625, https://doi.org/10.1029/98JE02496.
Pope, K.O., 2002, Impact dust not the cause of the Cretaceous–Tertiary mass extinction: Geology, v. 30, p. 99–102, https://doi.org/10.1130/0091-7613(2002)030<0099:IDNTCO>2.0.CO;2.
Pope, K.O., Baines, K.H., Ocampo, A.C., and Ivanov, B.A., 1994, Impact winter and the Cretaceous/Tertiary extinctions: Results of a Chicxulub asteroid impact model: Earth and Planetary Science Letters, v. 128, p. 719–725, https://doi.org/10.1016/0012-821X(94)90186-4.
Pope, K.O., Baines, K.H., Ocampo, A.C., and Ivanov, B.A., 1997, Energy, volatile production, and climatic effects of the Chicxulub Cretaceous/Tertiarty impact: Journal of Geophysical Research, v. 102, p. 21645–21664, https://doi.org/10.1029/97JE01743.
Rasmussen, B., and Koeberl, C., 2004, Iridium anomalies and shocked quartz in a Late Archean spherule layer from Pilbara craton: New evidence for a major asteroid impact at 2.63 Ga: Geology, v. 32, p. 1029–1032, https://doi.org/10.1130/G20825.1.
Reimold, W.U., Köber, C., Fletcher P., Killick, A.M., and Wilson, J.D., 1999, Pseudotachylitic breccias from fault zones in the Witwatersrand Basin, South Africa: Evidence of autometasomatism and post-brecciation alteration processes: Mineralogy and Petrology, v. 66, p. 25–53, https://doi.org/10.1007/BF01161721.
Reimold, W.U., Koeberl, C., Gibson, R.L., and Dressler, B.O., 2005, Economic mineral deposits in impact structures: A review, *in* Koeberl, C., and Henkel, H., *eds.*, Impact Tectonics: Springer, Heidelberg, p. 479–552, https://doi.org/10.1007/3-540-27548-7_20.
Robb, L.J., and Robb, V.M., 1998, Gold in the Witwatersrand Basin, *in* Wilson, M.G.C., and Anhaeusser, C.R., *eds.*, The Mineral Resources of South Africa: Geoscience Council of South Africa, Handbook 16, Pretoria, p. 294–349.
Robertson, D.S., Lewis, W.M., Sheehan, P.M., and Toon, O.B., 2013, K–Pg extinction: Reevaluation of the heat-fire hypothesis: Journal of Geophysical Research, v. 118, p. 329–336, https://doi.org/10.1002/jgrg/20018.
Santiago-Acevedo, J., 1980, Giant fields of the southern zone-Mexico, *in* Halbouty, M.T., *ed.*, Giant Oil and Gas Fields of the Decade 1968–1978: American Association of Petroleum Geologists, Memoir 30, Tulsa, p. 339–385.
Sawatzky, H.B., 1977, Buried impact structures in the Williston Basin and adjacent area, *in* Roddy, D.J., Pepin, R.O., and Merrill, R.B., *eds.*, Impact and Explosion Cratering: Pergamon, New York, p. 461–480.
Schaller, M.F., Fung, M.K., Wright, J.D., Katz, M.E., and Kent, D.V., 2016, Impact ejecta at the Paleocene–Eocene boundary: Science, v. 354, p. 225–229, https://doi.org/10.1126/science.aaf5466.
Schulte, P., and 40 others, 2010, The Chicxulub asteroid impact and mass extinction at the Cretaceous–Paleogene boundary: Science, v. 327, p. 1214–1218, https://doi.org/10.1126/science.1177265.
Scott, R.G., and Spray, J.G., 2000, The South Range breccia belt of the Sudbury impact structure; a possible terrace collapse feature: Meteoritics and Planetary Science, v. 35, p. 505–520, https://doi.org/10.1111/j.1945-5100.2000.tb01432.x.
Sharpton, V.L., Marín, L.E., Carney, J.L., Lee, S., Ryder, G., Schuraytz, B.C., Sikora, P., and Spudis, P.D., 1996, A model of the Chicxulub impact basin based on evaluation of geophysical data, well logs, and drill core samples, *in* Ryder, G., Fastovsky, D.E., and Gartner, S., *eds.*, The Cretaceous–Tertiary Event and Other Catastrophes in Earth History: Geological Society of America Special Papers,

v. 307, p. 55–74, https://doi.org/10.1130/0-8137-2307-8.55.
Shuvalov, V.V., and Artemieva, N.A., 2002, Atmospheric erosion and radiation impulse induced by impacts, *in* Koeberl, C., and Macleod, K.G., *eds*., Catastrophic Events and Mass Extinctions: Impacts and Beyond: Geological Society of America Special Papers, v. 356, p. 695–703, https://doi.org/10.1130/0-8137-2356-6.695.
Simonson, B.M., and Glass, B.P., 2004, Spherule layers–records of ancient impacts: Annual Review of Earth and Planetary Science, v. 32, p. 329–361, https://doi.org/10.1146/annurev.earth.32.101802.120458.
Simonson, B.M., Sumner, D.Y., Beukes, N.J., Johnson, S., and Gutzmer, J., 2009, Correlating multiple Neoarchean–Paleoproterozoic impact spherule layers between South Africa and Western Australia: Precambrian Research, v. 169, p. 100–111, https://doi.org/10.1016/j.precamres.2008.10.016.
Smith, F.C., Glass, B.P., Simonson, B.M., Smith, J.P., Krull-Davatzes, A.E., and Booksh, K.S., 2016, Shock-metamorphosed rutile grains containing the high pressure polymorph TiO_2-II in four Neoarchean spherule layers: Geology, v. 44, p. 775–778, https://doi.org/10.1130/G38327.1.
Stöffler, D., Deutsch, A., Avermann, A., Bischoff, L., Brockmeyer, P., Buhl, D., Lakomv, R., and Müller-Mohr, V., 1994, The formation of the Sudbury Structure, Canada: Toward a unified impact model, *in* Dressler, B.O., Grieve, R.A.F., and Sharpton, V.L., *eds*., Large Meteorite Impacts and Planetary Evolution: Geological Society of America Special Papers, v. 293, p. 303–318, https://doi.org/10.1130/SPE293-p303.
Stöffler, D., Ryder, G., Ivanov, B.A., Artemieva, N.A., Cintala, M.J., and Grieve, R.A.F., 2006, Cratering history and lunar chronology: Reviews in Mineralogy and Geochemistry, v. 60, p. 519–596, https://doi.org/10.2138/rmg.2006.60.05.
Therriault, A.M., Grieve, R.A.F., and Reimold, W.U., 1997, Original size of the Vredefort structure: Implications for the geological evolution of the Witwatersrand Basin: Meteoritics and Planetary Science, v. 32, p. 71–77, https://doi.org/10.1111/j.1945-5100.1997.tb01242.x.
Therriault, A.M., Fowler, A.D., and Grieve, R.A.F., 2002, The Sudbury Igneous Complex: A differentiated impact melt sheet: Economic Geology, v. 97, p. 1521–1540, https://doi.org/10.2113/gsecongeo.97.7.1521.
Thomas, P.J., Hicks, R.D., Chyba, C.F., and McKay, C.P., *editors*, 1997, Comets and the Origin Evolution of Life: Springer, Berlin, 357 p., https://doi.org/10.1007/10903490.
Toon, O.B., Zahnle, K., Morrison, D., Turco, R.P., and Covey, C., 1997, Environmental perturbations caused by the impact of asteroids and comets: Reviews of Geophysics, v. 35, p. 41–78, https://doi.org/10.1029/96RG03038.
Tuchscherer, M.G., and Spray, J.G., 2002, Geology, mineralization and emplacement of the Foy offset dike, Sudbury impact structure: Economic Geology, v. 97, p. 1377–1398, https://doi.org/10.2113/gsecongeo.97.7.1377.
Tucker, R.T., Viljoen, R.P., and Viljoen, M.J., 2016, A review of the Witwatersrand Basin–the world's greatest goldfield: Episodes, v. 39, p. 105–133, https://doi.org/10.18814/epiiugs/2016/v39i2/95771.
Vellekoop, J., Esmeray-Senlet, S., Miller, K.G., Browning, J.V., Sluijs, A., van de Schootbrugge, B., Sinninghe Damsté, J.S., and Brinkhuis, H., 2016, Evidence for Cretaceous–Paleogene boundary bolide "impact winter" conditions from New Jersey, USA: Geology, v. 44, p. 619–622, https://doi.org/10.1130/G37961.1.
Vonhof, H.B., Smit, J., Brinkhuis, H., Montanari, A., and Nederbragt, A.J., 2000, Global cooling accelerated by early late Eocene impacts?: Geology, v. 28, p. 687–690, https://doi.org/10.1130/0091-7613(2000)28<687:GCABEL>2.0.CO;2.
Walkden, G., Parker, J., and Kelley, S., 2002, A late Triassic impact ejecta layer in southwestern Britain: Science, v. 298, p. 2185–2188, https://doi.org/10.1126/science.1076249.
Walker, R.J., Morgan, J.W., Naldrett, A.J., Li, C., and Fassett, J.D., 1991, Re–Os isotope systematics of Ni–Cu sulphide ores, Sudbury Igneous Complex, Ontario: Evidence for a major crustal component: Earth and Planetary Science Letters, v. 105, p. 416–429, https://doi.org/10.1016/0012-821X(91)90182-H.
Ward, P.L., 2009, Sulfur dioxide initiates global climate change in four ways: Thin Solid Films, v. 517, p. 3188–3203, https://doi.org/10.1016/j.tsf.2009.01.005.
Warner, S., Martin, R.F., Abdel-Raham, A.F.M., and Doig, R., 1998, Apatite as a monitor of fractionation, degassing and metamorphism in the Sudbury Igneous Complex, Ontario: Canadian Mineralogist, v. 36, p. 981–999.
Watson, E.B., and Harrison, T.M., 2005, Zircon thermometer reveals minimum melting conditions on earliest Earth: Science, v. 308, p. 841–844, https://doi.org/10.1126/science.1110873.
Wiechert, U., Halliday, A.N., Lee, D.-C., Snyder, G.A., Taylor, L.A., and Rumble, D., 2001, Oxygen isotopes and the moon-forming giant impact: Science, v. 294, p. 345–348, https://doi.org/10.1126/science.1063037.
Wielicki, M.M., Harrison, T.M., and Schmitt, A.K., 2012, Geochemical signature and magmatic stability of terrestrial impact produced zircons: Earth and Planetary Science Letters, v. 321–322, p. 20–31, https://doi.org/10.1016/j.epsl.2012.01.009.
Woolbach, W.S., Gilmour, I., and Anders, E., 1990, Major wildfires at the Cretaceous/Tertiary boundary, *in* Sharpton, V.L., and Ward, P.D., *eds*., Global Catastrophes in Earth History: An Interdisciplinary Conference on Impacts, Volcanism, and Mass Mortality: Geological Society of America Special Papers, v. 247, p. 391–400, https://doi.org/10.1130/SPE247-p391.
Zahnle, K.J., and Sleep, N.H., 1997, Impacts and the early evolution of life, *in* Thomas, P.J., Chyba, C.F., and McKay, C.P., *eds*., Comets and the Origin of Life: Springer-Verlag, New York, p. 175–208, https://doi.org/10.1007/978-1-4757-2688-6_8.
Zhang, J., Dauphas, N., Davis, A.M., Leya, I., and Fedkin, A., 2012, The proto-Earth as a significant source of lunar material: Nature Geoscience, v. 5, p. 251–255, https://doi.org/10.1038/ngeo1429.
Zhao, B., Robb, L.J., Harris, C., and Jordaan, L.J., 2006, Origin of hydrothermal fluids and gold mineralization associated with the Ventersdorp Contact Reef, Witwatersrand Basin, South Africa: Constraints from S, O, and H isotopes, *in* Reimold, W.U., and Gibson, R.L., *eds*., Processes on the Early Earth: Geological Society of America Special Papers, v. 405, p. 333–352, https://doi.org/10.1130/2006.2405(17).

Received November 2016
Accepted as revised January 2017
First published on the web February 2017

ARTICLE

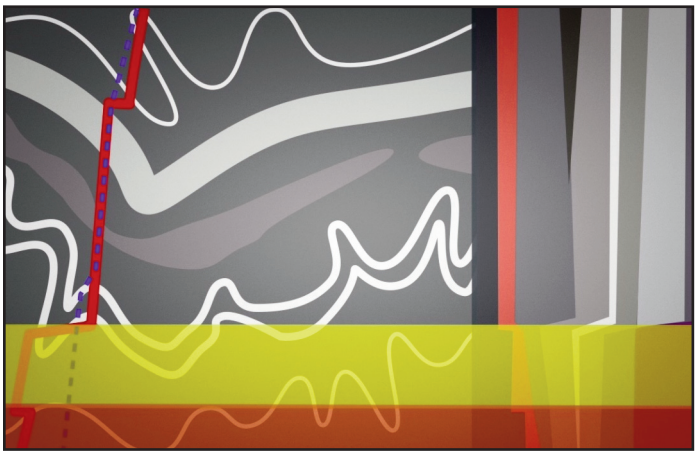

Applying Phase Equilibria Modelling to Metamorphic and Geological Processes: Recent Developments and Future Potential

Chris Yakymchuk

Department of Earth and Environmental Sciences
University of Waterloo, 200 University Ave West
Waterloo, Ontario, N2L 3G1, Canada
Email: cyakymchuk@uwaterloo.ca

SUMMARY

Phase equilibria modelling has played a key role in enhancing our understanding of metamorphic processes. An important breakthrough in the last three decades has been the ability to construct phase diagrams by integrating internally consistent datasets of the thermodynamic properties of minerals, fluids and melts with activity–composition models for mixed phases that calculate end-member activities from end-member proportions. A major advance in applying phase equilibria modelling to natural rocks is using isochemical phase diagrams to explore the phase assemblages and reaction sequences applicable for a particular sample. The chemical systems used for modelling phase equilibria are continually evolving to provide closer approximations to the natural compositions of rocks and allow wider varieties of compositions to be modelled. Phase diagrams are now routinely applied to metasedimentary rocks, metabasites and intermediate to felsic intrusive rocks and more recently to ultramafic rocks and meteorites.

While the principal application of these phase diagrams is quantifying the pressure and temperature evolution of metamorphic rocks, workers are now applying them to other fields across the geosciences. For example, phase equilibria modelling of hydrothermal alteration and the metamorphism of hydrothermally altered rocks can be used to determine 'alteration vectors' to hydrothermal mineral deposits. Combining the results of phase equilibria of rock-forming minerals with solubility equations of accessory minerals has provided new insights into the geological significance of U–Pb ages of accessory minerals commonly used in geochronology (e.g. zircon and monazite). Rheological models based on the results of phase equilibria modelling can be used to evaluate how the strength of the crust and mantle can change through metamorphic and metasomatic processes, which has implications for a range orogenic processes, including the localization of earthquakes. Finally, phase equilibria modelling of fluid generation and consumption during metamorphism can be used to explore links between metamorphism and global geochemical cycles of carbon and sulphur, which may provide new insights into the secular change of the lithosphere, hydrosphere and atmosphere.

RÉSUMÉ

La modélisation des équilibres de phases a joué un rôle clé dans l'amélioration de notre compréhension des processus métamorphiques. Une percée importante au cours des trois dernières décennies a été la capacité de construire des diagrammes de phase en y intégrant des ensembles de données cohérentes des propriétés thermodynamiques des minéraux, des fluides et des bains magmatiques avec des modèles d'activité-composition pour des phases mixtes qui déduisent l'activité des membres extrêmes à partir des proportions des membres extrêmes. Une avancée majeure dans l'application de la modélisation d'équilibre de phase aux roches naturelles consiste à utiliser des diagrammes de phases isochimiques pour étudier les assemblages de phase et les séquences de réaction applicables pour un échantillon particulier. Les systèmes chimiques utilisés pour la modélisation des équilibres de phase évoluent continuellement pour fournir des approximations plus proches des compositions naturelles des roches et permettent de modéliser de plus grandes variétés de compositions. Les diagrammes de phase sont maintenant appliqués de façon routinière aux roches métasédimentaires, aux métabasites et aux roches intrusives intermédiaires à felsiques et plus récemment aux roches ultramafiques et aux météorites.

Geoscience Canada, v. 44, https://doi.org/10.12789/geocanj.2017.44.114 pages 27–45

Bien que l'application principale de ces diagrammes de phase consiste à quantifier l'évolution de la pression et de la température des roches métamorphiques, les utilisateurs les appliquent maintenant à d'autres spécialités des géosciences. Par exemple, la modélisation des équilibres de phase de l'altération hydrothermale et du métamorphisme des roches d'altération hydrothermale peut être utilisée pour déterminer les « vecteurs d'altération » des gisements minéraux hydrothermaux. La combinaison des résultats des équilibres de phase des minéraux constitutifs des roches avec des équations de solubilité des minéraux accessoires a permis d'en savoir davantage sur la signification géologique des âges U–Pb des minéraux accessoires couramment utilisés en géochronologie (par exemple zircon et monazite). Les modèles rhéologiques basés sur les résultats de la modélisation des équilibres de phase peuvent être utilisés pour évaluer comment la résistance de la croûte et du manteau peut changer à travers des processus métamorphiques et métasomatiques, ce qui a des implications sur une gamme de processus orogéniques, y compris la localisation des séismes. Enfin, la modélisation des équilibres de phase de la génération et de l'absorption des fluides pendant le métamorphisme peut être utilisée pour explorer les liens entre le métamorphisme et les cycles géochimiques globaux du carbone et du soufre, ce qui peut fournir de nouvelles perspectives sur le changement séculaire de la lithosphère, de l'hydrosphère et de l'atmosphère.

Traduit par le Traducteur

INTRODUCTION

Phase diagrams are graphical representations of the phases that coexist in a system as a function of different thermodynamic variables. In metamorphic geology, phase diagrams are commonly used to evaluate the absolute pressures (*P*) and temperatures (*T*) experienced by metamorphic rocks from which their geodynamic settings can be inferred (e.g. England and Thompson 1984; Spear 1995; Brown 2007, 2014). These diagrams are also combined with the results of accessory or major mineral geochronology to elucidate the *P*–*T*–*time(t)* paths experienced by metamorphic rocks (e.g. petrochronology; Mottram et al. 2014; Ambrose et al. 2015; Stevens et al. 2015; Dragovic et al. 2016). However, metamorphic phase diagrams have much broader applications across the geosciences.

Here, I review some recent applications of phase equilibria modelling of metamorphic rocks and processes and discuss some of the broader implications of these studies. First, I review some basics of phase equilibria modelling and phase diagrams. Second, I present some of the recent applications of phase equilibria modelling to different fields of the geosciences, including tectonics, earthquakes, linking deep mantle petrology with the observations from geophysics, mineral deposits and hydrothermal alteration, the behaviour of accessory minerals, metamorphism of meteorites, and linking fluid production in metamorphic rocks to global geochemical cycles. Finally, I discuss some of the assumptions and limitations of applying the equilibrium approach to understanding metamorphic processes. A review by Spear et al. (2016) provides an excellent summary of additional advances in metamorphic geology over the last 50 years and discusses some outstanding questions to be addressed in this evolving field of research.

PHASE DIAGRAMS

Phase Equilibria Modelling

Phase equilibria modelling can be used to predict the stable metamorphic phase assemblage in a rock for a set of thermodynamic variables (usually variations in *P* and *T*). Note that I prefer the term *phase assemblage* to *mineral assemblage* because most metamorphic assemblages develop with a fluid and/or melt *phase* in equilibrium with the mineral assemblage and this needs to be considered in phase equilibria modelling. Constructing phase diagrams that display equilibrium phase assemblages requires an understanding of the phase rule and of equilibrium thermodynamics (e.g. Powell 1978; Spear 1995) that is beyond the scope of this contribution. There are several resources that provide good introductions to the fundamentals of phase equilibria including short-course notes by R. Powell (1991) on the THERMOCALC website (http://www.metamorph.geo.uni-mainz.de/thermocalc/) and the textbooks by Spear (1995) and Vernon and Clarke (2008). Here, I provide a general overview of the common types of phase diagrams, discuss some recent examples, and explore how the results of phase equilibria modelling can be linked to various geological processes. Throughout, I assume that the modelled system has achieved equilibrium, meaning that the proportions and compositions of all phases in a system (e.g. rock) at a given set of conditions (usually *P* and *T*) reflect the minimum free energy configuration. This is a main principle of phase equilibria modelling. The limitations of applying this approach to natural systems are discussed later.

Phase diagrams are graphical representations of the equilibrium phase assemblages in a system as a function of intensive and/or extensive variables (e.g. Powell et al. 2005). *Intensive* variables are independent of the amount of material in a system, and are identical in all parts of an equilibrated system. Examples of these are temperature, pressure and chemical potential that are equalized in metamorphic systems through conduction, deformation and diffusion, respectively. *Extensive* variables depend on the number of moles of the components in the system (e.g. volume, entropy, composition).

The majority of metamorphic phase diagrams use intensive variables as axes (mostly *P* and *T*) because these are the most useful diagrams for linking metamorphic phase assemblages to tectonic processes and to tectonic models of orogenesis. Such tectonic models can predict the pressure–temperature (*P*–*T*) paths of different tectonic processes and against which constraints from phase equilibria modelling and geochronology can be evaluated (e.g. England and Thompson 1984; Thompson and England 1984; Jamieson et al. 1996, 1998, 2004, 2010). Phase diagrams with *extensive* variables as axes are less common but are particularly useful for investigating metamorphic processes, such as evaluating volume changes in metamorphic

systems (e.g. Powell et al. 2005; Guiraud and Powell 2006) and modelling the redox budget of metamorphic rocks (e.g. Evans et al. 2013).

Petrogenetic Grids

Metamorphic phase diagrams have evolved in complexity since their conception in the early half of the 20th century. Bowen (1940) was one of the first researchers to *project* a series of univariant equilibrium curves onto a *P–T* plane to evaluate the metamorphic reactions that can occur over a range of pressures and temperatures. The projection of all of these univariant curves onto a common surface results in a network of lines (and points) that define a *petrogenetic grid* for the modelled chemical system. The topology of these diagrams can be constrained using the method of Schreinemakers (e.g. Zen 1966).

Bowen (1940) modelled the metamorphic reactions of siliceous limestone and dolostone in the relatively simple $CaO–MgO–SiO_2–CO_2$ chemical system. Over the latter part of the 20th century, phase diagrams in larger chemical systems were developed and applied to a wider variety of rock types. Petrogenetic grids were constructed and refined using a combination of experimental studies of metamorphic reactions (e.g. Carrington and Harley 1995) and natural equilibrated phase assemblages (e.g. Pattison and Harte 1985). Grids applicable to metapelitic rocks were constructed in the $K_2O–FeO–MgO–Al_2O_3–SiO_2–H_2O$ (KFMASH) system (e.g. Albee 1965). Following on from this work the chemical systems of petrogenetic grids continued to expand to become closer approximations of the true chemical composition of metamorphic rocks. The KFMASH system was expanded to include Na_2O (Thompson and Algor 1977) and later CaO (Thompson and Tracy 1979), which were critical for modelling the anatexis of pelitic rocks.

Other important components were later included in petrogenetic grids, such as manganese, which is of particular importance for garnet-bearing univariant equilibria (e.g. Spear and Cheney 1989; Symmes and Ferry 1992; Tinkham and Ghent 2005; White et al. 2005), and ferric iron and titanium, which allowed Fe-Ti oxides to be considered (e.g. White et al. 2007; White et al. 2014a). A wide variety of petrogenetic grids is now available to investigate rocks from low to high grade (e.g. White et al. 2014a; Kelsey and Hand 2015) and for a range of compositions (e.g. Will et al. 1990; Frey et al. 1991; Riesco et al. 2004; White et al. 2007; Groppo et al. 2013). A recent example of a petrogenetic grid constructed in the KFMASHTO system applicable for suprasolidus rocks is shown in Figure 1a. Univariant reactions are displayed as lines that connect at invariant points. All phase abbreviations in this figure and the remainder of this contribution are summarized in Table 1.

While petrogenetic grids provide an essential framework in which to understand the reactions that take place in metamorphic systems, there are two main limitations when applying them to natural rocks. The first is that petrogenetic grids are a projection of all possible univariant reactions in a specified chemical system onto a *P–T* plane. A specific rock will only 'see' a subset of the total number of univariant reactions; the specific reactions that are encountered depend on the particular bulk composition of the rock. While this can be accounted for by using complementary chemographic diagrams in simple chemical systems (e.g. KFMASH; Thompson 1957), this approach does not easily lend itself to the larger chemical systems (e.g. MnNCKFMASHTO) where higher-dimensional chemographic diagrams would be required. The second limitation is that phase assemblages in metamorphic rocks generally change through continuous or multivariant reactions rather than univariant (discontinuous) reactions (e.g. Stüwe and Powell 1995). These multivariant reactions are not displayed on petrogenetic grids. Furthermore, univariant reaction curves on petrogenetic grids may yield the false impression that phase assemblages change over narrow intervals in *P–T* space. In reality, phase proportions (also known as *modes*) and compositions continuously change along a *P–T* evolution due to the operation of multivariant reactions.

Table 1. Phase abbreviations used in the text and figures (from Holland and Powell 2011).

ab	albite	g	garnet	po	pyrrhotite
atg	antigorite	H_2O	water	pyr	pyrite
bi	biotite	ilm	ilmenite	q	quartz
br	brucite	ksp	K-feldspar	ru	rutile
cc	calcite	ky	kyanite	spr	sapphirine
cd	cordierite	liq	liquid	sid	siderite
chl	chlorite	mt	magnetite	sill	sillimanite
cm	chromite	mu	muscovite	sp	spinel
cpx	clinopyroxene	ol	olivine		
dol	dolomite	opx	orthopyroxene		
ep	epidote	pl	plagioclase		

Isochemical Phase Diagrams

One of the most significant advances in metamorphic geology in the last 30 years has been the development of isochemical phase diagrams that are applicable to fixed bulk rock compositions (e.g. individual rock samples). The concept goes back to Hensen (1971) who constructed schematic *P–T* phase diagrams for particular bulk rock compositions in the $MgO–FeO–Al_2O_3–SiO_2$ chemical system. R. Powell and colleagues popularized this approach by developing the THERMOCALC software package that solves a set of independent non-linear equations to determine the stable phase assemblages (which may include minerals, fluids and/or melts) as well as their compositions and modes across a *P–T* diagram for a fixed bulk composition (Powell et al. 1998). THERMOCALC calculates individual phase boundaries (and invariant points), which are then combined manually into complete phase diagrams. As computational power increased, automated software packages were developed to generate similar diagrams, but using Gibbs free energy minimization as the numerical method to determine the equilibrium phase assemblage (e.g. Connolly and Petrini 2002; de Capitani and Petrakakis 2010).

Phase diagrams constructed for a fixed bulk composition are called isochemical phase diagrams and have also been called *pseudosections* in the metamorphic literature. Pseudosections are not true sections because the compositions of phases

https://doi.org/10.12789/geocanj.2017.44.114

in the system may lie off the plane of the section (Powell 1991). Although *pseudosection* also applies to non-isochemical phase diagrams, the term has largely become synonymous with isochemical phase diagrams. The same term is also used in geophysics to display 2-dimensional multi-electrode resistivity data (e.g. Everett 2013). To avoid confusion, I will not use this term from this point forward.

Isochemical phase diagrams consist of a series of geometric domains (e.g. panels) that are bounded by lines (Fig. 1b). Each domain represents a stable phase assemblage and these domains are commonly shaded (mainly for convenience) so that darker shades indicate relatively high-variance assemblages and lighter shades represent low-variance assemblages. Each domain is generally labelled with the stable phase assemblage.

In contrast to the lines representing reactions in a petrogenetic grid, the lines on an isochemical phase diagram represent the *P*–*T* conditions where the mode of a mineral, fluid or melt goes to zero. Isochemical phase diagrams can be more powerful than petrogenetic grids because they can be contoured for phase proportions and compositions that can be used to quantify the *P*–*T* conditions and the reaction sequence of a particular rock during prograde and retrograde metamorphism. These contours are commonly referred to as *isopleths* in the metamorphic community. This information can be combined with petrographic observations and the results of electron probe microanalysis of mineral compositions to constrain a *P*–*T* path.

The two most important factors in constructing an isochemical phase diagram for a rock is choosing an appropriate chemical system and using a representative bulk composition for the assumed volume of equilibration. The modelled chemical system is a necessary simplification of the more complex natural system, but it should include the key components that make up the phases of interest in a sample. For example, the KFMASH system is appropriate for modelling many metapelitic rocks but the calculated equilibria would not include plagioclase. This system also does not consider manganese, which can significantly extend the stability of garnet to lower temperatures (e.g. Symmes and Ferry 1992; Mahar et al. 1997; Tinkham et al. 2003; White et al. 2014b). In general, it is good practice to model in the largest chemical system possible, which represents the closest approximation to the natural rock composition.

Bulk composition can be determined in several ways: (1) crushed and milled rock samples can be analyzed using X-ray fluorescence or other bulk analytical techniques, (2) major element mapping of thin sections using μXRF or scanning electron microscopy (e.g. Indares et al. 2008), and (3) combining point counting or automated mineral mode analysis (e.g. QEMSCAN and MIL) with mineral compositions obtained by electron microprobe analysis (e.g. Carson et al. 2000; Lasalle and Indares 2014). Each of these methods has advantages and disadvantages, but the result should be a bulk composition that approximates the equilibration volume of the rock. Additional factors that need to be considered in some cases are the concentration of CO_2 and H_2S in the fluid phase (Tomkins and Evans 2015), the amount of H_2O in the bulk composition (e.g. White et al. 2007), as well as the oxidation state of the system (e.g. Boger et al. 2012; Evans et al. 2013).

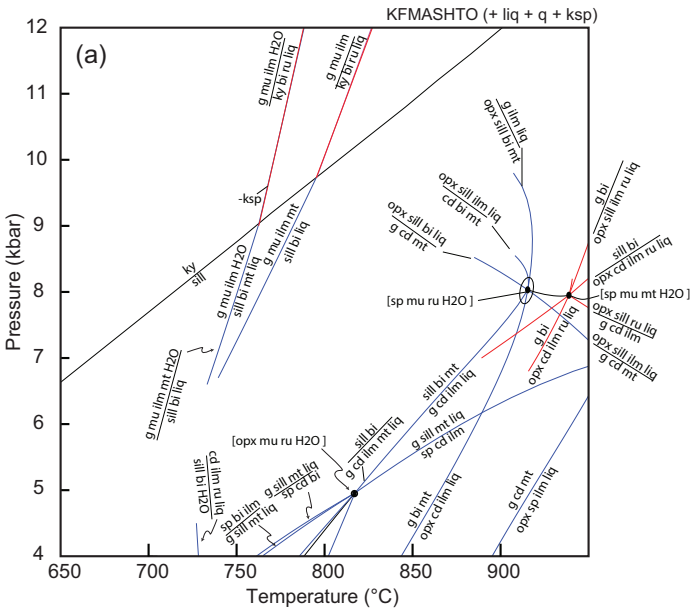

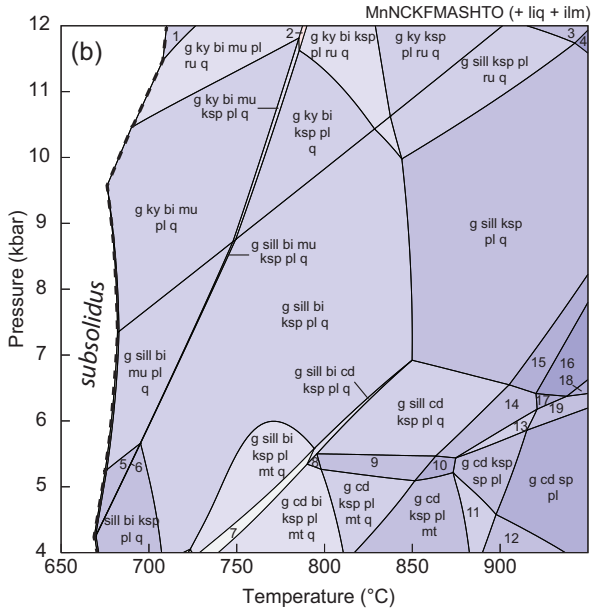

1: g bi mu pl ru q
2: g ky bi mu ksp pl ru q
3: g sill ksp ru q
4: g sill ksp q
5: sill bi mu pl q
6: sill ksp bi mu pl q
7: g sill cd bi ksp pl mt q
8: g cd bi ksp pl q
9: g cd ksp pl q
10: g cd ksp pl
11: g cd ksp sp pl mt
12: g cd sp pl mt
13: g sill cd ksp sp pl
14: g sill cd ksp pl
15: g sill ksp pl
16: g sill pl
17: g sill cd pl
18: g sill sp pl
19: g sill cd sp pl

Figure 1. (a) Petrogenetic grid of selected suprasolidus univariant reactions for metapelitic rocks in the K_2O–FeO–MgO–Al_2O_3–SiO_2–H_2O–TiO_2–O system (modified from White et al. 2014a). Blue lines are for reactions that include magnetite and red lines are for reactions that include rutile. Note that some labels are omitted for clarity. (b) Isochemical *P*–*T* phase diagram for the average amphibolite-facies metapelite composition of Ague (1991) and modified from Yakymchuk et al. (2017). Each field contains the equilibrium phase assemblage and each line is where the proportion of one phase goes to zero. Fields are shaded so that light shades are low-variance assemblages and dark shades represent high-variance assemblages. Silicate melt (liq) and ilmenite (ilm) are present in each field of the diagram.

Once a bulk composition is determined, there are two main computational approaches to constructing isochemical phase

diagrams. Both approaches require an internally consistent thermodynamic database (e.g. Helgeson et al. 1978; Berman 1988; Holland and Powell 1998, 2011) and activity–composition models that relate end-member proportions to end-member activities for the solid-solution minerals as well as for complex fluid and melt phases (e.g. Evans et al. 2010; White et al. 2014a; Green et al. 2016).

The first computational approach is to use Gibbs free energy minimization to determine the stable phase assemblages at a given *P–T* condition. Two common software packages available for this approach are Perple_X (Connolly and Petrini 2002; http://www.perplex.ethz.ch) and THERIAK–DOMINO (de Capitani and Brown 1987; de Capitani and Petrakakis 2010; http://titan.minpet.unibas.ch/minpet/theriak/theruser.html). They are user-friendly and can automatically calculate most phase diagrams relatively quickly (generally minutes to hours). The output is a complete phase diagram and associated files with other calculation information. An additional benefit of Gibbs free energy minimization programs is the ability to easily explore thermodynamic data and activity–composition models of end-member activities.

A second approach is to determine the solution of simultaneous non-linear equations to build up an array of points and lines that make up a metamorphic phase diagram (THERMOCALC: Powell and Holland 1988, 2008; Powell et al. 1998). This is a more time-consuming approach, but workers acquire a deeper understanding of how phase diagrams are developed.

Compositional Phase Diagrams

The most common type of phase diagrams in metamorphic studies is isochemical *P–T* phase diagrams. Another class of phase diagrams is used to evaluate changes in the chemical composition of the system. In these diagrams, one or more axes represent compositional variables that can be intensive (e.g. molar ratios) or extensive (e.g. weight % or mol. % of a component). Compositional phase diagrams include *Pressure–Composition* (*P–X*), *Temperature–Composition* (*T–X*), and *Composition–Composition* diagrams (*X–X*). Figure 2 shows examples of each of these. Note that the same topological features described above for isochemical phase diagrams also apply to the compositional phase diagrams.

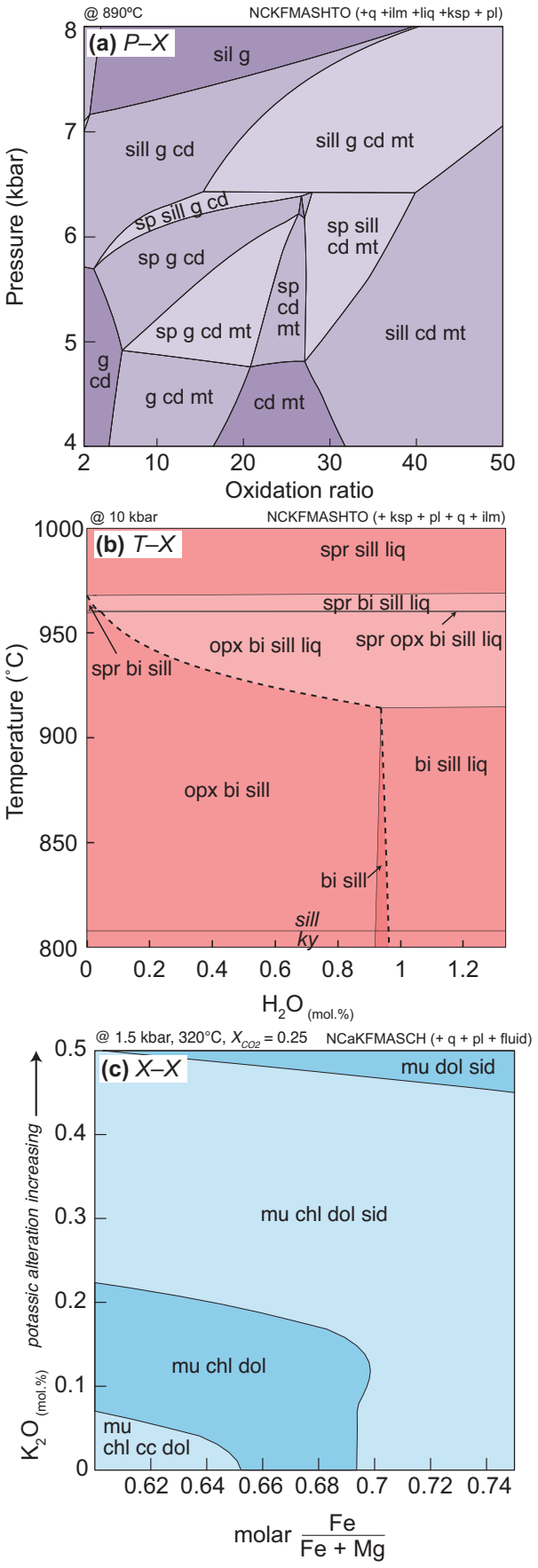

Figure 2. *(opposite)* Selection of phase diagrams calculated where one or more axes are compositional variables. (a) *Pressure–Composition* calculated at 890°C showing the sensitivity of phase assemblages in pelite to the oxidation ratio, which is defined as molar ([2 x Fe_2O_3 x 100] / [2Fe_2O_3 + FeO]). The vertical axis on the left-hand side of the diagram is for metapelite with ~1% of iron in the ferric state and the right-hand side is the same metapelite but with roughly ~33% of the iron in the ferric state. Note that the oxidation ratio affects the stability of oxides (e.g. magnetite) and silicate minerals (e.g. garnet and sillimanite). Modified from Boger et al. (2012). (b) *Temperature–Composition* phase diagram calculated at 10 kbar for sapphirine–quartz granulite (modified from Korhonen et al. 2012). The horizontal axis is the amount of H_2O in the modelled bulk composition ranging from 0 mol.% (left side) to 1.34 mol.% (right side). The solidus (dashed line) is sensitive to the amount of H_2O. (c) *Composition–Composition* diagram calculated at 1.5 kbar and 320°C for greenschist-facies metabasite (with a constant fluid composition of X_{CO2} = 0.25) from an orogenic gold deposit illustrating the sensitivity of carbonate minerals to the bulk composition of K_2O on the vertical axis and the relative amount of Fe to Mg on the horizontal axis (modified from White et al. 2003).

https://doi.org/10.12789/geocanj.2017.44.114

The *P–X* diagram in Figure 2a is from Boger et al. (2012) and has *P* on the vertical axis (similar to most *P–T* phase diagrams) and the horizontal axis relates to the ratio of ferric to ferrous iron in the bulk composition, which is a proxy for the oxidation state of the system. Here the diagram illustrates that the stability of oxide (e.g. magnetite) and silicate minerals (e.g. garnet and sillimanite) is sensitive to changes in the oxidation state of the system. For example, garnet is stable and magnetite is unstable over the modelled pressure range for relatively reducing systems (left side of diagram), whereas on the right side of the diagram the opposite is true.

A *T–X* diagram from Korhonen et al. (2012) in Figure 2b illustrates the sensitivity of the solidus temperature in a metasedimentary rock to changes in bulk rock water content. The solidus is at higher temperatures for drier bulk compositions (left side of the diagram). A prediction of this phase diagram is that melting can initiate due to an increase in the proportion of water in the system at a constant temperature. For example, the addition of ~1 mol.% (~0.4 wt.%) of H_2O to a completely dry rock at 900°C will cause it to melt at < 800°C.

While not common, *X–X* diagrams are particularly useful in studies of hydrothermal alteration and metasomatism (e.g. White et al. 2003; Riesco et al. 2005). An example from White et al. (2003) is shown in Figure 2c. This diagram was calculated at 1.5 kbar at 320°C with a constant fluid composition of X_{CO2} = 0.25 (molar CO_2 / [H_2O + CO_2]). Here the vertical axis represents the molar proportion of K_2O in the bulk composition. Higher values approximate the degree of potassic alteration. The horizontal axis extends along a range of mafic protolith compositions with variable X_{Fe} (molar Fe/[Fe+Mg]). Note that in some cases an equivalent amount of potassic alteration will produce the same alteration minerals (e.g. mu+chl+dol+sid at K_2O = 0.3) across the range of protolith compositions. In other scenarios, potassic alteration will produce different alteration minerals for protoliths with variable X_{Fe} values. For example, at a K_2O value of 0.2, siderite is stable in the high X_{Fe} compositions but is absent in compositions with X_{Fe} < 0.64.

Volumetric Phase Diagrams

One of the assumptions when constructing isochemical *P–T* phase diagrams is that changes in pressure are accommodated by changes in volume (e.g. via deformation of the rock). Likewise, we generally assume that heat flow accommodates changes in *T*. The effects of volume change are particularly important in studies of migmatites (e.g. Powell et al. 2005) and ultra-high pressure mineral assemblages (e.g. Guiraud and Powell 2006), as well as in studies of the serpentinization of ultramafic rocks (Kelemen and Hirth 2012).

For a *P–T* isochemical phase diagram to be an effective model of a natural system, we assume that the rock deforms relatively quickly to maintain a constant pressure. Melt is a relatively high-volume phase relative to most silicate minerals and the production of melt can potentially induce large volume changes in a rock. For some rock types, such as metabasite and some greywackes, melt is predicted to be produced more or less continuously along a prograde *P–T* path (e.g. Johnson et al. 2008; Yakymchuk and Brown 2014a; Palin et al. 2016b). However, rocks such as metapelite also contain narrow low-variance fields. In these fields, melt is generated over relatively small temperature intervals, which potentially represents a more pulsed nature of melt generation. In these cases, a relatively small increase in temperature is predicted to generate a large quantity of melt resulting in a correspondingly large volume increase.

Some of these aspects were explored by Powell et al. (2005) for a model aluminous metapelite composition. An isochemical *P–T* phase diagram for this composition is shown in Figure 3a and it is contoured for molar volume. A complementary *Volume–Temperature* diagram from Powell et al. (2005) is shown in Figure 3b. Note that the volume is presented as molar volume. The diagram is contoured for isobars (lines of constant pressure) to illustrate the changes in volume that occur at different pressures during isobaric heating. Consider an isobaric heating path at 5 kbar. There are two nearly vertical segments (one at ~680°C and one at ~725°C) that relate to the relatively low-variance fields that represent muscovite and biotite breakdown. As the isobaric path crosses these fields there is a large volume change due to melt generation. If this relatively rapid volume increase cannot be accommodated by local deformation in the rock's environment, then the rock will respond to the increase in melt volume and concomitant pressure increase by fracturing or otherwise deforming to allow the melt to escape, thereby re-establishing the ambient lithostatic pressure. If melt is lost, the composition of the residue will change and the isochemical phase diagrams calculated for the protolith composition (Fig. 3a, b) are no longer valid. Some techniques for accounting for melt loss are discussed later.

SOME RECENT APPLICATIONS OF PHASE EQUILIBRIA MODELLING

P–T Determinations in Metamorphic Rocks

One of the principal applications of isochemical phase diagrams is linking the observed phase assemblages, reaction sequences and phase modes and compositions to the *P–T* conditions of metamorphism. Figure 4 is an example of an isochemical *P–T* phase diagram from Pearce et al. (2015a) for a greywacke composition that is contoured for the X_{Fe} (molar Fe/[Fe+Mg]) of chlorite. For the example in Figure 4, note that the X_{Fe} isopleths for chlorite are generally steeply dipping. This indicates that this parameter is mostly sensitive to changes in temperature. For the modelled rock, a peak assemblage of epidote–chlorite–albite (plus the other phases that are stable across the diagram) and a chlorite X_{Fe} value of 0.60 would constrain the *P–T* conditions to *P* > 6 kbar at ~350°C. Isopleths for other parameters can also be used to refine these *P–T* estimates.

While mineral composition isopleths are useful for low-temperature metamorphic rocks, their use at high temperatures is complicated by retrograde exchange reactions during cooling that change the compositions of the minerals from what they were at peak conditions (e.g. Indares and Martignole 1985; Spear and Florence 1992; Pattison and Bégin 1994; Kohn and Spear 2000; Pattison et al. 2003). For these rocks, a better

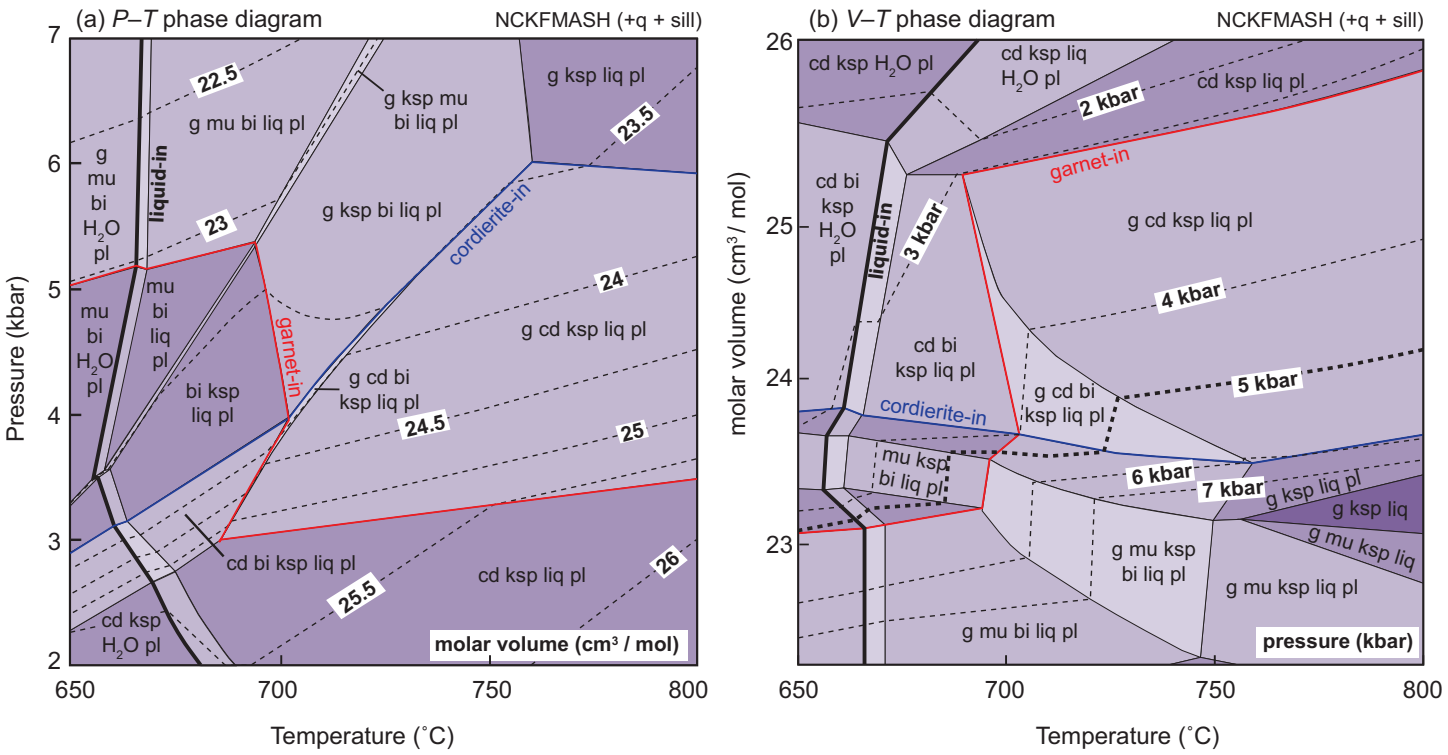

Figure 3. (a) Isochemical *P–T* phase diagram for a metapelite composition (modified from Powell et al. 2005). Contours are the molar volume of the system. (b) Isochemical *Temperature–Volume* phase diagram contoured for pressure (modified from Powell et al. 2005) for a metapelite composition. For all isobaric paths except 2 kbar, molar volume increases with temperature. In general, it is assumed that the increase in volume is accommodated by deformation in the rock (e.g. fracturing) to maintain a constant pressure. For the 5 kbar isobaric path, note the large volume increases for a relatively small temperature change in the muscovite–K-feldspar field at ~680°C and the cordierite–biotite field at ~725°C. These relatively rapid volume changes may be accommodated by deformation or the expulsion of high-volume melt from the rock.

approach is to use the preserved assemblage to determine the conditions of peak metamorphism and the modes of various minerals to constrain the *P–T* path.

A simple example of using mode isopleths to interpret a *P–T* path is shown in Figure 5 for a metasedimentary migmatite from Yakymchuk et al. (2015). Here, the peak pressure assemblage contains biotite, garnet, sillimanite and liquid, which defines a field of 850–900°C at $P > 7$–7.5 kbar (Fig. 5a). The microstructures in the rock suggest the consumption of biotite, garnet and sillimanite to produce cordierite (see inset in Fig. 5a). The *P–T* field for the cordierite-bearing assemblage is restricted to 840–890°C at 6–7.5 kbar, which is at a slightly lower pressure than the earlier garnet–biotite–sillimanite assemblage. A schematic *P–T* path was constructed to connect these two assemblage fields and the mineral and melt modes were calculated along this path. The *Pressure–Mode* diagram in Figure 5b summarizes the oxide-molar proportions (approximately equivalent to vol.% of phases in a rock) along the decompression path. The modelling predicts that garnet, biotite and sillimanite are consumed to produce cordierite and melt during decompression, which links well with the inferred petrogenesis.

Mineral Deposits and Hydrothermal Alteration

Phase equilibria modelling can be used to understand the genesis of mineral deposits in both direct and indirect ways. Some ore-forming processes can be directly modelled using phase diagrams, such as the role of partial melting and melt extraction on upgrading magnetite and hematite concentrations in iron ore (e.g. Morrissey et al. 2016). Other scenarios can be modelled that are indirectly associated with mineralizing systems. For example, isochemical *P–T* phase diagrams can be used to assess the quantity of melt generated from different protoliths and the melting reactions that are responsible for generating the magmas that ultimately differentiate to form uranium deposits (e.g. Jeanneret et al. 2016).

Phase equilibria modelling can also be used to (1) predict alteration mineral assemblages (e.g. Elmer et al. 2007, 2008; Evans et al. 2013; White et al. 2013, 2014c), (2) assess how metamorphic assemblages develop in hydrothermally altered rocks (e.g. Pattison and Seitz 2012), (3) determine the compositions of fluids released during metamorphic reactions (White et al. 2003; Phillips and Powell 2010), and (4) quantify the amounts of mineralizing fluids responsible for forming hydrothermal ore deposits (e.g. Pearce et al. 2015b). These applications of phase equilibria modelling can provide 'alteration vectors' to mineralization because alteration zones around hydrothermal mineral deposits are usually much larger than ore zones.

One of the strengths of phase equilibria modelling is that a wide variety of alteration styles (e.g. carbonatization, potassic alteration, fenitization, silicification) can be examined in numerous rock types at different *P–T* conditions. The outputs of phase equilibria modelling can provide predictions of alter-

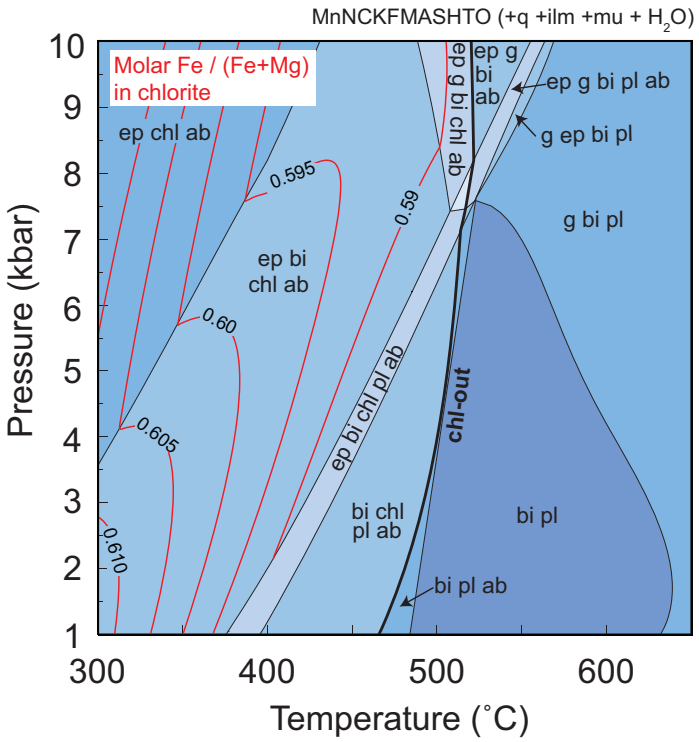

Figure 4. *Pressure–Temperature* isochemical phase diagram for a metagreywacke contoured for the value of X_{Fe} (molar Fe/[Fe + Mg]) in chlorite (modified from Pearce et al. 2015a). The chlorite composition isopleths are generally steeply sloping, which indicates that this variable is sensitive to temperature in this example. The modelled plagioclase is roughly oligoclase in composition, which is predicted to coexist with albite reflecting the 'peristerite gap' (e.g. Vry et al. 2008)

ation at several levels of detail ranging from the mineral assemblage (outcrop scale), to mineral modes (core and hand sample scale) to mineral compositions (thin section scale).

White et al. (2003) applied phase equilibria modelling to investigate potassic alteration of greenschist-facies metabasites that host orogenic gold mineralization in the Kalgoorlie area of Western Australia. Orogenic gold mineralization at Kalgoorlie is associated with carbonic and potassic alteration zones. Figure 6a shows a temperature–composition phase diagram where the amount of potassium in the bulk rock ranges from negligible at the left side of the diagram to strong potassic alteration at the right. Consider a constant temperature of 310°C on this diagram, which is approximately the temperature of gold deposition at Kalgoorlie (White et al. 2003). With increasing potassic alteration (e.g. K_2O being introduced into the rock by an externally derived fluid) chlorite eventually disappears from the assemblage when the amount of K_2O in the bulk rock reaches ~3.2 mol.% (Fig. 6a). While this is of some use to an exploration geologist, a more detailed model of the amounts of key alteration minerals is shown in Figure 6b. In this diagram, the modes of alteration minerals vary as potassic alteration increases. The amounts of muscovite and siderite increase during potassic alteration at the expense of chlorite, plagioclase and dolomite. At the far right of this diagram, the amount of siderite reaches ~20 mol.% (roughly equivalent to 20 vol.%), which should be apparent in hand and core samples or from the results of mineral liberation analysis (QEMSCAN

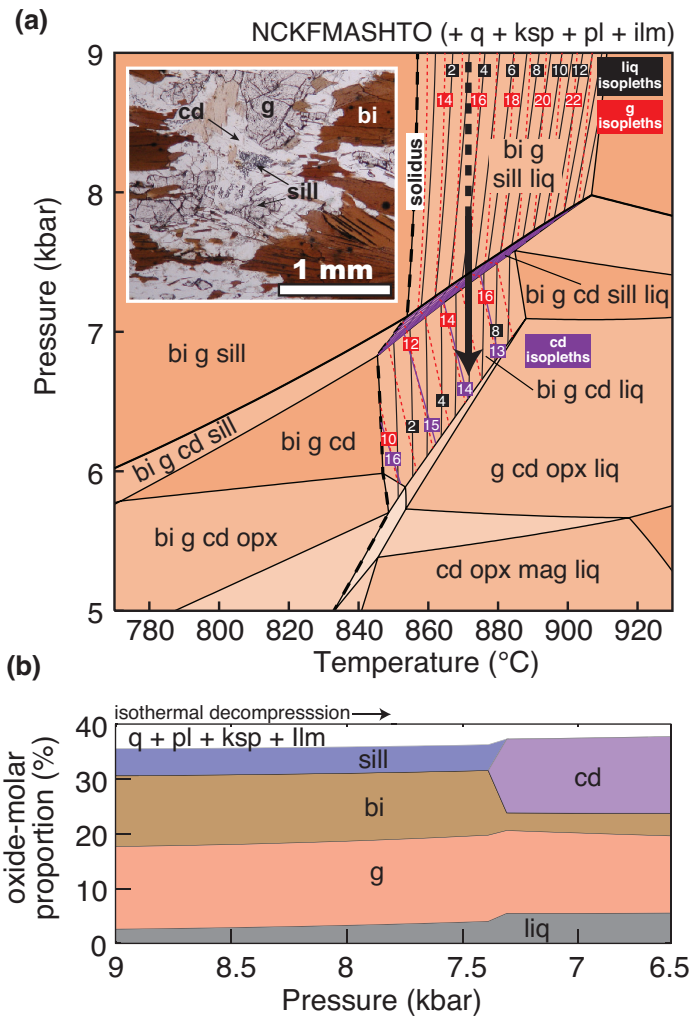

Figure 5. An example of linking the predictions of phase equilibria modelling with microstructural observations. (a) Isochemical *Pressure–Temperature* phase diagram for a suprasolidus metapelite (modified from Yakymchuk et al. 2015). The isopleths are for the modes of liquid, cordierite and garnet. The inset shows the breakdown of garnet, sillimanite and biotite to cordierite. A schematic isothermal decompression *P–T* path is shown by the bold arrow. (b) *Pressure–Mode* diagram showing the change in the proportions of the key ferromagnesian minerals along the *P–T* path in (a). Note that the modelling predicts the consumption of sillimanite, biotite and minor garnet to produce cordierite, which is consistent with the microstructural observations.

or MLA). Although not discussed by White et al. (2003), additional outputs from the modelling can include the composition of the different minerals (e.g. plagioclase). This information can be linked with the results of electron probe microanalysis to quantify the amount of potassic alteration.

Open System Behaviour and Melt Drainage

One of the key benefits of phase equilibria modelling is the ability to model a large number of petrogenetic scenarios, which can be prohibitively time-consuming for experimental petrologists. An example of this is modelling open-system behaviour in migmatites. The preservation of high-grade metamorphic assemblages requires the loss of anatectic melt to preserve high-temperature minerals such as garnet and orthopyroxene (e.g. Spear et al. 1999; White and Powell 2002).

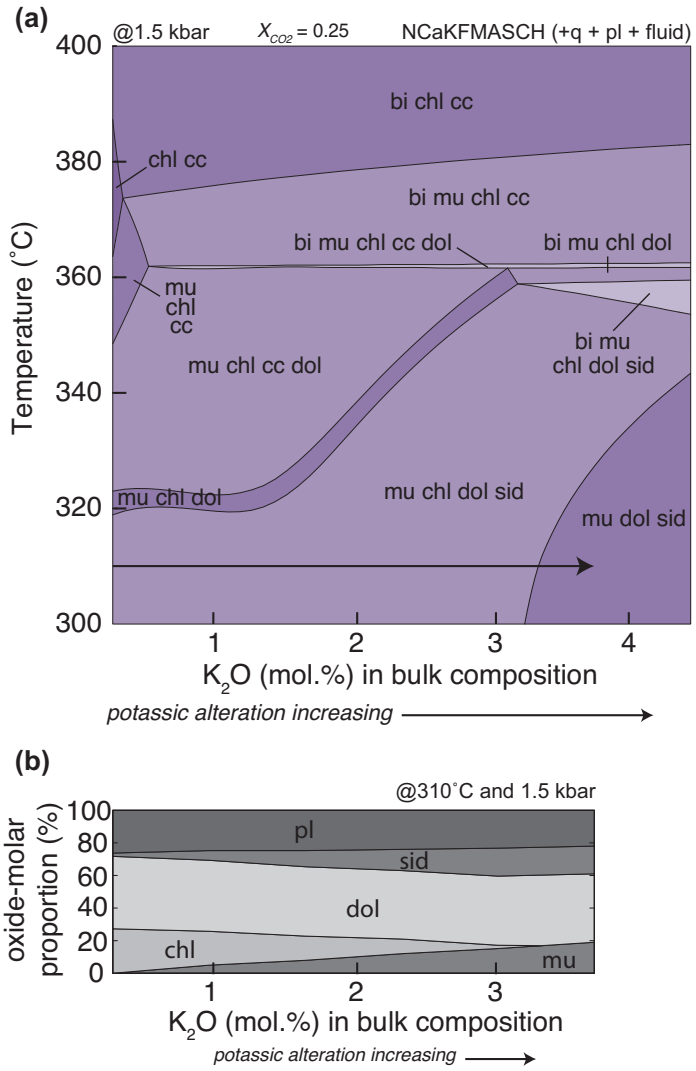

Figure 6. An example of phase equilibria modelling applied to alteration associated with gold mineralization. (a) *Temperature–Composition (Alteration)* phase diagram calculated at 1.5 kbar for a metabasite (modified from White et al. 2003). The horizontal axis represents an increasing intensity of potassic alteration towards the right-hand side of the diagram. The left-hand side of the diagram represents an approximate protolith composition. (b) An isothermal (310°C) and isobaric (1.5 kbar) *Composition–Mode* diagram showing the change in the proportion of phases with increasing potassic alteration. Note that the amounts of muscovite and siderite increase at the expense of chlorite, plagioclase and dolomite. Excess quartz and fluid (X_{CO2} = 0.25) are assumed for both diagrams.

If melt stayed in the system, high-temperature minerals are expected to retrogress to lower-temperature minerals during cooling and melt crystallization. Because phase equilibria modelling predicts the composition and mode of melt at *P–T*, a specified amount of melt can be subtracted out of the bulk composition leaving behind a more residual composition. This has implications for quantification of the amount of melt extracted from a system, determination of the change(s) in the rheological behaviour (e.g. strength) of migmatite during prograde metamorphism and evaluation of the tectonic processes that operate in the anatectic crust.

Yakymchuk and Brown (2014a) modelled the changes in the fertility (i.e. amount of melt that can be produced during anatexis) and density of a metapelite during a metamorphic evolution with periodic melt drainage events. These authors assumed that melt drains from the system when the proportion of melt reached a critical threshold. This critical value was set at 7% melt, which is a rheological threshold where melt is assumed to form an interconnected network along grain boundaries (e.g. Rosenberg and Handy 2005) that allows melt drainage out of the system. Yakymchuk and Brown (2014a) assumed that when the melt proportion reached the 7% threshold, 6% melt was drained from the system, which leaves 1% in the system. However, this exercise can easily be done for different melt thresholds including quasi-continuous melt extraction, which may be applicable to migmatites with high melt fractions undergoing syn-anatectic deformation (e.g. Vigneresse and Burg 2000). Figure 7a shows *Temperature–Mode* diagrams calculated for closed system (undrained) and open system (drained) metamorphism along an isobaric heating path at 12 kbar. Note that the changes in mineral modes are roughly equivalent up-temperature between the two scenarios. One notable exception is that the proportion of melt produced in an open system (30%) is less than the amount generated in a closed system (36%). The effect of melt drainage on the reduced ability of the rock to generate additional melt is even more significant for decompression *P–T* paths (cf. Yakymchuk and Brown 2014a).

The effect of anatexis and melt drainage on rock density for an isothermal decompression path at 820°C for the same metapelite is shown in Figure 7b. The density of the migmatite (e.g. the density of the residue plus any melt in the system) is compared with the density of the immediately overlying subsolidus crust for the same protolith composition. Similar to the isobaric heating path, melt loss events are labelled on the diagram at the 7% melt threshold. During decompression from 12 kbar the migmatite is of equivalent or greater density to the overlying subsolidus crust until ~ 6 kbar. At this pressure, biotite and sillimanite break down to produce cordierite, which is a relatively low-density mineral. This causes the density of the migmatite to decrease to values below that of the overlying crust during further decompression, which creates a buoyancy contrast. The positive buoyancy of the migmatite relative to the overlying crust may be a mechanism that enhances the exhumation of migmatite gneiss domes and metamorphic core complexes (e.g. Whitney et al. 2013).

Mayne et al. (2016) developed an algorithm that models the same open-system melting scenario as Yakymchuk and Brown (2014a), but for a much larger number of *P–T* paths. The conclusions of Mayne et al. (2016) were the same as Yakymchuk and Brown (2014a), although their new algorithm can be applied to numerous other path-dependent open-system processes.

Deformation and Tectonics

Partial melting has significant implications for the rheology of the deep crust. The decrease in strength of the crust during anatexis is well established for closed systems (e.g. Rosenberg and Handy 2005), but the consequences of melt extraction on the strength of the remaining residuum in the deep crust are

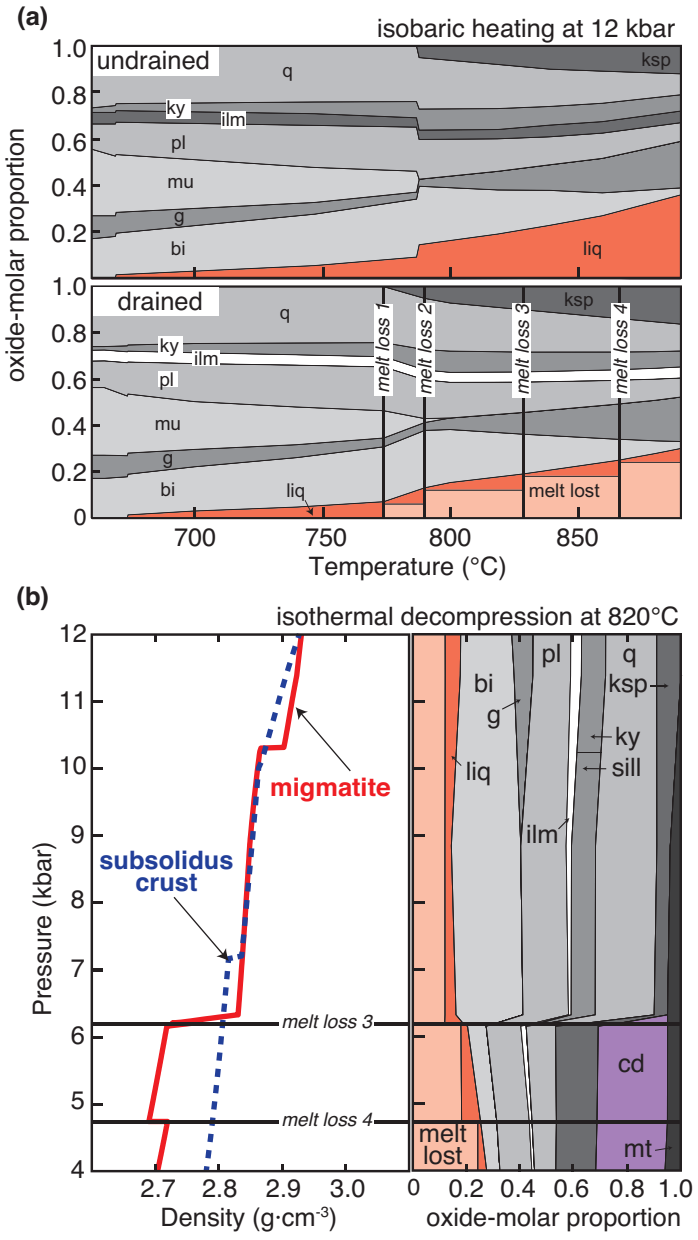

Figure 7. An example of phase equilibria modelling applied to open system behaviour and melt loss during high-temperature metamorphism (modified from Yakymchuk and Brown 2014a). (a) *Temperature–mode* diagrams for isobaric heating at 12 kbar for an average amphibolite-facies metapelite. Two scenarios are shown: a closed system (undrained) where all of the melt produced remains in the rock and an open system (drained) where melt is periodically extracted at each 'melt loss' event resulting in a more residual composition for the next segment of the heating path. Note that the amount of melt generated in the open system is less. (b) *Pressure–Mode* diagrams and density evolution curves (relative to subsolidus crust) for isothermal decompression of the same rock and the change in density of the modelled rock. Note the large density decrease during the growth of cordierite. The result is a migmatite that is less dense than the overlying (subsolidus) crust.

not as well understood. This issue has important implications for stabilizing the deep crust during orogenesis and cratonization.

Diener and Fagereng (2014) combined the results of phase equilibria modelling with equations for plastic flow of rocks and minerals to quantify the strength of migmatite during partial melting and melt extraction. They evaluated the phases and modes in the melt-bearing part of the migmatite (leucosome) and the residual material after melt extraction (residuum, restite or melanosome). This information was combined with rheological models of plastic deformation to quantify the strength of different parts of the migmatite along *P–T* paths for a metapelite and a greywacke, which generally represent the most fertile rock types in orogenic systems.

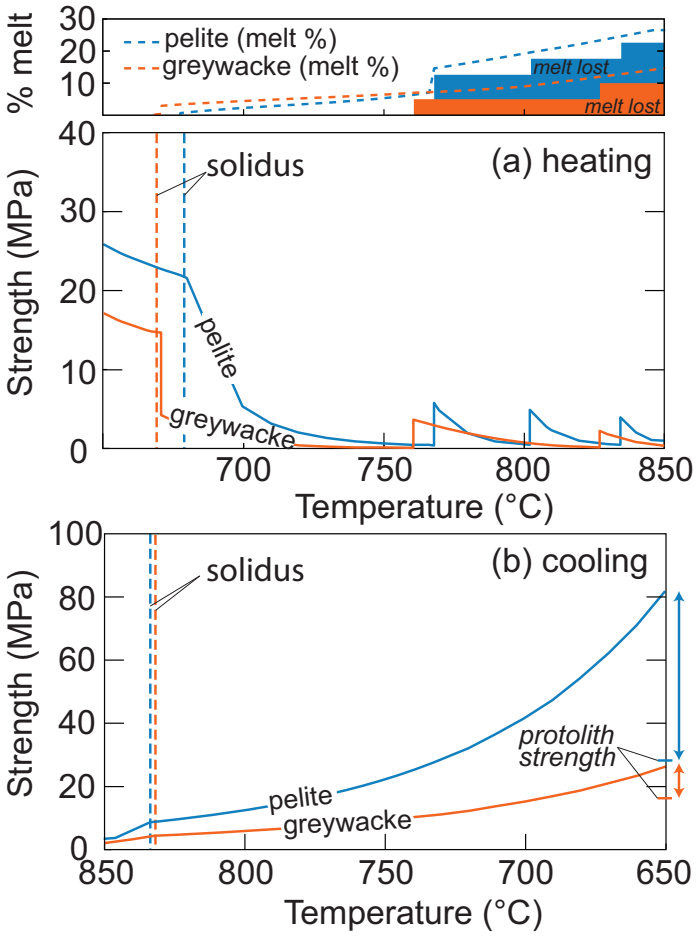

Figure 8. An example of phase equilibria modelling applied to the strength of the crust (modified from Diener and Fagereng 2014). (a) Strength evolution curves for a pelite and greywacke during heating and partial melting at 10 kbar. The episodic strength increases are from the extraction of melt from the system at various temperatures. (b) Strength profiles for the same rock types at the same pressure during cooling. Note that the strength of both rocks is much greater than for the same rocks prior to high-temperature metamorphism and melt loss (see arrows on right hand side of diagram).

The results of their modelling are summarized in Figure 8. There is a non-linear change in the expected strength of the metapelite and metagreywacke during heating and cooling. During heating, the strength of both rock types is predicted to decrease significantly after crossing the solidus and minor punctuated strength increases are expected during punctuated melt extraction episodes (Fig. 8a). For both rock types, the strength decreases by nearly an order of magnitude from the solidus to the peak of metamorphism at 850°C. During cooling and melt crystallization, the melt-depleted residuum can become up to 400% stronger than the unmelted protoliths

(Fig. 8b)—mainly due to the prograde replacement of relatively weak quartz and mica by relatively strong feldspar and garnet—resulting in a dry and strong deep crust. Ultimately, anatectic reworking of the continental crust can lead to cratonization, which then serves as a locus for arc development and accretionary orogens. The study by Diener and Fagereng (2014) provides the first attempt to quantitatively link phase equilibria modelling with crustal rheology and future studies should aim to include intermediate to mafic rocks.

Mantle Rocks

A relatively recent development in phase equilibria modelling is the compilation of an internally consistent database and solution models for phases in ultrabasic compositions that apply to mantle petrology (e.g. Stixrude and Lithgow-Bertelloni 2005, 2011; Holland et al. 2013; Jennings and Holland 2015). The use of phase equilibria modelling to predict phase assemblages in the deep mantle is a complementary technique to time-consuming high-pressure experiments that are usually conducted in relatively simple chemical systems (e.g. MgO–FeO–SiO_2; Ito et al. 1984).

Holland et al. (2013) modelled several bulk compositions to evaluate the main phase transitions that occur from the upper mantle through the transition zone to the uppermost lower mantle. This modelling was conducted in the NCFMAS system, which ignores ferric iron and chromium. The main mineral stabilities calculated from their modelling for a representative peridotite composition are summarized in Figure 9a. A mantle geotherm from Stixrude and Lithgow-Bertelloni (2007) is shown in Figure 9a and a *Pressure–Mode* diagram along this geotherm is shown in Figure 9b. There are several transitions that occur along the geotherm, but most striking is the appearance of MgSi-perovskite and ferropericlase at a depth of ~660 km, which generally corresponds to current interpretations of the depth of the transition zone between the upper and lower mantle.

Jennings and Holland (2015) expanded the NCFMAS system to include ferric iron and chromium for pressures up to 60 kbar. An important implication of their work is that the mantle oxidation state depends on *P, T* and the phase assemblage and the oxidation state varies in a complex way for a single phase assemblage. This chemical system can also be used to investigate the phase transitions in the non-hydrous components of subducting lithospheric slabs.

While these studies are preliminary, they are some of the first applications of phase equilibria modelling to mantle petrology and have the potential to allow the phase relations to be evaluated for a wide variety of compositions. Experimental data are still limited for some deep mantle phases and complex solution models that contain K and Ti have not yet been developed. Nonetheless, phase equilibria modelling of ultrabasic compositions at mantle conditions is an evolving field and studies that link the development and testing of these models with observations from geophysical studies of the deep Earth are a fruitful avenue for further research.

Geochemical Cycles and Subduction Zones

The depths and temperatures of fluid production in down-

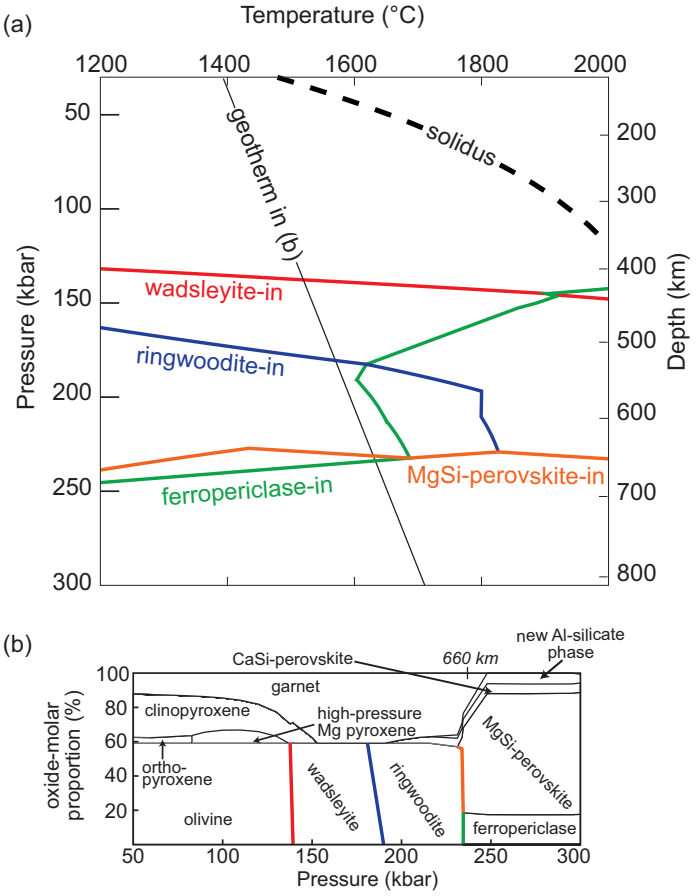

Figure 9. Phase equilibria modelling applied to deep mantle assemblages. (a) *Pressure–Temperature* phase diagram illustrating the main mineral-in reactions applicable to mantle rocks (modified from Holland et al. 2013). Note that pressure increases towards the bottom of the diagram. (b) *Pressure–Mode* diagram showing the proportions of the different minerals along the geothermal gradient in (a) (modified from Holland et al. 2013). An important link to geophysical studies is the breakdown of ringwoodite to MgSi-perovskite (and other phases) that roughly coincides with a depth of ~660 km.

going slabs have important implications for subduction-related earthquakes, geochemical cycling of carbon and the generation of arc-related magmas and mineral deposits. The fluids released during metamorphism of the subducted crust and lithospheric mantle can be investigated with phase equilibria modelling. Evans and Powell (2015) modelled the change in phase assemblages, modes, and compositions for a metasomatized ultramafic rock along two geothermal gradients appropriate for different tectonic settings. A selection of their results for a cold geothermal gradient is shown in Figure 10.

The *Temperature–Mode* diagram in Figure 10a displays three main phase transitions along the geotherm: (1) pyrrhotite breaks down to produce pyrite at ~430°C, (2) brucite reacts out to olivine and fluid at ~520°C, and (3) antigorite breaks down to olivine, orthopyroxene, trace amounts of chlorite and fluid from 520°C to 570°C. The breakdown of antigorite generates a large quantity of fluid. The transition from pyrrhotite to pyrite does not change the H_2S composition of the fluid significantly and the H_2S proportion in the fluid phase remains low (Fig. 10b). The modelling of Evans and Powell (2015) also

https://doi.org/10.12789/geocanj.2017.44.114

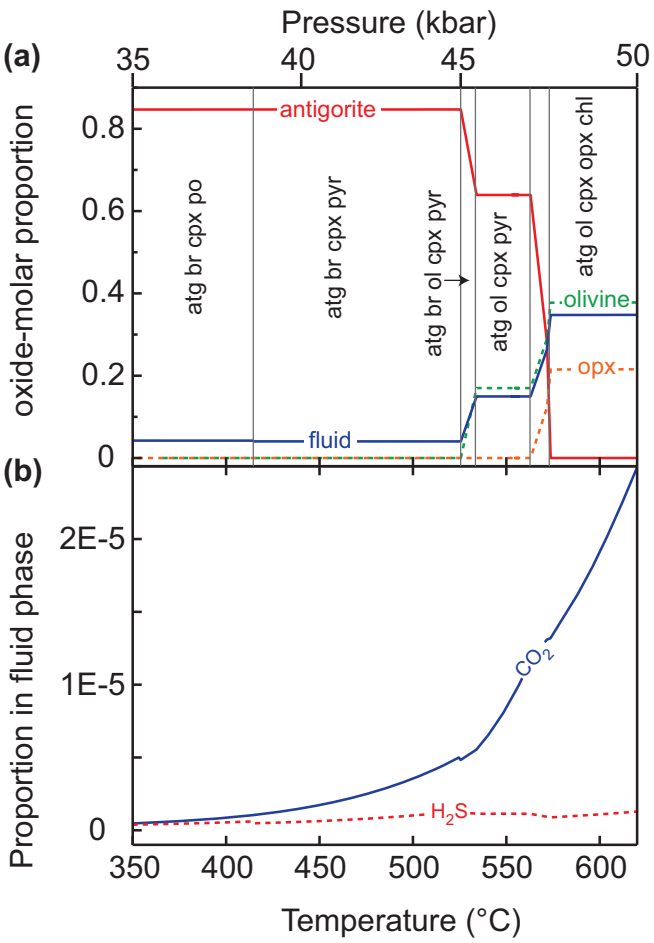

Figure 10. An example of phase equilibria modelling applied to fluid generation from a hydrated ultramafic rock during subduction (modified from Evans and Powell 2015). Note that magnesian carbonate and magnetite are in excess. (a) *Temperature–Mode* diagram for a relatively cold geothermal gradient. The important fluid-producing reactions involve the breakdown of antigorite and brucite to olivine at temperatures > 525°C. (b) Concentration of CO_2 and H_2S in the fluid phase along the same geotherm.

suggests that most sulphur will be transported to the deep mantle and relatively little is recycled back to the surface in arc magmas. Nonetheless, the H_2S that does make it into an arc system may act as a ligand to transport and ultimately act to concentrate elements of economic interest, especially precious metals, in magmatic–hydrothermal mineral deposits.

Although pyrrhotite breakdown is modelled to occur at ~430°C along the modelled geothermal gradient, the temperature of pyrrhotite breakdown is sensitive to other factors such as closed versus open system behaviour and redox state, which are explored in more detail by Evans and Powell (2015). A broader implication of this type of modelling is that the breakdown of pyrrhotite may also liberate trapped platinum group elements into the fluid (and/or melt) phase, which has implications for the generation of Ni–PGE deposits as well as for Re–Os geochronology of mantle samples.

Figure 10 shows that the concentration of CO_2 in the fluid is predicted to increase during prograde metamorphism in a subduction setting. A prediction of the modelling by Evans and Powell (2015) is that < 5% of the CO_2 in the rock will enter the fluid phase. The remainder is subducted into the deep mantle where it may influence mantle-melting reactions. While phase equilibria modelling of C–O–H–S fluids in the mantle is still relatively underexplored, it represents an opportunity to link the predictions of phase equilibria modelling with measurements of mantle xenoliths and experimental studies to better understand the geochemical cycling of carbon and sulphur as well as diamond growth in the lithospheric mantle.

Earthquakes

Changes in rock strength during metamorphism and metasomatism in subduction and collisional tectonic settings—including implications for earthquake localization—can be evaluated with phase equilibria modelling (e.g. Fagereng and Diener 2011; Getsinger et al. 2013). Fagereng and Diener (2011) used phase equilibria modelling to investigate prograde and retrograde reactions of rocks from the Franciscan Complex at the depths and temperatures thought to be appropriate for seismicity related to the San Andreas 'tectonic tremor.' They suggested that mantle-derived fluids may induce retrograde metamorphism of mafic rocks and greywacke leading to the production of abundant phyllosilicate minerals that result in fault-zone weakening and localization.

Getsinger et al. (2013) combined microstructural constraints with phase equilibria modelling of water activity in mafic rocks to understand how mineralogical changes in response to fluid infiltration affect the rheology of the lower crust. They showed that deformation in the lower crust is strongly partitioned into relatively narrow fluid-altered zones leaving the bulk of the lower crust relatively strong. This has implications for how the lower crust responds to tectonic stresses and the localization of low-frequency earthquakes.

Climate Change

Metamorphic fluid compositions can be predicted through phase equilibria modelling for a variety of geological settings, which has implications for the geochemical cycles of carbon and sulphur and the generation of greenhouse gases in metamorphic settings (Aarnes et al. 2010; Skora et al. 2015; Tomkins and Evans 2015). Aarnes et al. (2010) evaluated the composition and volumes of metamorphic fluids produced through contact metamorphism of organic-rich metasedimentary rocks. These authors calculated that basin-scale contact metamorphism could have generated up to ~16,200 Gt of thermogenic CH_4 in the Karoo Basin (South Africa) within 10–1000 years. This quantity of CH_4 was predicted to produce a global $\delta^{13}C$ excursion of –3 to –5‰. Aarnes et al. (2010) proposed a link between large igneous provinces, contact metamorphism of organic-rich sedimentary rocks, global warming and mass extinction in the Toarcian stage of the Lower Jurassic.

Meteorites

Phase equilibria modelling can also be applied to extraterrestrial rocks to evaluate how parental asteroid bodies are constructed. Johnson et al. (2016) modelled metamorphism of three

groups of ordinary chondrite compositions. A *P–T* isochemical phase diagram for an average of the 'LL' group of ordinary chondrites is shown in Figure 11. Note that garnet is restricted to $P > 10$ kbar and plagioclase is stable at $P < 9$–15 kbar with increasing temperature. Considering that nearly all ordinary chondrites are thought to record metamorphic conditions at pressures < 1 kbar, the results of Johnson et al. (2016) are consistent with the observation that most, or all, ordinary chondrites contain plagioclase and lack garnet. While the model results of Johnson et al. (2016) are preliminary, their study opens the door for further work to evaluate how oxidation affects chondrite mineralogy (e.g. McSween and Labotka 1993), the effects of melt loss on the chemical differentiation of planetesimals and the 'onion-shell' versus 'rubble-pile' hypotheses of the parent asteroids of ordinary chondrites (e.g. Harrison and Grimm 2010).

Accessory Minerals

Accessory minerals make up a small proportion of most rocks, but they are disproportionately large repositories of trace elements. Furthermore, many accessory minerals contain suitable quantities of U and Th to be dated through U–Pb geochronology. The behaviour of some accessory minerals used in metamorphic studies such as epidote and titanite as well as oxides (e.g. rutile, ilmenite) and sulphides can be quantified for different bulk compositions and *P–T* conditions using phase equilibria modelling (e.g. White et al. 2007; Evans et al. 2010; Palin et al. 2016b). However, the behaviour of the most commonly used U–Pb chronometers (zircon and monazite) are more difficult to quantify with current phase equilibria modelling techniques (e.g. Spear and Pyle 2010; Kelsey and Powell 2011). This is because some of their essential structural constituents (Zr, P, LREE) are not usually considered in model chemical systems.

For subsolidus metamorphic rocks, accessory minerals can be produced through solid-state reactions (Rubatto et al. 2001; Wing et al. 2003) and may also precipitate from fluids (Ayers et al. 1999; Schaltegger 2007). Zircon is generally expected to be unreactive or consumed during subsolidus metamorphism (e.g. Kohn et al. 2015), whereas monazite is generally more reactive and can be used to date particular portions of subsolidus *P–T* paths. Phase equilibria modelling of subsolidus monazite behaviour is restricted to relatively few studies (Spear 2010; Spear and Pyle 2010). Spear and Pyle (2010) compiled a thermodynamic database that included apatite, monazite and xenotime and they were the first to develop a *P–T* isochemical phase diagram that includes phosphates. Spear (2010) used phase equilibria modelling to show that the temperature of allanite breakdown to monazite is sensitive to bulk rock concentrations of calcium and aluminum. Both of these studies have implications for interpreting the reaction sequence of monazite growth in metapelitic rocks and the geological significance of monazite U–Pb ages.

For suprasolidus rocks, accessory mineral behaviour is strongly linked with the amount and composition of anatectic melt in the system. Because the composition and mode of melt in a metamorphic system can be predicted with phase

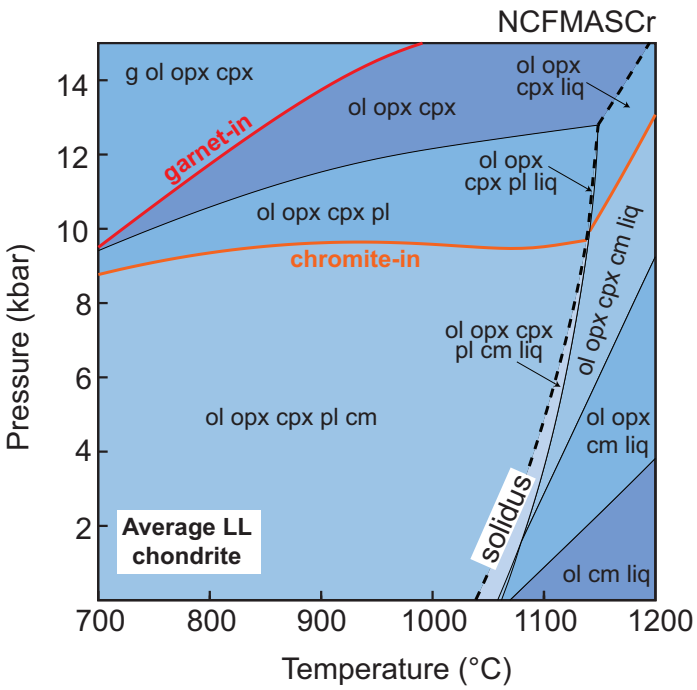

Figure 11. A *Pressure–Temperature* phase diagram for a LL ordinary chondrite (modified from Johnson et al. 2016). The modelling does not predict garnet at pressures < 9 kbar, which is consistent with the absence of garnet from LL ordinary chondrites and the hypothesis that most were metamorphosed in a parent body at $P < 1$ kbar.

equilibria modelling, this information can be combined with solubility equations of accessory minerals (determined from experimental studies) to evaluate when these minerals are expected to grow and be consumed along a metamorphic *P–T* path (e.g. Kelsey et al. 2008; Spear and Pyle 2010; Kelsey and Powell 2011; Yakymchuk and Brown 2014b; Kohn et al. 2015; Yakymchuk et al. 2017; Yakymchuk 2017).

Kelsey et al. (2008) combined zircon and monazite solubility equations with the mode and composition of anatectic melt predicted for pelite and greywacke compositions to determine the amount of accessory mineral dissolution for a wide range of suprasolidus *P–T* conditions. Their study was followed by the development of solution models for Zr-bearing silicate melt and garnet that allowed quantitative phase equilibria modelling of suprasolidus zircon behaviour (Kelsey and Powell 2011). Further experimental work on zircon and monazite solubility (Stepanov et al. 2012; Boehnke et al. 2013) refined the solubility equations for these minerals. Yakymchuk and Brown (2014b) used these revised solubility equations to evaluate the effects of open-system behaviour on the stability of monazite and zircon.

An example of the behaviour of zircon and monazite in suprasolidus rocks from Yakymchuk et al. (2017) is shown in Figure 12. Figure 12a is a *Temperature–Composition* (*T–X*) phase diagram that shows the phase assemblages and melt proportion isopleths for compositions ranging linearly from an average metapelite (left side) to an average passive margin greywacke (right side). Figure 12b and 12c show the percentage of zircon and monazite dissolution (relative to the amount

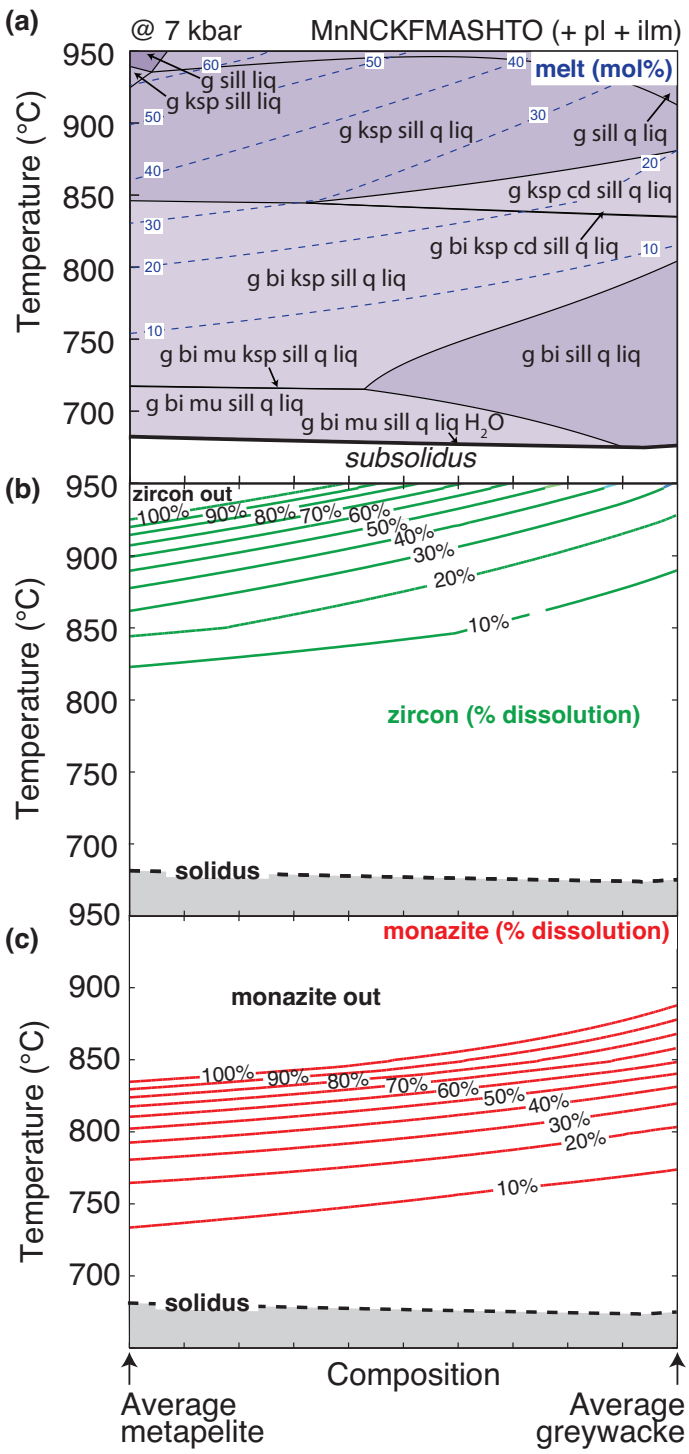

Figure 12. *Temperature–Composition* diagrams exploring the behaviour of zircon and monazite during partial melting for compositions ranging linearly between an average metapelite at the left side of the diagram and an average greywacke at right side of the diagram in a closed system with no melt loss (modified from Yakymchuk et al. 2017). (a) Phase diagram showing the change in melt mode (mol.%) and phase assemblages across the modelled compositional range. (b) Contours for the amount of zircon dissolution (%) relative to the amount existing at the solidus. Note that zircon is predicted to be completely consumed at 930°C for a pelite and only 20% of zircon is expected to be consumed for the greywacke. (c) Contours for the amount of monazite dissolution (%) relative to the amount existing at the solidus. Monazite dissolution is less sensitive to changing bulk composition than zircon and monazite is expected to be completely consumed in both rock types by 900°C.

present at the solidus) required to maintain zirconium and light rare earth element (LREE) saturation of the anatectic melt, respectively. The calculations are conducted for specific bulk rock compositions of zirconium and the LREE. In this case, both are assumed to be 150 ppm, which is interpreted to represent a reasonable value for most pelites and greywackes and their high-grade equivalents (e.g. Yakymchuk and Brown 2014b).

Dissolution contours have negative slopes on Figure 12b and 12c and the spacing between contours decreases up temperature. The negative slopes indicate that, at a given temperature, the amounts of zircon and monazite dissolution are greater for the metapelite composition (left-hand side of the diagram) than for the greywacke composition (right-hand side of the diagram). The main controlling factor for the difference between the two rocks is that the metapelite is predicted to generate more melt at a given T than the greywacke. Therefore, proportionally more zircon and monazite dissolution are required to maintain melt saturation with respect to these minerals for the pelite. The closer spacing of the contours at high temperatures suggests that the amount of zircon and monazite dissolution is non-linear with temperature. This is a function of the rate of melt production and the increased solubility of the accessory minerals at high temperatures.

For the metapelite, zircon is expected to be completely consumed (i.e. 100% contours in Fig. 12b, c) by ~930°C (left-hand side of the diagram) and monazite is exhausted by ~840°C (left-hand side of the diagram). For the greywacke, some zircon is expected to survive up to 950°C and monazite is expected to be completely consumed by 880°C. Conversely, melt crystallization during cooling is predicted to result in new zircon and monazite growth. The assumptions and limitations of an equilibrium approach to modelling accessory mineral behaviour in metamorphic rocks are discussed elsewhere (Kelsey et al. 2008; Yakymchuk and Brown 2014b; Yakymchuk et al. 2017). In particular, these models do not consider phosphorus, which has important implications for the stability of monazite (and apatite) in melt (e.g. Duc-Tin and Keppler 2015; Yakymchuk 2017).

ASSUMPTIONS AND LIMITATIONS OF PHASE EQUILIBRIA MODELLING

Like any model, phase equilibria modelling represents a necessary simplification of complex natural systems. There are two main categories of uncertainties when applying equilibrium thermodynamics to metamorphic phase assemblages: systematic uncertainties (Powell 1985) and random uncertainties (Palin et al. 2016a). The first are the systematic uncertainties in the thermodynamic properties of phase end-members in thermodynamic databases (Helgeson et al. 1978; Berman 1988; Holland and Powell 2011) and those related to the formulation of activity–composition models (e.g. O'Brien 2008; White et al. 2014a). For example, Pattison and Debuhr (2015) demonstrated that natural phase assemblages in subsolidus cordierite-bearing metapelite are reproduced by a modified version of the Berman (1988) database and associated activity–composition models (Pattison et al. 2002; Spear and Pyle 2010), but not

by the Holland and Powell (1998, 2011) databases and associated activity–composition models. The systematic uncertainties of phase equilibria modelling will decrease as more experimental data become available and more natural rock assemblages are examined and integrated into activity–composition models. In some cases, error propagation can be used to assess the uncertainty in *P–T* estimates (e.g. Powell 1985) and, more recently, Monte Carlo simulations were used to quantify systematic uncertainties (Jennings and Holland 2015; Palin et al. 2016a).

The second category of uncertainties comprises geological uncertainties that are difficult to quantify. These include: (1) choosing an *effective* bulk composition of a system (e.g. Guevara and Caddick 2016), and (2) evaluating if a phase assemblage is in equilibrium and assessing any kinetic barriers to attaining equilibrium (e.g. Pattison et al. 2011; Spear et al. 2016). Another source of uncertainty is the misidentification of reaction sequences and equilibrium phase assemblages (e.g. Vernon et al. 2008), but this needs to be assessed on a case-by-case basis.

The effective bulk composition of a metamorphic system can change along a *P–T* evolution. The partitioning of particular cations into growing porphyroblasts (e.g. Mn into garnet) and different diffusion rates for cations can result in growth-zoned minerals where the cores are not in equilibrium with the surrounding phase assemblage. In some cases, this can be examined by *forward modelling* of porphyroblast growth (e.g. Zuluaga et al. 2005; Gaidies et al. 2008; Moynihan and Pattison 2013).

Melt loss during suprasolidus metamorphism produces more residual compositions, elevated solidus temperatures and a greater proportion of peritectic minerals relative to the undrained protolith compositions (e.g. Yakymchuk and Brown 2014a; Guevara and Caddick 2016). While these residual compositions are useful for determining peak *P–T* and portions of the retrograde path, they may not be appropriate for investigating prograde metamorphic reactions that require an estimate of the effective bulk composition before melt extraction. *Inverse modelling* has been used to add melt back into the bulk composition while working down temperature (White et al. 2004; Indares et al. 2008; Guilmette et al. 2011), but this requires an assumption of the *P–T* trajectory of the prograde path, which is not always clear.

Assessing if a metamorphic phase assemblage is in equilibrium is a matter of interpretation and the scale of observation. Most petrologists would interpret high-temperature metamorphic minerals that are compositionally homogeneous with low-energy grain shapes (e.g. triple junctions at grain boundaries) to represent an equilibrium assemblage. However, very few metamorphic rocks fit these criteria. Reaction microstructures (e.g. coronae around porphyroblasts) may be interpreted by one geologist to record disequilibrium at the scale of a hand sample or thin section and by another to represent equilibrium at the scale of grain boundaries. Therefore, the interpretation comes down to the scale of observation. Equilibrium volumes are anticipated to be larger for high-temperature systems that may permit relatively rapid cation transport, such as through melt along grain boundaries, and smaller for lower-temperature systems where intergranular diffusion rates of cations may be very slow. However, this temperature-related generality may be secondary to the presence and nature of intergranular volatile species (e.g. Carlson et al. 2015a).

Metamorphic reactions may not proceed at the *P–T* conditions predicted from phase equilibria modelling due to kinetic barriers related to nucleation, interface reaction and intergranular transport (Ridley and Thompson 1986; Rubie 1998; Gaidies et al. 2011; Carlson et al. 2015b). Kinetic barriers to nucleation are generally considered to be the dominant rate-limiting step in metamorphic phase assemblages reaching equilibrium (e.g. Ague and Carlson 2013). Kelly et al. (2013) used numerical modelling of diffusion-controlled nucleation (and growth) of garnet to show that garnet nucleation begins after 5–67°C of thermal overstep. Waters and Lovegrove (2002) and Pattison et al. (2011) showed how reaction affinity modelling could be used to predict the degrees of overstepping to be expected for different reactions, the results of which agreed with observations from the Bushveld aureole (Waters and Lovegrove 2002) and Nelson aureole (Pattison and Tinkham 2009). Reaction overstepping and disequilibrium processes are probably more widespread than previously acknowledged and are essential components of a rock's metamorphic history.

All of the limitations discussed above need to be considered when applying the results of phase equilibria modelling to natural metamorphic rocks and in particular to detailed studies of *P–T–t* paths. Nonetheless, the equilibrium approach to metamorphic assemblages reproduces many first-order observations from metamorphic rocks and this methodology can be applied to various geological questions in a relatively fast and inexpensive way. Thermodynamics and phase equilibrium modelling also provide some of the theoretical tools to evaluate the possible consequences of disequilibrium processes (e.g. Pattison et al. 2011).

CONCLUSIONS AND OUTLOOK

Phase equilibria modelling has evolved over the last few decades and now allows for a variety of phase diagrams to be calculated with different variables for a wide range of compositions. While there may be limitations to the equilibrium approach to understanding metamorphic rocks and processes, it provides an excellent framework to test and refine hypotheses and opens up connections to many other areas of the geosciences. Linking the predictions of phase equilibria modelling of mantle rocks with observations from geophysical studies is a fruitful avenue for further work. Developing alteration vectors to mineralization using phase diagrams is an underexplored connection to economic geology. Integrating metamorphic phase diagrams into global geochemical cycles from the Archean to the present may provide new insights into the secular change of the lithosphere, hydrosphere and atmosphere. The continual refinement of activity–composition models of different phases and expanding model chemical systems may soon allow a more quantitative method to evaluate accessory mineral behaviour in metamorphic systems. Finally, the interplay between equilibrium and kinetics in the pressure-temper-

https://doi.org/10.12789/geocanj.2017.44.114

ature-fluid-deformation history of rocks is at an early stage of investigation and will be the focus of much future research.

ACKNOWLEDGEMENTS

This admittedly biased review has benefited from numerous interactions with colleagues and students. Discussions with M Brown, MJ Caddick, C Clark, DRM Pattison and RW White were particularly insightful. I thank T Rivers and DRM Pattison for very thorough and constructive reviews of this manuscript. I thank Andrew Kerr for the invitation to write this contribution and for his editorial handling. I acknowledge funding from a Natural Sciences and Engineering Council of Canada Discovery Grant.

REFERENCES

Aarnes, I., Svensen, H., Connolly, J.A.D., and Podladchikov, Y.Y., 2010, How contact metamorphism can trigger global climate changes: Modeling gas generation around igneous sills in sedimentary basins: Geochimica et Cosmochimica Acta, v. 74, p. 7179–7195, https://doi.org/10.1016/j.gca.2010.09.011.

Ague, J.J., 1991, Evidence for major mass transfer and volume strain during regional metamorphism of pelites: Geology, v. 19, p. 855–858, https://doi.org/10.1130/0091-7613(1991)019<0855:EFMMTA>2.3.CO;2.

Ague, J.J., and Carlson, W.D., 2013, Metamorphism as garnet sees it: The kinetics of nucleation and growth, equilibration, and diffusional relaxation: Elements, v. 9, p. 439–445, https://doi.org/10.2113/gselements.9.6.439.

Albee, A.L., 1965, A petrogenetic grid for the Fe-Mg silicates of pelitic schists: American Journal of Science, v. 263, p. 512–536, https://doi.org/10.2475/ajs.263.6.512.

Ambrose, T.K., Larson, K.P., Guilmette, C., Cottle, J.M., Buckingham, H., and Rai, S., 2015, Lateral extrusion, underplating, and out-of-sequence thrusting within the Himalayan metamorphic core, Kanchenjunga, Nepal: Lithosphere, v. 7, p. 441–464, https://doi.org/10.1130/L437.1.

Ayers, J.C., Miller, C., Gorisch, B., and Milleman, J., 1999, Textural development of monazite during high-grade metamorphism; hydrothermal growth kinetics, with implications for U, Th–Pb geochronology: American Mineralogist, v. 84, p. 1766–1780, https://doi.org/10.2138/am-1999-11-1206.

Berman, R.G., 1988, Internally-consistent thermodynamic data for minerals in the system Na_2O–K_2O–CaO–MgO–FeO–Fe_2O_3–Al_2O_3–SiO_2–TiO_2–H_2O–CO_2: Journal of Petrology, v. 29, p. 445–522, https://doi.org/10.1093/petrology/29.2.445.

Boehnke, P., Watson, E.B., Trail, D., Harrison, T.M., and Schmitt, A.K., 2013, Zircon saturation re-revisited: Chemical Geology, v. 351, p. 324–334, https://doi.org/10.1016/j.chemgeo.2013.05.028.

Boger, S.D., White, R.W., and Schulte, B., 2012, The importance of iron speciation (Fe^{+2}/Fe^{+3}) in determining mineral assemblages: an example from the high-grade aluminous metapelites of southeastern Madagascar: Journal of Metamorphic Geology, v. 30, p. 997–1018, https://doi.org/10.1111/jmg.12001.

Bowen, N.L., 1940, Progressive metamorphism of siliceous limestone and dolomite: The Journal of Geology, v. 48, p. 225–274, https://doi.org/10.1086/624885.

Brown, M., 2007, Metamorphic conditions in orogenic belts: A record of secular change: International Geology Review, v. 49, p. 193–234, https://doi.org/10.2747/0020-6814.49.3.193.

Brown, M., 2014, The contribution of metamorphic petrology to understanding lithosphere evolution and geodynamics: Geoscience Frontiers, v. 5, p. 553–569, https://doi.org/10.1016/j.gsf.2014.02.005.

Carlson, W.D., Hixon, J.D., Garber, J.M., and Bodnar, R.J., 2015a, Controls on metamorphic equilibration: the importance of intergranular solubilities mediated by fluid composition: Journal of Metamorphic Geology, v. 33, p. 123–146, https://doi.org/10.1111/jmg.12113.

Carlson, W.D., Pattison, D.R.M., and Caddick, M.J., 2015b, Beyond the equilibrium paradigm: How consideration of kinetics enhances metamorphic interpretation: American Mineralogist, v. 100, p. 1659–1667, https://doi.org/10.2138/am-2015-5097.

Carrington, D.P., and Harley, S.L., 1995, Partial melting and phase relations in high-grade metapelites: an experimental petrogenetic grid in the KFMASH system: Contributions to Mineralogy and Petrology, v. 120, p. 270–291, https://doi.org/10.1007/BF00306508.

Carson, C.J., Clarke, G.L., and Powell, R., 2000, Hydration of eclogite, Pam Peninsula, New Caledonia: Journal of Metamorphic Geology, v. 18, p. 79–90, https://doi.org/10.1046/j.1525-1314.2000.00245.x.

Connolly, J.A.D., and Petrini, K., 2002, An automated strategy for calculation of phase diagram sections and retrieval of rock properties as a function of physical conditions: Journal of Metamorphic Geology, v. 20, p. 697–708, https://doi.org/10.1046/j.1525-1314.2002.00398.x.

de Capitani, C., and Brown, T.H., 1987, The computation of chemical equilibrium in complex systems containing non-ideal solutions: Geochimica et Cosmochimica Acta, v. 51, p. 2639–2652, https://doi.org/10.1016/0016-7037(87)90145-1.

de Capitani, C., and Petrakakis, K., 2010, The computation of equilibrium assemblage diagrams with Theriak/Domino software: American Mineralogist, v. 95, p. 1006–1016, https://doi.org/10.2138/am.2010.3354.

Diener, J.F.A., and Fagereng, Å., 2014, The influence of melting and melt drainage on crustal rheology during orogenesis: Journal of Geophysical Research, v. 119, p. 6193–6210, https://doi.org/10.1002/2014JB011088.

Dragovic, B., Guevara, V.E., Caddick, M.J., Baxter, E.F., and Kylander-Clark, A.R.C., 2016, A pulse of cryptic granulite-facies metamorphism in the Archean Wyoming Craton revealed by Sm–Nd garnet and U–Pb monazite geochronology: Precambrian Research, v. 283, p. 24–49, https://doi.org/10.1016/j.precamres.2016.07.010.

Duc-Tin, Q., and Keppler, H., 2015, Monazite and xenotime solubility in granitic melts and the origin of the lanthanide tetrad effect: Contributions to Mineralogy and Petrology, v. 169, Article 8, https://doi.org/10.1007/s00410-014-1100-9.

Elmer, F.L., Powell, R., White, R.W., and Phillips, G.N., 2007, Timing of gold mineralization relative to the peak of metamorphism at Bronzewing, Western Australia: Economic Geology, v. 102, p. 379–392, https://doi.org/10.2113/gsecongeo.102.3.379.

Elmer, F.L., Dugdale, A.L., and Wilson, C.J.L., 2008, Application of mineral equilibria modeling to constrain T and X_{CO2} conditions during the evolution of the Magdala gold deposit, Stawell, Victoria, Australia: Mineralium Deposita, v. 43, p. 759–776, https://doi.org/10.1007/s00126-008-0192-4.

England, P.C., and Thompson, A.B., 1984, Pressure–Temperature–Time paths of regional metamorphism I. Heat transfer during the evolution of regions of thickened continental crust: Journal of Petrology, v. 25, p. 894–928, https://doi.org/10.1093/petrology/25.4.894.

Evans, K.A., and Powell, R., 2015, The effect of subduction on the sulphur, carbon and redox budget of lithospheric mantle: Journal of Metamorphic Geology, v. 33, p. 649–670, https://doi.org/10.1111/jmg.12140.

Evans, K.A., Powell, R., and Holland, T.J.B., 2010, Internally consistent data for sulphur-bearing phases and application to the construction of pseudosections for mafic greenschist facies rocks in Na_2O–CaO–K_2O–FeO–MgO–Al_2O_3–SiO_2–CO_2–O–S–H_2O: Journal of Metamorphic Geology, v. 28, p. 667–687, https://doi.org/10.1111/j.1525-1314.2010.00890.x.

Evans, K.A., Powell, R., and Frost, B.R., 2013, Using equilibrium thermodynamics in the study of metasomatic alteration, illustrated by an application to serpentinites: Lithos, v. 168–169, p. 67–84, https://doi.org/10.1016/j.lithos.2013.01.016.

Everett, M.E., 2013, Near-surface applied geophysics: Cambridge University Press, Cambridge, 415 p., https://doi.org/10.1017/CBO9781139088435.

Fagereng, Å., and Diener, J.F.A., 2011, San Andreas Fault tremor and retrograde metamorphism: Geophysical Research Letters, v. 38, L23303, https://doi.org/10.1029/2011GL049550.

Frey, M., de Capitani, C., and Liou, J.G., 1991, A new petrogenetic grid for low-grade metabasites: Journal of Metamorphic Geology, v. 9, p. 497–509, https://doi.org/10.1111/j.1525-1314.1991.tb00542.x.

Gaidies, F., de Capitani, C., and Abart, R., 2008, THERIA_G: a software program to numerically model prograde garnet growth: Contributions to Mineralogy and Petrology, v. 155, p. 657–671, https://doi.org/10.1007/s00410-007-0263-z.

Gaidies, F., Pattison, D.R.M., and de Capitani, C., 2011, Toward a quantitative model of metamorphic nucleation and growth: Contributions to Mineralogy and Petrology, v. 162, Article 975, https://doi.org/10.1007/s00410-011-0635-2.

Getsinger, A.J., Hirth, G., Stünitz, H., and Goergen, E.T., 2013, Influence of water on rheology and strain localization in the lower continental crust: Geochemistry, Geophysics, Geosystems, v. 14, p. 2247–2264, https://doi.org/10.1002/ggge.20148.

Green, E.C.R., White, R.W., Diener, J.F.A., Powell, R., Holland, T.J.B., and Palin, R.M., 2016, Activity–composition relations for the calculation of partial melting equilibria in metabasic rocks: Journal of Metamorphic Geology, v. 34, p. 845–869, https://doi.org/10.1111/jmg.12211.

Groppo, C., Rolfo, F., Castelli, D., and Connolly, J.A.D., 2013, Metamorphic CO_2 production from calc-silicate rocks via garnet-forming reactions in the CFAS–H_2O–CO_2 system: Contributions to Mineralogy and Petrology, v. 166, p. 1655–1675, https://doi.org/10.1007/s00410-013-0947-5.

Guevara, V.E., and Caddick, M.J., 2016, Shooting at a moving target: phase equilibria modelling of high-temperature metamorphism: Journal of Metamorphic Geology, v. 34, p. 209–235, https://doi.org/10.1111/jmg.12179.

Guilmette, C., Indares, A., and Hébert, R., 2011, High-pressure anatectic paragneiss-

es from the Namche Barwa, Eastern Himalayan Syntaxis: Textural evidence for partial melting, phase equilibria modeling and tectonic implications: Lithos, v. 124, p. 66–81, https://doi.org/10.1016/j.lithos.2010.09.003.

Guiraud, M., and Powell, R., 2006, *P–V–T* relationships and mineral equilibria in inclusions in minerals: Earth and Planetary Science Letters, v. 244, p. 683–694, https://doi.org/10.1016/j.epsl.2006.02.021.

Harrison, K.P., and Grimm, R.E., 2010, Thermal constraints on the early history of the H-chondrite parent body reconsidered: Geochimica et Cosmochimica Acta, v. 74, p. 5410–5423, https://doi.org/10.1016/j.gca.2010.05.034.

Helgeson, H.C., Delany, J.M., Nesbitt, H.W., and Bird, D.K., 1978, Summary and critique of the thermodynamic properties of rock-forming minerals: American Journal of Science, v. 278, p. 1–229.

Hensen, B.J., 1971, Theoretical phase relations involving cordierite and garnet in the system MgO–FeO–Al_2O_3–SiO_2: Contributions to Mineralogy and Petrology, v. 33, p. 191–214, https://doi.org/10.1007/BF00374063.

Holland, T.J.B., and Powell, R., 1998, An internally consistent thermodynamic data set for phases of petrological interest: Journal of Metamorphic Geology, v. 16, p. 309–343, https://doi.org/10.1111/j.1525-1314.1998.00140.x.

Holland, T.J.B., and Powell, R., 2011, An improved and extended internally consistent thermodynamic dataset for phases of petrological interest, involving a new equation of state for solids: Journal of Metamorphic Geology, v. 29, p. 333–383, https://doi.org/10.1111/j.1525-1314.2010.00923.x.

Holland, T.J.B., Hudson, N.F.C., Powell, R., and Harte, B., 2013, New thermodynamic models and calculated phase equilibria in NCFMAS for basic and ultrabasic compositions through the transition zone into the uppermost lower mantle: Journal of Petrology, v. 54, p. 1901–1920, https://doi.org/10.1093/petrology/egt035.

Indares, A., and Martignole, J., 1985, Biotite-garnet geothermometry in granulite-facies rocks; evaluation of equilibrium criteria: The Canadian Mineralogist, v. 23, p. 187–193.

Indares, A., White, R.W., and Powell, R., 2008, Phase equilibria modelling of kyanite-bearing anatectic paragneisses from the central Grenville Province: Journal of Metamorphic Geology, v. 26, p. 815–836, https://doi.org/10.1111/j.1525-1314.2008.00788.x.

Ito, E., Takahashi, E., and Matsui, Y., 1984, The mineralogy and chemistry of the lower mantle: an implication of the ultrahigh-pressure phase relations in the system MgO–FeO–SiO_2: Earth and Planetary Science Letters, v. 67, p. 238–248, https://doi.org/10.1016/0012-821X(84)90119-5.

Jamieson, R.A., Beaumont, C., Hamilton, J., and Fullsack, P., 1996, Tectonic assembly of inverted metamorphic sequences: Geology, v. 24, p. 839–842, https://doi.org/10.1130/0091-7613(1996)024<0839:TAOIMS>2.3.CO;2.

Jamieson, R.A., Beaumont, C., Fullsack, P., and Lee, B., 1998, Barrovian regional metamorphism: where's the heat?, *in* Treloar, P.J., and O'Brien, P.J., *eds.*, What Drives Metamorphism and Metamorphic Reactions?: Geological Society, London, Special Publications, v. 138, p. 23–51, https://doi.org/10.1144/GSL.SP.1996.138.01.03.

Jamieson, R.A., Beaumont, C., Medvedev, S., and Nguyen, M.H., 2004, Crustal channel flows: 2. Numerical models with implications for metamorphism in the Himalayan-Tibetan orogen: Journal of Geophysical Research, v. 109, B06407, https://doi.org/10.1029/2003JB002811.

Jamieson, R.A., Beaumont, C., Warren, C.J., and Nguyen, M.H., 2010, The Grenville Orogen explained? Applications and limitations of integrating numerical models with geological and geophysical data: Canadian Journal of Earth Sciences, v. 47, p. 517–539, https://doi.org/10.1139/E09-070.

Jeanneret, P., Goncalves, P., Durand, C., Trap, P., Marquer, D., Quirt, D., and Ledru, P., 2016, Tectono-metamorphic evolution of the pre-Athabasca basement within the Wollaston–Mudjatik Transition Zone, Saskatchewan: Canadian Journal of Earth Sciences, v. 53, p. 231–259, https://doi.org/10.1139/cjes-2015-0136.

Jennings, E.S., and Holland, T.J.B., 2015, A simple thermodynamic model for melting of peridotite in the system NCFMASOCr: Journal of Petrology, v. 56, p. 869–892, https://doi.org/10.1093/petrology/egv020.

Johnson, T.E., White, R.W., and Powell, R., 2008, Partial melting of metagreywacke: a calculated mineral equilibria study: Journal of Metamorphic Geology, v. 26, p. 837–853, https://doi.org/10.1111/j.1525-1314.2008.00790.x.

Johnson, T.E., Benedix, G.K., and Bland, P.A., 2016, Metamorphism and partial melting of ordinary chondrites: Calculated phase equilibria: Earth and Planetary Science Letters, v. 433, p. 21–30, https://doi.org/10.1016/j.epsl.2015.10.035.

Kelemen, P.B., and Hirth, G., 2012, Reaction-driven cracking during retrograde metamorphism: Olivine hydration and carbonation: Earth and Planetary Science Letters, v. 345–348, p. 81–89, https://doi.org/10.1016/j.epsl.2012.06.018.

Kelly, E.D., Carlson, W.D., and Ketcham, R.A., 2013, Magnitudes of departures from equilibrium during regional metamorphism of porphyroblastic rocks: Journal of Metamorphic Geology, v. 31, p. 981–1002, https://doi.org/10.1111/jmg.12053.

Kelsey, D.E., and Hand, M., 2015, On ultrahigh temperature crustal metamorphism: Phase equilibria, trace element thermometry, bulk composition, heat sources, timescales and tectonic settings: Geoscience Frontiers, v. 6, p. 311–356, https://doi.org/10.1016/j.gsf.2014.09.006.

Kelsey, D.E., and Powell, R., 2011, Progress in linking accessory mineral growth and breakdown to major mineral evolution in metamorphic rocks: a thermodynamic approach in the Na_2O–CaO–K_2O–FeO–MgO–Al_2O_3–SiO_2–H_2O–TiO_2–ZrO_2 system: Journal of Metamorphic Geology, v. 29, p. 151–166, https://doi.org/10.1111/j.1525-1314.2010.00910.x.

Kelsey, D.E., Clark, C., and Hand, M., 2008, Thermobarometric modelling of zircon and monazite growth in melt-bearing systems: examples using model metapelitic and metapsammitic granulites: Journal of Metamorphic Geology, v. 26, p. 199–212, https://doi.org/10.1111/j.1525-1314.2007.00757.x.

Kohn, M.J., and Spear, F., 2000, Retrograde net transfer reaction insurance for pressure-temperature estimates: Geology, v. 28, p. 1127–1130, https://doi.org/10.1130/0091-7613(2000)28<1127:RNTRIF>2.0.CO;2.

Kohn, M.J., Corrie, S.L., and Markley, C., 2015, The fall and rise of metamorphic zircon: American Mineralogist, v. 100, p. 897–908, https://doi.org/10.2138/am-2015-5064.

Korhonen, F.J., Powell, R., and Stout, J.H., 2012, Stability of sapphirine + quartz in the oxidized rocks of the Wilson Lake terrane, Labrador: calculated equilibria in NCKFMASHTO: Journal of Metamorphic Geology, v. 30, p. 21–36, https://doi.org/10.1111/j.1525-1314.2011.00954.x.

Lasalle, S., and Indares, A., 2014, Anatectic record and contrasting *P–T* paths of aluminous gneisses from the central Grenville Province: Journal of Metamorphic Geology, v. 32, p. 627–646, https://doi.org/10.1111/jmg.12083.

Mahar, E.M., Baker, J.M., Powell, R., Holland, T.J.B., and Howell, N., 1997, The effect of Mn on mineral stability in metapelites: Journal of Metamorphic Geology, v. 15, p. 223–238, https://doi.org/10.1111/j.1525-1314.1997.00011.x.

Mayne, M.J., Moyen, J.-F., Stevens, G., and Kaislaniemi, L., 2016, Rcrust: a tool for calculating path-dependent open system processes and application to melt loss: Journal of Metamorphic Geology, v. 34, p. 663–682, https://doi.org/10.1111/jmg.12199.

McSween Jr., H.Y., and Labotka, T.C., 1993, Oxidation during metamorphism of the ordinary chondrites: Geochimica et Cosmochimica Acta, v. 57, p. 1105–1114, https://doi.org/10.1016/0016-7037(93)90044-W.

Morrissey, L.J., Hand, M., Lane, K., Kelsey, D.E., and Dutch, R.A., 2016, Upgrading iron-ore deposits by melt loss during granulite facies metamorphism: Ore Geology Reviews, v. 74, p. 101–121, https://doi.org/10.1016/j.oregeorev.2015.11.012.

Mottram, C.M., Warren, C.J., Regis, D., Roberts, N.M.W., Harris, N.B.W., Argles, T.W., and Parrish, R.R., 2014, Developing an inverted Barrovian sequence; insights from monazite petrochronology: Earth and Planetary Science Letters, v. 403, p. 418–431, https://doi.org/10.1016/j.epsl.2014.07.006.

Moynihan, D.P., and Pattison, D.R.M., 2013, An automated method for the calculation of *P–T* paths from garnet zoning, with application to metapelitic schist from the Kootenay Arc, British Columbia, Canada: Journal of Metamorphic Geology, v. 31, p. 525–548, https://doi.org/10.1111/jmg.12032.

O'Brien, P.J., 2008, Challenges in high-pressure granulite metamorphism in the era of pseudosections: reaction textures, compositional zoning and tectonic interpretation with examples from the Bohemian Massif: Journal of Metamorphic Geology, v. 26, p. 235–251, https://doi.org/10.1111/j.1525-1314.2007.00758.x.

Palin, R.M., Weller, O.M., Waters, D.J., and Dyck, B., 2016a, Quantifying geological uncertainty in metamorphic phase equilibria modelling; a Monte Carlo assessment and implications for tectonic interpretations: Geoscience Frontiers, v. 7, p. 591–607, https://doi.org/10.1016/j.gsf.2015.08.005.

Palin, R.M., White, R.W., Green, E.C.R., Diener, J.F.A., Powell, R., and Holland, T.J.B., 2016b, High-grade metamorphism and partial melting of basic and intermediate rocks: Journal of Metamorphic Geology, v. 34, p. 871–892, https://doi.org/10.1111/jmg.12212.

Pattison, D., and Harte, B., 1985, A petrogenetic grid for pelites in the Ballachulish and other Scottish thermal aureoles: Journal of the Geological Society, v. 142, p. 7–28, https://doi.org/10.1144/gsjgs.142.1.0007.

Pattison, D.R.M., and Bégin, N.J., 1994, Zoning patterns in orthopyroxene and garnet in granulites: implications for geothermometry: Journal of Metamorphic Geology, v. 12, p. 387–410, https://doi.org/10.1111/j.1525-1314.1994.tb00031.x.

Pattison, D.R.M., and DeBuhr, C.L., 2015, Petrology of metapelites in the Bugaboo aureole, British Columbia, Canada: Journal of Metamorphic Geology, v. 33, p. 437–462, https://doi.org/10.1111/jmg.12128.

Pattison, D.R.M., and Seitz, J.D., 2012, Stabilization of garnet in metamorphosed altered turbidites near the St. Eugene lead–zinc deposit, southeastern British

Columbia: Equilibrium and kinetic controls: Lithos, v. 134–135, p. 221–235, https://doi.org/10.1016/j.lithos.2011.12.007.
Pattison, D.R.M., and Tinkham, D.K., 2009, Interplay between equilibrium and kinetics in prograde metamorphism of pelites: an example from the Nelson aureole, British Columbia: Journal of Metamorphic Geology, v. 27, p. 249–279, https://doi.org/10.1111/j.1525-1314.2009.00816.x.
Pattison, D.R.M., Spear, F.S., Debuhr, C.L., Cheney, J.T., and Guidotti, C.V., 2002, Thermodynamic modelling of the reaction muscovite+cordierite→ Al_2SiO_5+biotite+quartz+H_2O: constraints from natural assemblages and implications for the metapelitic petrogenetic grid: Journal of Metamorphic Geology, v. 20, p. 99–118, https://doi.org/10.1046/j.0263-4929. 2001.356.356.x.
Pattison, D.R.M., Chacko, T., Farquhar, J., and McFarlane, C.R.M., 2003, Temperatures of granulite-facies metamorphism: Constraints from experimental phase equilibria and thermobarometry corrected for retrograde exchange: Journal of Petrology, v. 44, p. 867–900, https://doi.org/10.1093/petrology/44.5.867.
Pattison, D.R.M., de Capitani, C., and Gaidies, F., 2011, Petrological consequences of variations in metamorphic reaction affinity: Journal of Metamorphic Geology, v. 29, p. 953–977, https://doi.org/10.1111/j.1525-1314.2011.00950.x.
Pearce, M.A., White, A.J.R., and Gazley, M.F., 2015a, TCInvestigator: automated calculation of mineral mode and composition contours for THERMOCALC pseudosections: Journal of Metamorphic Geology, v. 33, p. 413–425, https://doi.org/10.1111/jmg.12126.
Pearce, M.A., White, A.J.R., Fisher, L.A., Hough, R.M., and Cleverley, J.S., 2015b, Gold deposition caused by carbonation of biotite during late-stage fluid flow: Lithos, v. 239, p. 114–127, https://doi.org/10.1016/j.lithos.2015.10.010.
Phillips, G.N., and Powell, R., 2010, Formation of gold deposits: a metamorphic devolatilization model: Journal of Metamorphic Geology, v. 28, p. 689–718, https://doi.org/10.1111/j.1525-1314.2010.00887.x.
Powell, R., 1978, Equilibrium Thermodynamics in Petrology, An Introduction: Harper & Row Ltd, London, 284 p.
Powell, R., 1985, Geothermometry and geobarometry: a discussion: Journal of the Geological Society, v. 142, p. 29–38, https://doi.org/10.1144/gsjgs.142.1.0029.
Powell, R., 1991, Metamorphic Mineral Equilibria Short Course: Course Notes: University of Melbourne. Available from: http://www.metamorph.geo.uni-mainz.de/thermocalc/documentation/introphasediagrams/index.html.
Powell, R., and Holland, T.J.B., 1988, An internally consistent dataset with uncertainties and correlations: 3. Applications to geobarometry, worked examples and a computer program: Journal of Metamorphic Geology, v. 6, p. 173–204, https://doi.org/10.1111/j.1525-1314.1988.tb00415.x.
Powell, R., and Holland, T.J.B., 2008, On thermobarometry: Journal of Metamorphic Geology, v. 26, p. 155–179, https://doi.org/10.1111/j.1525-1314.2007.00756.x.
Powell, R., Holland, T., and Worley, B., 1998, Calculating phase diagrams involving solid solutions via non-linear equations, with examples using THERMOCALC: Journal of Metamorphic Geology, v. 16, p. 577–588, https://doi.org/10.1111/j.1525-1314.1998.00157.x.
Powell, R., Guiraud, M., and White, R.W., 2005, Truth and beauty in metamorphic phase-equilibria: conjugate variables and phase diagrams: The Canadian Mineralogist, v. 43, p. 21–33, https://doi.org/10.2113/gscanmin.43.1.21.
Ridley, J., and Thompson, A.B., 1986, The role of mineral kinetics in the development of metamorphic microtexture, *in* Walther, J.V., and Wood, B.J., *eds.*, Fluid-Rock Interactions During Metamorphism: Springer, New York, p. 154–193.
Riesco, M., Stüwe, K., Reche, J., and Martinez, F.J., 2004, Silica depleted melting of pelites. Petrogenetic grid and application to the Susqueda Aureole, Spain: Journal of Metamorphic Geology, v. 22, p. 475–494, https://doi.org/10.1111/j.1525-1314.2004.00527.x.
Riesco, M., Stüwe, K., and Reche, J., 2005, Formation of corundum in metapelites around ultramafic bodies. An example from the Saualpe region, Eastern Alps: Mineralogy and Petrology, v. 83, p. 1–25, https://doi.org/10.1007/s00710-004-0062-4.
Rosenberg, C.L., and Handy, M.R., 2005, Experimental deformation of partially melted granite revisited: implications for the continental crust: Journal of Metamorphic Geology, v. 23, p. 19–28, https://doi.org/10.1111/j.1525-1314.2005.00555.x.
Rubatto, D., Williams, I.S., and Buick, I.S., 2001, Zircon and monazite response to prograde metamorphism in the Reynolds Range, central Australia: Contributions to Mineralogy and Petrology, v. 140, p. 458–468, https://doi.org/10.1007/PL00007673.
Rubie, D.C., 1998, Disequilibrium during metamorphism: the role of nucleation kinetics, *in* Treloar, P.J., and O'Brien, P.J., *eds.*, What Drives Metamorphism and Metamorphic Reactions?: Geological Society, London, Special Publications, v. 138, p. 199–214, https://doi.org/10.1144/GSL.SP.1996.138.01.12.
Schaltegger, U., 2007, Hydrothermal Zircon: Elements, v. 3, p. 51–79, https://doi.org/10.2113/gselements.3.1.51.
Skora, S., Blundy, J.D., Brooker, R.A., Green, E.C.R., de Hoog, J.C.M., and Connolly, J.A.D., 2015, Hydrous phase relations and trace element partitioning behaviour in calcareous sediments at subduction-zone conditions: Journal of Petrology, v. 56, p. 953–980, https://doi.org/10.1093/petrology/egv024.
Spear, F.S., 1995, Metamorphic phase equilibria and Pressure–Temperature–Time paths: Mineralogical Society of America, Washington, DC, 799 p.
Spear, F.S., 2010, Monazite–allanite phase relations in metapelites: Chemical Geology, v. 279, p. 55–62, https://doi.org/10.1016/j.chemgeo.2010.10.004.
Spear, F.S., and Cheney, J.T., 1989, A petrogenetic grid for pelitic schists in the system SiO_2–Al_2O_3–FeO–MgO–K_2O–H_2O: Contributions to Mineralogy and Petrology, v. 101, p. 149–164, https://doi.org/10.1007/BF00375302.
Spear, F.S., and Florence, F.P., 1992, Thermobarometry in granulites: pitfalls and new approaches: Precambrian Research, v. 55, p. 209–241, https://doi.org/10.1016/0301-9268(92)90025-J.
Spear, F.S., and Pyle, J.M., 2010, Theoretical modeling of monazite growth in a low-Ca metapelite: Chemical Geology, v. 273, p. 111–119, https://doi.org/10.1016/j.chemgeo.2010.02.016.
Spear, F.S., Kohn, M.J., and Cheney, J.T., 1999, *P–T* paths from anatectic pelites: Contributions to Mineralogy and Petrology, v. 134, p. 17–32, https://doi.org/10.1007/s004100050466.
Spear, F.S., Pattison, D.R.M., and Cheney, J.T., 2016, The metamorphosis of metamorphic petrology: Geological Society of America Special Papers, v. 523, p. SPE523-02, https://doi.org/10.1130/2016.2523(02).
Stepanov, A.S., Hermann, J., Rubatto, D., and Rapp, R.P., 2012, Experimental study of monazite/melt partitioning with implications for the REE, Th and U geochemistry of crustal rocks: Chemical Geology, v. 300–301, p. 200–220, https://doi.org/10.1016/j.chemgeo.2012.01.007.
Stevens, L.M., Baldwin, J.A., Cottle, J.M., and Kylander-Clark, A.R.C., 2015, Phase equilibria modelling and LASS monazite petrochronology: *P–T–t* constraints on the evolution of the Priest River core complex, northern Idaho: Journal of Metamorphic Geology, v. 33, p. 385–411, https://doi.org/10.1111/jmg.12125.
Stixrude, L., and Lithgow-Bertelloni, C., 2005, Thermodynamics of mantle minerals — I. Physical properties: Geophysical Journal International, v. 162, p. 610–632, https://doi.org/10.1111/j.1365-246X.2005.02642.x.
Stixrude, L., and Lithgow-Bertelloni, C., 2007, Influence of phase transformations on lateral heterogeneity and dynamics in Earth's mantle: Earth and Planetary Science Letters, v. 263, p. 45–55, https://doi.org/10.1016/j.epsl.2007.08.027.
Stixrude, L., and Lithgow-Bertelloni, C., 2011, Thermodynamics of mantle minerals - II. Phase equilibria: Geophysical Journal International, v. 184, p. 1180–1213, https://doi.org/10.1111/j.1365-246X.2010.04890.x.
Stüwe, K., and Powell, R., 1995, *PT* Paths from modal proportions: application to the Koralm Complex, Eastern Alps: Contributions to Mineralogy and Petrology, v. 119, p. 83–93, https://doi.org/10.1007/BF00310719.
Symmes, G.H., and Ferry, J.M., 1992, The effect of whole-rock MnO content on the stability of garnet in pelitic schists during metamorphism: Journal of Metamorphic Geology, v. 10, p. 221–237, https://doi.org/10.1111/j.1525-1314.1992.tb00080.x.
Thompson, A.B., and Algor, J.R., 1977, Model systems for anatexis of pelitic rocks: Contributions to Mineralogy and Petrology, v. 63, p. 247–269, https://doi.org/10.1007/BF00375575.
Thompson, A.B., and England, P.C., 1984, Pressure—Temperature—Time paths of regional metamorphism II. Their inference and interpretation using mineral assemblages in metamorphic rocks: Journal of Petrology, v. 25, p. 929–955, https://doi.org/10.1093/petrology/25.4.929.
Thompson, A.B., and Tracy, R.J., 1979, Model systems for anatexis of pelitic rocks: Contributions to Mineralogy and Petrology, v. 70, p. 429–438, https://doi.org/10.1007/BF00371049.
Thompson, J.B., 1957, The graphical analysis of mineral assemblages in pelitic schists: American Mineralogist, v. 42, p. 842–858.
Tinkham, D.K., and Ghent, E.D., 2005, Estimating *P–T* conditions of garnet growth with isochemical phase-diagram sections and the problem of effective bulk-composition: The Canadian Mineralogist, v. 43, p. 35–50, https://doi.org/10.2113/gscanmin.43.1.35.
Tinkham, D.K., Zuluaga, C.A., and Stowell, H.H., 2003, Metapelite phase equilibria modeling in MnNCKFMASH: The effect of variable Al_2O_3 and MgO/(MgO + FeO) on mineral stability: American Mineralogist, v. 88, p. 1174–1174.
Tomkins, A.G., and Evans, K.A., 2015, Separate zones of sulfate and sulfide release from subducted mafic oceanic crust: Earth and Planetary Science Letters, v. 428, p. 73–83, https://doi.org/10.1016/j.epsl.2015.07.028.
Vernon, R.H., and Clarke, G.L., 2008, Principles of Metamorphic Petrology: Cambridge University Press, 478 p.
Vernon, R.H., White, R.W., and Clarke, G.L., 2008, False metamorphic events

inferred from misinterpretation of microstructural evidence and *P–T* data: Journal of Metamorphic Geology, v. 26, p. 437–449, https://doi.org/10.1111/j.1525-1314.2008.00762.x.

Vigneresse, J.L., and Burg, J.P., 2000, Continuous vs. discontinuous melt segregation in migmatites: insights from a cellular automaton model: Terra Nova, v. 12, p. 188–192, https://doi.org/10.1046/j.1365-3121.2000.00299.x.

Vry, J.K., Powell, R., and Williams, J., 2008, Establishing the *P–T* path for Alpine Schist, Southern Alps near Hokitika, New Zealand: Journal of Metamorphic Geology, v. 26, p. 81–97, https://doi.org/10.1111/j.1525-1314.2007.00746.x.

Waters, D.J., and Lovegrove, D.P., 2002, Assessing the extent of disequilibrium and overstepping of prograde metamorphic reactions in metapelites from the Bushveld Complex aureole, South Africa: Journal of Metamorphic Geology, v. 20, p. 135–149, https://doi.org/10.1046/j.0263-4929.2001.00350.x.

White, A.J.R., Waters, D.J., and Robb, L.J., 2013, The application of *P–T–X*(CO_2) modelling in constraining metamorphism and hydrothermal alteration at the Damang gold deposit, Ghana: Journal of Metamorphic Geology, v. 31, p. 937–961, https://doi.org/10.1111/jmg.12051.

White, A.J.R., Legras, M., Smith, R.E., and Nadoll, P., 2014c, Deformation-driven, regional-scale metasomatism in the Hamersley Basin, Western Australia: Journal of Metamorphic Geology, v. 32, p. 417–433, https://doi.org/10.1111/jmg.12078.

White, R.W., and Powell, R., 2002, Melt loss and the preservation of granulite facies mineral assemblages: Journal of Metamorphic Geology, v. 20, p. 621–632, https://doi.org/10.1046/j.1525-1314.2002.00206_20_7.x.

White, R.W., Powell, R., and Phillips, G.N., 2003, A mineral equilibria study of the hydrothermal alteration in mafic greenschist facies rocks at Kalgoorlie, Western Australia: Journal of Metamorphic Geology, v. 21, p. 455–468, https://doi.org/10.1046/j.1525-1314.2003.00454.x.

White, R.W., Powell, R., and Halpin, J.A., 2004, Spatially-focussed melt formation in aluminous metapelites from Broken Hill, Australia: Journal of Metamorphic Geology, v. 22, p. 825–845, https://doi.org/10.1111/j.1525-1314.2004.00553.x.

White, R.W., Pomroy, N.E., and Powell, R., 2005, An *in situ* metatexite–diatexite transition in upper amphibolite facies rocks from Broken Hill, Australia: Journal of Metamorphic Geology, v. 23, p. 579–602, https://doi.org/10.1111/j.1525-1314.2005.00597.x.

White, R.W., Powell, R., and Holland, T.J.B., 2007, Progress relating to calculation of partial melting equilibria for metapelites: Journal of Metamorphic Geology, v. 25, p. 511–527, https://doi.org/10.1111/j.1525-1314.2007.00711.x.

White, R.W., Powell, R., Holland, T.J.B., Johnson, T.E., and Green, E.C.R., 2014a, New mineral activity–composition relations for thermodynamic calculations in metapelitic systems: Journal of Metamorphic Geology, v. 32, p. 261–286, https://doi.org/10.1111/jmg.12071.

White, R.W., Powell, R., and Johnson, T.E., 2014b, The effect of Mn on mineral stability in metapelites revisited: new *a–x* relations for manganese-bearing minerals: Journal of Metamorphic Geology, v. 32, p. 809–828, https://doi.org/10.1111/jmg.12095.

Whitney, D.L., Teyssier, C., Rey, P., and Buck, W.R., 2013, Continental and oceanic core complexes: Geological Society of America Bulletin, v. 125, p. 273–298, https://doi.org/10.1130/B30754.1.

Will, T.M., Powell, R., and Holland, T.J.B., 1990, A calculated petrogenetic grid for ultramafic rocks in the system CaO–FeO–MgO–Al_2O_3–SiO_2–CO_2–H_2O at low pressures: Contributions to Mineralogy and Petrology, v. 105, p. 347–358, https://doi.org/10.1007/BF00306544.

Wing, B.A., Ferry, J.M., and Harrison, T.M., 2003, Prograde destruction and formation of monazite and allanite during contact and regional metamorphism of pelites: petrology and geochronology: Contributions to Mineralogy and Petrology, v. 145, p. 228–250, https://doi.org/10.1007/s00410-003-0446-1.

Yakymchuk, C., 2017, Behaviour of apatite during partial melting of metapelites and consequences for prograde suprasolidus monazite growth: Lithos, v. 274–275, p. 421–426, https://doi.org/10.1016/j.lithos.2017.01.009.

Yakymchuk, C., and Brown, M., 2014a, Consequences of open-system melting in tectonics: Journal of the Geological Society, v. 171, p. 21–40, https://doi.org/10.1144/jgs2013-039.

Yakymchuk, C., and Brown, M., 2014b, Behaviour of zircon and monazite during crustal melting: Journal of the Geological Society, v. 171, p. 465–479, https://doi.org/10.1144/jgs2013-115.

Yakymchuk, C., Brown, M., Clark, C., Korhonen, F.J., Piccoli, P.M., Siddoway, C.S., Taylor, R.J.M., and Vervoort, J.D., 2015, Decoding polyphase migmatites using geochronology and phase equilibria modelling: Journal of Metamorphic Geology, v. 33, p. 203–230, https://doi.org/10.1111/jmg.12117.

Yakymchuk, C., Clark, C., and White, R.W., 2017, Phase relations, reaction sequences and petrochronology: Reviews in Mineralogy and Geochemistry, (in press), https://doi.org/10.2138/rmg.2017.83.2.

Zen, E-A., 1966, Construction of pressure-temperature diagrams for multicomponent systems after the method of Schreinemakers–A geometric approach: USGS Bulletin 1225, 56 p.

Zuluaga, C.A., Stowell, H.H., and Tinkham, D.K., 2005, The effect of zoned garnet on metapelite pseudosection topology and calculated metamorphic *P–T* paths: American Mineralogist, v. 90, p. 1619–1628, https://doi.org/10.2138/am.2005.1741.

Received November 2016
Accepted as revised February 2017
First published on the web February 2017

ARTICLE

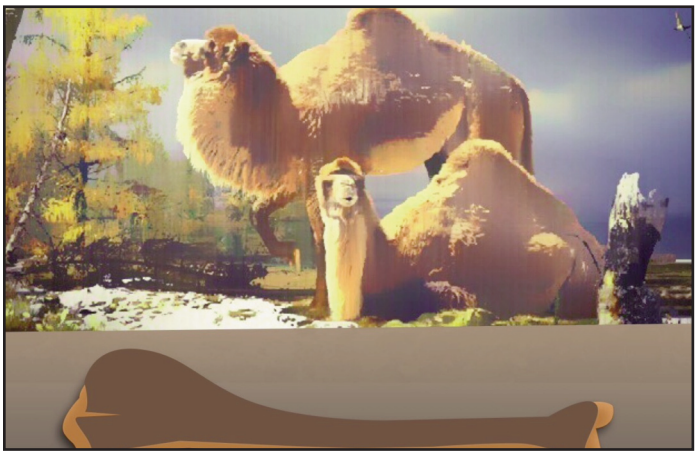

PoLAR-FIT: Pliocene Landscapes and Arctic Remains—Frozen in Time

J.C. Gosse[1], A.P. Ballantyne[2], J.D. Barker[3,4], A.Z. Csank[5], T.L. Fletcher[2], G.W. Grant[4], D.R. Greenwood[6], R.D.E. MacPhee[7] and N. Rybczynski[8]

[1]*Department of Earth Sciences, Dalhousie University*
1459 Oxford St, Halifax, Nova Scotia, B3H 4R2, Canada
Email: john.gosse@dal.ca

[2]*College of Forestry and Conservation, University of Montana*
32 Campus Drive, Missoula, Montana, 59801, U.S.A.

[3]*School of Earth Sciences, The Ohio State University*
Marion, Ohio, 43302, U.S.A.

[4]*Byrd Polar and Climate Research Centre*
Columbus, Ohio, 43210, U.S.A.

[5]*Department of Geography at the University of Nevada Reno*
1664 N Virginia Street, Reno, Nevada, 89557, U.S.A.

[6]*Department of Biology, Brandon University*
270 18th Street, Brandon, Manitoba, R7A 6A9, Canada

[7]*Department of Mammalogy, Division of Vertebrate Zoology*
American Museum of Natural History,
Central Park West at 79th Street
New York, New York, 10024-5192, U.S.A.

[8]*Canadian Museum of Nature*
PO Box 3443, Station D, Ottawa, Ontario, K1P 6P4, Canada

SUMMARY

This short summary presents selected results of an ongoing investigation into the feedbacks that contribute to amplified Arctic warming. The consequences of warming for Arctic biodiversity and landscape response to global warmth are currently being interpreted. Arctic North American records of large-scale landscape and paleoenvironmental change during the Pliocene are exquisitely preserved and locked in permafrost, providing an opportunity for paleoenvironmental and faunal reconstruction with unprecedented quality and resolution. During a period of mean global temperatures only ~2.5°C above modern, the Pliocene molecular, isotopic, tree-ring, paleofaunal, and paleofloral records indicate that the High Arctic mean annual temperature was 11–19°C above modern values, pointing to a much shallower latitudinal temperature gradient than exists today. It appears that the intense Neogene warming caused thawing and weathering to liberate sediment and create a continuous and thick (>2.5 km in places) clastic wedge, from at least Banks Island to Meighen Island, to form a coastal plain that provided a highway for camels and other mammals to migrate and evolve in the High Arctic. In this summary, we highlight the opportunities that exist for research on these and related topics with the *PoLAR-FIT* community.

RÉSUMÉ

Ce bref résumé présente les résultats choisis d'une enquête en cours sur les déclencheurs qui contribuent à l'amplification du réchauffement de l'Arctique. Les conséquences du réchauffement sur la biodiversité arctique et de la réponse du paysage au réchauffement climatique sont en cours d'être interprété. Des dossiers nord-américains de paysage à grande échelle et le changement paléoenvironnementales durant le Pliocène sont exceptionnellement préservés et scellées dans un état de congélation qui fournissant une occasion pour la reconstruction paléoenvironnementale et faunistique avec une qualité et une résolution sans précédent. Pendent une période de réchauffement global seulement ~2,5°C au-dessus de moderne les dossiers, moléculaire, isotopique, annaux de croissance, paléofaunistique et paléovégétation indiquent que l'Arctique a connu une augmentation de la température annuelle moyenne de 11–19°C au-dessus de moderne, en montrant un inferieur gradient de température latitudinal qu'aujourd'hui. Il semble que le réchauffement intense pendent le Néogène a provoqué la décongélation et erosion pour libérer les sédiments et créer une plaine côtière continuel et épaisse (> 2,5 km dans lieux) qui a fourni une route pour les chameaux et autres mam-

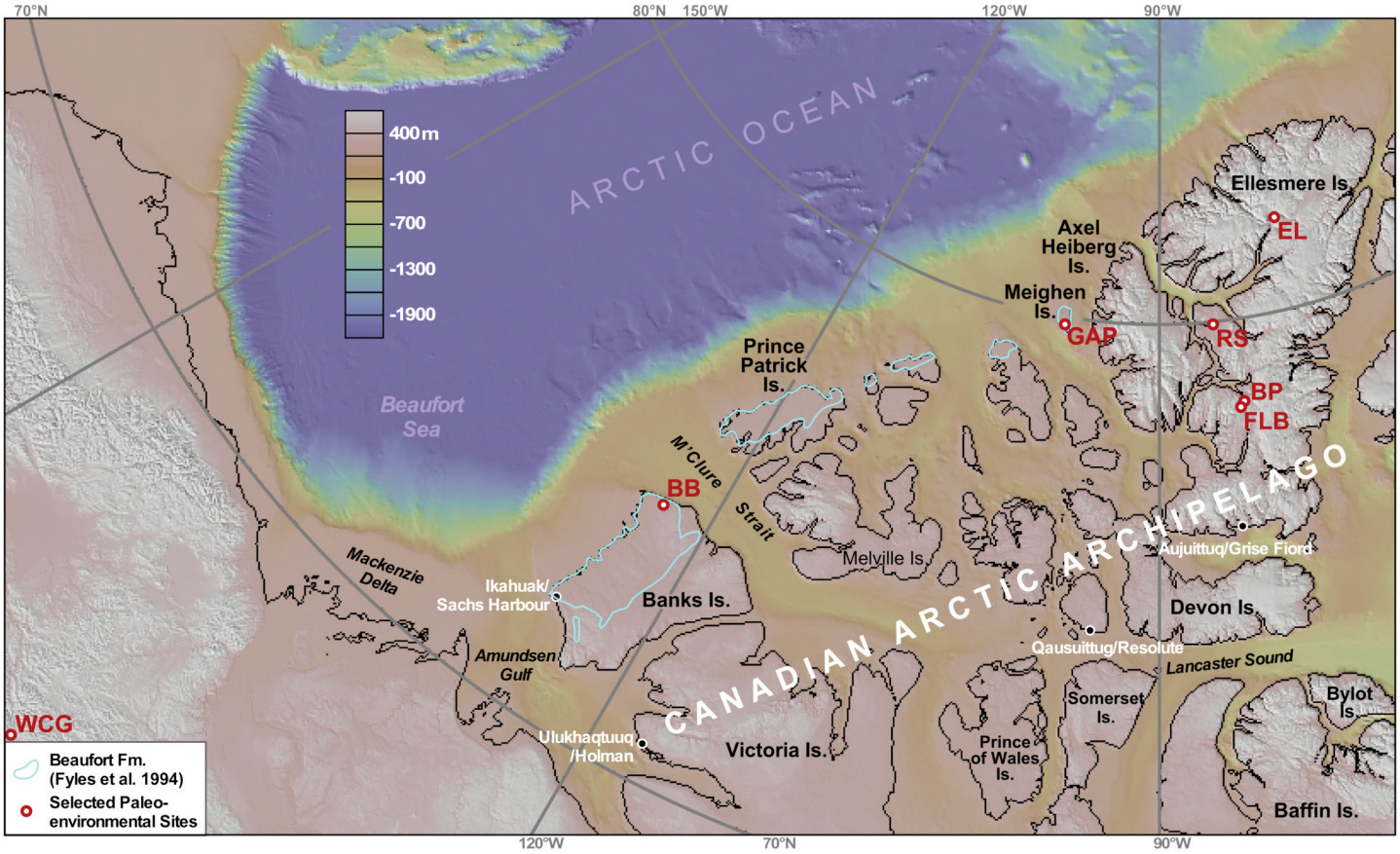

Figure 1. Map of Arctic North America with geographic features described in the text. Previous '*Pliocene Landscape and Arctic Remains—Frozen In Time*', (*PoLAR-FIT*) sites include: BP –Beaver Pond, BB –Ballast Brook, EL –Ekblaw Lake, FLB –Fyles Leaf Bed, GAP –'The Gap' on Meighen Island, RS –Remus Section, WCG –White Channel Gravel in the Klondike District, Yukon. The blue outline represents the modern onshore distribution of Beaufort Formation (Fyles et al. 1994). The original Beaufort Formation has been interpreted by others to have formed a continuous Arctic Coastal Plain from Banks Island to Meighen Island, and possibly from the Mackenzie Delta to beyond Axel Heiberg Island. North Polar Projection DEM constructed with GEOMAPAPP v 3.6.4 using International Bathymetric Chart of the Arctic Ocean v 3, 30 arc-second resolution.

mifères pour migrer et évoluer dans l'Haut-Arctique. Dans ce résumé, nous soulignons les opportunités qui existent pour la recherche sur ces sujets et les sujets connexes avec la communauté *PoLAR-FIT*.

INTRODUCTION

Today's thawing of permanently frozen Pliocene clastic sediments and organic layers in Arctic Canada and Alaska (Fig. 1) provides access to exquisitely preserved, sub-fossilized floral, faunal, molecular, and isotopic records. These records document amplification of temperature change in polar regions (e.g. Ballantyne et al. 2013) during periods of global warmth on the magnitude predicted for our next century (Masson-Delmotte et al. 2013). The Pliocene sediments exposed onshore, including the Beaufort Formation, span a variety of depositional environments (marine, lacustrine, paludal, alluvial, fluvial, and possibly glacial) over a wide temporal range (ca. 3.8 to 2.6 Ma; see later discussion of Geochronology), including varves and possible annual couplets of sand and leaf layers spanning a millennium. Until recently (e.g. Feng et al. 2017) numerical models of Pliocene climate were unable to reproduce the high paleo-temperatures in the High Arctic while reliably replicating low-latitude temperature proxies (Salzmann et al. 2013). The collective record suggests that there may be feedbacks that are not adequately represented by the models. Temperature, humidity, CO_2, and continentality may be controlled by factors such as different forest types and densities, sea-ice cover, the effects of forest fires, and the possibility that ocean circulation through the High Arctic was limited until the Beaufort Formation was incised and the Northwest Passages were opened. Despite the discovery of well-preserved wood by explorers on Banks Island 150 years ago (Heer 1868), the paleoenvironmental and paleoclimate research is still in its infancy and the biochronostratigraphy is too imprecise to test synchroneity and reconcile the disparities among the sites. Furthermore, accelerated processes such as retrogressive thaw slumping is rapidly removing or exposing previously entombed sedimentary, macrofossil, and biochemical records before they can be examined within their stratigraphic context.

To tackle these challenges, an international multidisciplinary team has assembled with the shared objective of studying these systems in an integrated way. The represented disciplines include paleoclimatology, geomorphology, geochronology, biogeochemistry, dendroclimatology, floral and faunal paleon-

tology, evolutionary biology, and landscape ecology. Members of the '*Pliocene Landscape and Arctic Remains—Frozen In Time*', or *PoLAR-FIT* working group span from early-career to senior scientists, some of whom have worked on the Pliocene records over the past four decades (Table 1 lists the founding members, but we hope that others will join).

The initial goals of *PoLAR-FIT* are to maximize synergy, minimize the prohibitive costs of fieldwork in the Arctic, and expedite progress toward common research objectives that will have the immediate and broadest impact on the global community. This article provides a short review and outline of past and planned *PoLAR-FIT* research and highlights the many opportunities for other scientists to contribute and join.

PROGRESS IN PLIOCENE ARCTIC PALEO-ENVIRONMENTAL RESEARCH

The Floral Record

The Pliocene Arctic and sub-Arctic were characterized by both a more northerly position of the tree line compared to today (e.g. the limit was ~80°N on Meighen Island, compared to ~69–61°N in the western Arctic or 56°N in Labrador [e.g. Tozer and Thorsteinsson 1964; Hills 1975; Matthews 1987; Fyles et al. 1991]) and, consequently, a broader latitudinal extent of the Boreal zone. Based on pollen and plant macrofossils a flora more diverse than a modern boreal forest was found for the Pliocene units, including 80–90 species of non-vascular plants and 90 different species of vascular plants. The taxonomic and comparative studies of these flora represent a substantial legacy inherited by the group (e.g. Matthews and Ovenden 1990; Matthews and Fyles 2000; Fletcher et al. 2017). Included in this list are 12 different tree taxa identified from leaves or reproductive parts including, larch (*Larix*), birch (*Betula*), spruce (*Picea*), hemlock (*Tsuga*), pine (*Pinus*), alder (*Alnus*), poplar (*Populus*), and fir (*Abies*) (e.g. Matthews and Ovenden 1990; Ballantyne et al. 2010). Wood found in many of the fossil forest sites has been identified as larch (*Larix*), spruce (*Picea*), pine (*Pinus*) and birch (*Betula*) (e.g. Matthews and Ovenden 1990; Csank et al. 2011a). Based on plant abundances Matthews and Ovenden (1990) concluded that the flora is closely similar to modern Asian forests rather than to a typical North American boreal forest, and more recent workers support this conclusion (Ballantyne et al. 2010; Csank et al. 2011a). Elements of modern-character tundra communities were also already in place both within boreal communities, and potentially at higher latitudes (Matthews and Ovenden 1990; Matthews and Fyles 2000). The woody elements of the flora are conspicuously well preserved in some areas (Devaney 1991; Davies et al. 2013) (Fig. 2) and present a rare but significant opportunity to construct overlapping annual sequences with tree ring records (e.g. Csank et al. 2013). Extensive peat deposits (Mitchell et al. 2016) record long, environmentally sensitive floral sequences from pollen, seeds, needles, cones, leaves (Fig. 3), flowers, and mosses. The flora can often be identified to modern genera and in some cases species, permitting precise climate and vegetation reconstructions (e.g. Ballantyne et al. 2010). In addition, these same deposits preserve faunal remains ranging from terrestrial (e.g. beetles) and aquatic invertebrates (e.g. Fyles et al. 1991; Elias and Matthews 2002) to the vertebrate inhabitants of these Arctic forests (e.g. Rybczynski et al. 2013).

Table 1. Founding *PoLAR-FIT* members.

Ballantyne, A.	University of Montana
Barendregt, R.	Lethbridge University
Barker, J.	Byrd Polar and Climate Research Centre
Braschi, L.	Dalhousie University
Brigham-Grette, J.	University of Massachusetts
Csank, A.	University Nevada, Reno
Fletcher, T.	University of Montana
Fortier, D.	University of Montreal
Froese, D.	University of Alberta
Gilbert, M.	Canadian Museum of Nature
Gosse, J.	Dalhousie University
Grant, G.	Byrd Polar and Climate Research Centre
Greenwood, D.	Brandon University
Harington, C.R.	Canadian Museum of Nature (Emeritus)
Lakeman, T.	Norwegian Geological Survey
Manion, P.	Dalhousie University
Matthews, J.	Geological Survey of Canada (Retired)
McPhee, R.	American Museum of Natural History
Rybczynski, N.	Canadian Museum of Nature; Carleton University
Smith, R.	University of Calgary
Telka, A.	Paleotec Services
West, C.	University of Saskatchewan
Zazula, G.	Yukon Geological Survey

Vertebrate Paleontology

Currently, the record of Pliocene vertebrates from the High Arctic is known almost entirely from sites on Ellesmere Island, notably the Beaver Pond site (Fig. 1) near the head of Strathcona Fiord. Elsewhere, isolated bone fragments of possible Pliocene age have been found on Banks Island (by the co-authors in 2013) and Meighen Island (by the co-authors in 2010) but remain under investigation (Fig. 1). Decades of field excavations from Beaver Pond have yielded a boreal forest community with no modern analogue. The assemblage is more diverse than modern treeline communities and includes fossil bear, horse, deerlet, rabbit, various small carnivores, shrew, beaver, fish, scaup duck and frog (Tedford and Harington 2003; Mitchell et al. 2016). Many fossils from the site represent new taxa, including the fish (*Sander taneri*), badger (*Arctomeles sotnikovae*), shrew (*Arctisorex polaris*), and deerlet (*Boreameryx braskerudi*) (Hutchison and Harington 2002; Tedford and Harington 2003; Dawson and Harington 2007; Murray et al. 2009). The deerlet is notable because it appears to be derived from an early branch of the deer lineage; however, its dentition is highly specialized, suggesting high latitude endemism.

Owing to the geographical remoteness of Ellesmere Island (Fig. 1) and its Pliocene fossils, the closest fossil communities of similar age available for comparisons are in Northeastern China and Idaho. Most taxa, such as the badger and horse (*Plesiohipparion*) show closest affinities to Pliocene fossil vertebrates of the Yushe Basin, China, whereas the rabbit (*Hypolagus*) and dog (*Eucyon*) represent lineages that originated in

https://doi.org/10.12789/geocanj.2017.44.116

Figure 2. A sub-fossil stick, long held in permafrost, exposes at its end the characteristic cut-marks made by the lower front teeth of the Pliocene beaver *Dipoides sp.* (photo credit: M. Lipman).

Figure 3. An ancient leaf protrudes from the slope where the enclosing sands have eroded as the permafrost face thaws (photo credit: M. Lipman).

North America. The Beaver Pond bear represents a species (*"Ursus" abstrusus*) also collected in Idaho, although the lineage originates in Eurasia (Tedford and Harington 2003). In recent years, fragments of fossil bone (Fig. 4) collected from the nearby Fyles Leaf Bed site belong to a giant camel, possibly *Paracamelus*, of North American lineage (Rybczynski et al. 2013) (Fig. 5). Significantly, taxonomic identification of the bone fragments as camel was aided by collagen fingerprinting. The discovery that these ~3.5 Ma fossils preserve collagen, a structural protein that makes up about 80% of the organic fraction of mammal bones is remarkable, providing a foundation for future ecological and taxonomic investigations.

Sedimentary Records of Landscape Responses to Climate Change

The Pliocene records described above were recovered from onshore exposures of the Beaufort Formation (from Banks

Figure 4. Fossil remains of an Arctic giant camel – lateral view of right tibia specimen (NUFV 210), from Fyles Leaf Bed (FLB) site, Strathcona Fiord (Ellesmere Island), shown within the tibia of a modern camel (*Camelus dromedaries*, ROM MAM 94191). The modern *Camelus* tibia has been scaled up 30% to match the size of the fossil tibia. Scale bar, 10 cm. (From Rybczynski et al. 2013: figure 3).

Figure 5. Mid-Pliocene camels prepare for the long dark winter along a shallow river channel in a beaver-cut larch and birch-dominated taiga forest, 100 km southeast of what is now the Eureka weather station, Ellesmere Island (digital image, J. Csotonyi).

Island to Meighen Island) or correlative deposits (e.g. on Ellesmere Island). Previous and ongoing efforts have focused on characterizing the depositional environments that contain the organic remains. The Beaufort Formation was originally described by Tozer (1956) but most recently defined by Fyles et al. (1994) as outcrops along the western Canadian Arctic Archipelago (Fig. 1). The Beaufort Formation formed the Arctic Coastal Plain (e.g. Devaney 1991) which is the uppermost unit of the Arctic Continental Terrace Wedge (Trettin 1989). The braided-stream deposit extends into a thick (up to 3 km) clastic wedge offshore. The marine extension of the clastic

wedge is the Iperk Formation and estuarine sediments are recognized onshore in the Beaufort Formation (England 1987; Fyles 1990; McNeil et al. 2001). Fyles et al. (1994) and others before documented sites at other locations, such as high terraces and alluvial fans throughout Ellesmere Island, which have a similar age and faunal and floral record, but a different depositional environment from the braided stream coastal plain Beaufort Formation sediments. The various depositional environments inform the paleoenvironmental reconstruction and the sedimentary architectural elements provide a sense of duration at single exposures. For instance, at the base of the Fyles Leaf Bed section (Fig. 1), varved lake sediments containing dropstones underlie hundreds of rhythmic beds of sand–leaf layer couplets interpreted to represent shallow overbank and crevasse splay deposits adjacent to a distributary sandy braided-stream system. The possible annularity of those beds is being investigated and could potentially be exploited to reveal the frequency of forest fires and other climatogenic events. Cross-bedded woody detritus (Davies et al. 2013) is an example of a sedimentary structure apparently unique to a Pliocene forested fluvial environment with long dark and subzero winters. The emerging chronostratigraphy seems to indicate that much of the Beaufort Formation, and perhaps regional correlatives (e.g. parts of the offshore Iperk Formation, the White Channel Gravel in Yukon (Fig. 1), and various high terraces and alluvial fans on Axel Heiberg and Ellesmere Islands), were deposited over a very short time period between about 3.8 to 2.6 Ma, spanning the Pliocene–Pleistocene climate transition.

If the mapped units of Beaufort Formation on each western island of the archipelago were part of a continuous coastal plain, then the Northwest Passages (e.g. M'Clure Strait, Fig. 1) may not have existed in the Pliocene. The absence of the Northwest Passages prior to the Quaternary has been considered since Tozer (1956) but not proven. However, ongoing research to evaluate the regional lithospheric flexural response to their excavation reveals that the topography of the islands is consistent with post-Beaufort Formation (i.e. Quaternary) excavation (Manion 2017). The subsequent drop in relative sea level with Pleistocene cooling likely caused fluvial incision initially, followed by glacial deepening under the Innuitian and Laurentide Ice Sheets. It also appears that lithospheric flexure by loading of the Neogene clastic wedge may have partly controlled the ribbon-like distribution of the mapped Beaufort Formation by providing accommodation space with (albeit low amplitude) flexural bulge parallel but inland of the western coast line (Manion 2017). Acquisition and interpretation of high resolution seismic reflection data throughout the Northwest Passages is needed to fully address the timing and evolution of the Northwest Passages.

We now are attempting to quantify the rates of sedimentation throughout the Beaufort Formation and correlative units such as the White Channel Gravel of the Klondike Gold District. Abundances of cosmogenic nuclides in quartz grains reflect duration of their exposure to cosmic radiation, decay duration during burial, and erosion rate of the exposed surface. In every sample, hundreds of thousands of quartz sand grains record the erosion rate from different locations throughout a Pliocene catchment and allow us to evaluate the spatial and temporal variability in catchment average paleoerosion rates. The results allow us to test landscape responses to climate change, such as the possibility that weathering before and during the mid-Pliocene warm period may have provided an easily accessed source of quartz-rich sand to form the Beaufort Formation clastic wedge (up to 3 km thick in places) during the Pliocene-Pleistocene transition.

Paleoclimate Indices

There is broad interest in the Pliocene as a deep-time laboratory for understanding near-future climate. The ages of the localities studied by this workgroup span 3.8–2.6 Ma covering a large portion of the Pliocene. These sediments would have recorded paleoclimate during the warm periods of the Pliocene, and the transition into cooler climates involving large-scale Northern Hemisphere glaciation. Overlain on this trend are damped periodicities which have been detected and are linked to obliquity and processional cycles (e.g. Draut et al. 2003) and variability in atmospheric CO_2 (Seki et al. 2010; Pagani et al. 2010; Martínez-Botí et al. 2015). Nested within the broader period considered by *PoLAR-FIT*, the mid-Pliocene warm period (*mPWP*; 3.29–2.97 Ma), has received the greatest attention in the literature as the time slice for the long-running Pliocene Research Interpretation and Synoptic Mapping (PRISM) project. The *mPWP* was defined on the basis of a recognizably high global temperature and the convenience of magnetostratigraphic boundaries (Haywood et al. 2009). Shorter time slices (e.g. 3.264–3.025 Ma) provide foci for the other studies (e.g. Pliocene Model Intercomparison Projects (PlioMIP), Haywood et al. 2009). The time recorded at our terrestrial localities is much broader, as are our uncertainties (see Geochronology) and thus precise correlation with the *mPWP* is not yet possible. Improving the precision and quantity of terrestrial observations of climate is currently a critical goal for providing data against which climate models may be verified.

The high-quality preservation of multiple proxies available from the sites currently investigated by *PoLAR-FIT* allows for the simultaneous reconstruction of paleoclimate and paleoenvironment from a single site. For example, we can determine atmospheric CO_2, air temperature, and water temperature all at the same locality. Terrestrial climate proxies used at the High Arctic sites so far include mutual range methods on the beetle fauna (Elias and Matthews 2002) and flora (Ballantyne et al. 2010), dendroclimatologic and isotopic approaches using tree rings (Ballantyne et al. 2006, 2010; Csank et al. 2011a), 'clumped isotopes' (i.e. using molecules of similar chemical composition but different isotopic composition) analysis of freshwater molluscs (Csank et al. 2011b), and bacterial tetraether analysis (Ballantyne et al. 2010) (Fig. 6). There is also potential for investigation using foliar physiognomic methods (e.g. variation in leaf margin attributes, cf. CLAMP: Yang et al. 2011), mutual climatic range methods with improvements to the statistical framework (e.g. CRACLE; Harbert and Nixon 2015), leaf stomatal methods to determine coeval CO_2 (Roth-Nebelsick 2005), and biogeochemical potential via functional

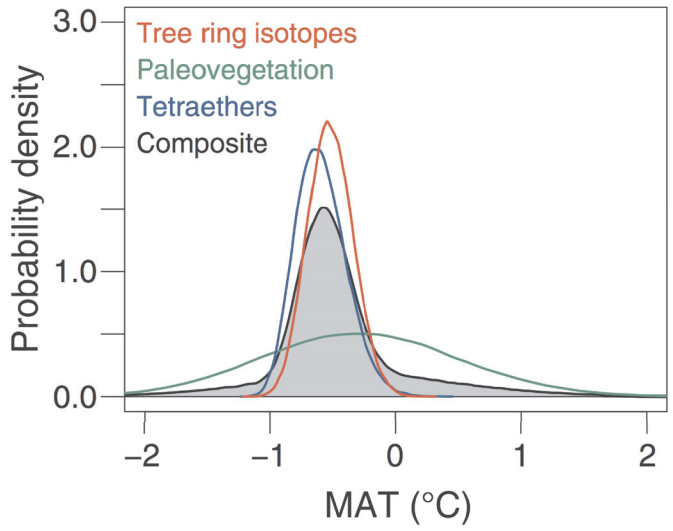

Figure 6. Using multiple proxies for paleoclimate analysis. Probability density functions of mean annual temperature (MAT) estimates for the Arctic during the Pliocene based on three independent proxies. Plotted are the three bootstrapped estimates of MAT derived from our three proxies (coloured lines) and the density function for the composite estimate of MAT derived from resampling the joint distribution across all three independent proxies (grey-filled; from Ballantyne et al. 2010: figure 2).

microbial genes (Xue et al. 2016). The group also is attempting to crossdate multiple *in situ* logs containing one or more burn scars to assist in the assessment of fire frequency. Some logs have over 200 tree rings.

Geochronology

The fossil-rich Beaufort Formation and correlative sediments have been dated with a combination of biostratigraphy, magnetostratigraphy, and numerical methods including cosmogenic $^{26}Al/^{10}Be$ burial and isochron methods on quartz sand, and amino acid racemization (AAR) and Sr isotope dating of marine shells (*Mya truncata* and *Hiatella arctica*). At Meighen Island (Fig. 1), AAR (>2.4 ± 0.5 Ma) and Sr (2.8–5.1 Ma) results (Brigham-Grette and Carter 1992) support the marine and terrestrial biostratigraphy. In the Klondike Gold District of Yukon, cosmogenic nuclide burial ages (Hidy et al. 2013) have confirmed the interpretation of magneto- and biostratigraphy pinned with tephrochronology using fission track dating of volcanic glass (Preece et al. 2011). Their burial age 2.64 +0.20/–0.18 Ma (1σ total external error; now 2.84 Ma adjusted for updates in cosmogenic nuclide production rates) for the top portion of the Upper White Channel Gravel dates the first Cordilleran Ice Sheet and provides a maximum age for the top of the White Channel Gravel (Fig. 1). As in the Yukon, the goal is to anchor paleomagnetic stratigraphy at sites throughout the Beaufort Formation to utilize the precision of the timing of polar reversals. Cosmogenic nuclide burial dating at the Beaver Pond Site (Fig. 1) yielding 3.4 +0.6/–0.4 Ma was interpreted as a minimum age for the Beaver Pond owing to the possibility of post-depositional production of the isotopes by deeply penetrating muons (Rybczynski et al. 2013). Twenty kilometres from the Beaver Pond, minimum burial ages of 3.8 +1.0/–0.7 Ma were reported for the Fyles Leaf Bed site (Fig. 1; Rybczynski et al. 2013). Additional samples have since been collected to improve on the precision of these sites, and unpublished and tentative ages have been measured at Meighen Island, Banks Island, and the Remus site on Ellesmere Island. Moving forward, *PoLAR-FIT* will use the $^{26}Al/^{10}Be$ burial and isochron methods at sites with key fossil or environmental records, where sediments are sufficiently thick to minimize the effect of post-depositional production by cosmic ray secondaries. However, to improve on the cosmogenic nuclide burial dating we will continue to further develop magnetostratigraphy where possible (e.g. Fyles et al. 1991). *PoLAR-FIT* will continue to collaborate with other researchers (including the Geological Survey of Canada and international groups) to build on this Arctic chronostratigraphy. The cosmogenic nuclide results also yield paleo-erosion rates, which provide insight into the variation in sedimentation rates during the climate transition.

EXAMPLES OF HYPOTHESES

The *PoLAR-FIT* workgroup has prioritized topics and hypotheses for testing initially, as follows:

(i) That Arctic forest processes, including forest fires, may be important feedbacks to polar amplification of temperature.

(ii) The 'regolith hypothesis,' that a thick saprolite or regolith was generated during the mid-Pliocene and stripped rapidly during the Pliocene–Pleistocene transition.

(iii) That the Northwest Passages were last opened after 2.7 Ma ago, beginning with fluvial incision in response to Pleistocene sea-level fall, and continuing with glacial erosion which widened and deepened the straits and sounds.

(iv) Consequently, we also hypothesize that the terrestrial distribution of the Beaufort Formation is tied to loading-induced lithospheric flexure and that unloading during excavation of the Northwest Passages may have caused strata and topography to experience uplift along the coasts of the straits.

(v) That records of summer temperature may provide insight into the nature of sea ice cover during the Pliocene.

(vi) The closest fossil relatives of the known High Arctic Pliocene flora and fauna are in mid-continental western North America and the Yushe Basin, China.

(vii) We hypothesize from biogeographical and phylogenetic evidence that an extensive, diverse polar Neogene forest biome existed in the warm part of the Pliocene, spanning Eurasia and northern North America. We will test this by searching for additional confirmatory fossil evidence in future field seasons.

PoLAR-FIT RESEARCH OBJECTIVES

The long-term research objectives of *PoLAR-FIT* are:

1. To understand the interaction of climate and landscape change and how this has affected the evolution and migration of organisms through the Western Arctic during the Pliocene.
2. To understand factors underlying Pliocene floral and faunal

diversity, and the role of the Neogene Arctic in patterning modern biodiversity.
3. Identify and quantify proxies of climatic and environmental conditions in the Pliocene Arctic that improve our understanding of ecological processes and climate interactions at high latitudes during periods of global warmth.
4. To develop a conceptual model, supported by sedimentology and stratigraphy, lithospheric flexure modelling, paleoecology, and paleoclimatology that captures the landscape evolution of the Canadian Arctic Archipelago since the middle Pliocene.

The short-term (5–10 year) research goals are:
1. To identify additional Pliocene sites, with well-constrained ages, to improve data-model comparisons for warm period climate modelling.
2. To build a Pliocene annual time series by crossdating fossil wood and to investigate whether multiple proxies derived from fossil tree rings can be used to characterize the annual and seasonal climate of the Arctic and understand its impacts on ecosystem dynamics.
3. To investigate the impact of currently hypothesized terrestrial feedbacks to polar amplification through climate and atmospheric proxies, and environmental and paleoecological reconstruction at key sites, and integration with current climate modelling.
4. To discover and describe Pliocene High Arctic vertebrate species, using morphological and proteomic techniques.
5. To enrich the faunal, floral, and paleoenvironmental proxy interpretations with improved chronostratigraphy and to investigate the archipelago-scale landscape evolution during the Pliocene-Pleistocene transition.

Targeted Sites

The Beaufort Formation has been recognized on all western Arctic Canada islands, from Banks Island to Meighen Island (Fig. 1). Correlative records have been studied at multiple sites throughout Ellesmere Island, and mid- to late-Pliocene fossil tree fragments on Axel Heiberg and Bylot Island (Fig. 1) have been studied (e.g. Csank et al. 2013), although the stratigraphy there needs further analysis and improved confidence for dating. Offshore, seismic and well data, and core samples from the Iperk Formation are being analyzed to help establish the timing of the post-Miocene transgression and other unconformities, and to separate Pleistocene and Holocene deposits from the Pliocene (Lakeman et al. 2014). With new tools, we are improving the bio- and chrono-stratigraphic correlation of new and existing Pliocene sections such as the White Channel Gravel (Fig. 1) and other well-studied records in western Yukon and northern Alaska. Unlike older and more resilient lithified records, most of these Pliocene beds may have survived only because of permafrost. While retrogressive thaw slumps, solifluction, and other gravitational erosion continue to rejuvenate and expose new records in unconsolidated sands—motivating revisits—key records at some locations are unlikely to survive decades. The next major target, planned for 2017, will be dozens of sections exposed on Prince Patrick Island, where the Beaufort Formation was first described by Tozer (1956).

ACKNOWLEDGEMENTS

PoLAR-FIT is grateful for the outstanding logistic support provided throughout the Canadian Arctic by the Polar Continental Shelf Program and in-kind support for accessing these sites. Without their professionalism and efficiency, our discoveries and knowledge growth could not be possible. We also thank the Canadian Museum of Nature for the past and recent support of critical research and meeting space, field equipment, and funding for research by members of their Arctic program. *PoLAR-FIT* members have benefited from financial support from Natural Science and Engineering Research Council of Canada Discovery Grant Program and NSERC-Northern Research Supplement Program, and the USA National Science Foundation. Special thanks to W. Garfield Weston Foundation for funding NR, a Post-doctoral Fellowship to TL, and a Graduate Student Fellowship to a past student; the National Geographic Society, who have provided field funding for NR and TF; and Byrd Polar and Climate Research Centre, Ohio State University Office of International Affairs, Geologic Society of America, the Columbus Rock and Mineral Society and the individual donors for their field funding for GG. Most significantly, we thank the northern hamlets of Resolute Bay (Qausuittuq), Grise Fiord (Aujuittuq), Sachs Harbour (Ikahuak), and Holman (Ulukhaqtuuq) and their Hunting and Trapping Committees for supporting our research over the past two decades. We hope past and future *PoLAR-FIT* landscape and climate research will be directly useful to their communities. We thank D. Froese for comments that improved an earlier version of this manuscript, and T. Bell, J. England, and A. Kerr for reviews which significantly improved its readability.

REFERENCES

Ballantyne, A.P., Rybczynski, N., Baker, P.A., Harington, C.R., and White, D., 2006, Pliocene Arctic temperature constraints from the growth rings and isotopic composition of fossil larch: Palaeogeography, Palaeoclimatology, Palaeoecology, v. 242, p. 188–200, https://doi.org/10.1016/j.palaeo.2006.05.016.

Ballantyne, A., Greenwood, D. Damsté, J., Csank, A., Eberle, J., and Rybczynski, N., 2010, Significantly warmer Arctic surface temperatures during the Pliocene indicated by multiple independent proxies: Geology, v. 38, p. 603–606, https://doi.org/10.1130/G30815.1.

Ballantyne, A.P., Axford, Y., Miller, G.H., Otto-Bliesner, B.L., Rosenbloom, N., and White, J.W.C., 2013, The amplification of Arctic terrestrial surface temperatures by reduced sea-ice extent during the Pliocene: Palaeogeography, Palaeoclimatology, Palaeoecology, v. 386, p 59–67, https://doi.org/10.1016/j.palaeo.2013.05.002.

Brigham-Grette, J., and Carter, L.D., 1992, Pliocene marine transgressions of Northern Alaska: Circumarctic correlations and paleoclimatic interpretations: Arctic, v. 45, p. 75–89, https://doi.org/10.14430/arctic1375.

Csank, A.Z., Patterson, W.P., Eglington, B.M., Rybczynski, N., and Basinger, J.F., 2011a, Climate variability in the Early Pliocene Arctic: Annually resolved evidence from stable isotope values of sub-fossil wood, Ellesmere Island, Canada: Palaeogeography, Palaeoclimatology, Palaeoecology, v. 308, p. 339–349, https://doi.org/10.1016/j.palaeo.2011.05.038.

Csank, A.Z., Tripati, A.K., Patterson, W.P., Eagle, R.A., Rybczynski, N., Ballantyne, A.P., and Eiler, J.M., 2011b, Estimates of Arctic land surface temperatures during the early Pliocene from two novel proxies: Earth and Planetary Science Letters, v. 304, p. 291–299, https://doi.org/10.1016/j.epsl.2011.02.030.

Csank, A.Z., Fortier, D., and Leavitt, S.W., 2013, Annually resolved temperature reconstructions from a late Pliocene–early Pleistocene polar forest on Bylot Island, Canada: Palaeogeography, Palaeoclimatology, Palaeoecology, v. 369, p. 313–322, https://doi.org/10.1016/j.palaeo.2012.10.040.

Davies, N., Gosse, J., and Rybczynski, N., 2014, Cross-bedded woody debris from a Pliocene forested river system in the High Arctic: Beaufort Formation, Meighen Island, Canada: Journal of Sedimentary Research, v. 84, p. 19–25, https://doi.org/10.2110/jsr.2014.5.

Dawson, M.R., and Harington, C.R., 2007, *Boreameryx*, an unusual new artiodactyl (Mammalia) from the Pliocene of Arctic Canada and endemism in Arctic fossil mammals: Canadian Journal of Earth Sciences, v. 44, p. 585–592, https://doi.org/10.1139/e06-111.

Devaney, J.R., 1991, Clastic sedimentology of the Beaufort Formation, Prince Patrick Island, Canadian Arctic Islands: Late Tertiary sandy braided river deposits with woody detritus beds: Arctic, v. 44, p. 206–216, https://doi.org/10.14430/arctic1540.

Draut, A.E., Raymo, M.E., McManus, J.F., and Oppo, D.W., 2003, Climate stability during the Pliocene warm period: Paleoceanography, v. 18, p. 1–12,

https://doi.org/10.1029/2003PA000889.

Elias, S.A., and Matthews Jr., J.V., 2002, Arctic North American seasonal temperatures from the latest Miocene to the Early Pleistocene, based on mutual climatic range analysis of fossil beetle assemblages: Canadian Journal of Earth Sciences, v. 39, p. 911–920, https://doi.org/10.1139/e01-096.

England, J., 1987, Glaciation and the evolution of the Canadian High Arctic landscape: Geology, v. 15, p. 419–424, https://doi.org/10.1130/0091-7613(1987)15<419:GATEOT>2.0.CO;2.

Feng, R., Otto-Bliesner, B.L., Fletcher, T.L., Tabor, C.R., Ballantyne, A.P., and Brady, E.C., 2017, Amplified Late Pliocene terrestrial warmth in northern high latitudes from greater radiative forcing and closed Arctic Ocean gateways: Earth and Planetary Science Letters, v. 466, p.129–138, https://doi.org/10.1016/j.epsl.2017.03.006.

Fletcher, T., Feng, R., Telka, A.M., Matthews Jr., J.V., and Ballantyne, A., 2017, Floral dissimilarity and the influence of climate in the Pliocene High Arctic: Biotic and abiotic influences on five sites on the Canadian Arctic Archipelago: Frontiers in Ecology and Evolution, v. 5, Article 19, https://doi.org/10.3389/fevo.2017.00019.

Fyles, J.G., 1990, Beaufort Formation (Late Tertiary) as seen from Prince Patrick Island, Arctic Canada: Arctic, v. 43, p. 393–403, https://doi.org/10.14430/arctic1632.

Fyles, J.G., Marincovich Jr., L., Matthews Jr., J.V., and Barendregt, R., 1991, Unique mollusc find in the Beaufort Formation (Pliocene) on Meighen Island, Arctic Canada: Geological Survey of Canada - Current Research B, v. 91, p. 105–112.

Fyles, J.G., Hills, L.V., Matthews Jr., J.V., Barendregt, R., Baker, J., Irving, E., and Jetté, H., 1994, Ballast Brook and Beaufort formations (Late Tertiary) on Northern Banks Island, Arctic Canada: Quaternary International, v. 22–23, p. 141–171, https://doi.org/10.1016/1040-6182(94)90010-8.

Harbert, R.S., and Nixon, K.C., 2015, Climate reconstruction analysis using coexistence likelihood estimation (CRACLE): A method for the estimation of climate using vegetation: American Journal of Botany, v. 102, p. 1277–1289, https://doi.org/10.3732/ajb.1400500.

Haywood, A.M., Dowsett, H.J., Valdes, P.J., Lunt, D.J., Francis, J.E., and Sellwood, B.W., 2009, Introduction. Pliocene climate, processes and problems: Philosophical Transactions of the Royal Society A, v. 367, p. 3–17, https://doi.org/10.1098/rsta.2008.0205.

Heer, O., 1868, Die Fossile Flora der Polarländer, die in Nordgronland, auf der Melville-Insel, im Banksland, am Mackenzie, in Island und in Spitzbergen entdeckten fossilen Pflanzen: Druck und Verlag von Friedrich Schulthess, Zurich, p. 1–192.

Hidy, A.J., Gosse, J.C., Froese, D.G., Bond, J.D., and Rood, D.H., 2013, A latest Pliocene age for the earliest and most extensive Cordilleran Ice Sheet in northwestern Canada: Quaternary Science Reviews, v. 61, p. 77–84, https://doi.org/10.1016/j.quascirev.2012.11.009.

Hills, L.V., 1975, Late Tertiary floras Arctic Canada: An interpretation: Proceedings of Circumpolar Conference on Northern Ecology, National Research Council of Canada, p I(63)–I(71).

Hutchison, J.H., and Harington, C.R., 2002, A peculiar new fossil shrew (*Lipotyphla, Soricidae*) from the High Arctic of Canada: Canadian Journal of Earth Sciences, v. 39, p. 439–443, https://doi.org/10.1139/e01-078.

Lakeman, T.R., Gosse, J.C., Blasco, S., Braschi, L.C., and Rybczynski, N., 2014, Reconstructing the nature of Pliocene–Pleistocene landscape dynamics in the Canadian Arctic from the age and architecture of the Iperk Fm. in the Beaufort Sea (Abstract): 'Past Gateways' First International Conference and Workshop, 2013, Abstracts, v. 1, p. 44.

Manion, P., 2017, Lithospheric flexural controls on landscape evolution during deposition and incision of the Beaufort Formation, western Canadian Arctic: Unpublished Honours Thesis, Dalhousie University, Halifax, NS, 81 p.

Martínez-Botí, M.A., Foster, G.L., Chalk, T.B., Rohling, E.J., Sexton, P.F., Lunt, D.J., Pancost, R.D., Badger, M.P.S., and Schmidt, D.N., 2015, Plio-Pleistocene climate sensitivity evaluated using high-resolution CO_2 records: Nature, v. 518, p. 49–54, https://doi.org/10.1038/nature14145.

Masson-Delmotte, V., Schulz, M., Abe-Ouchi, A., Beer, J., Ganopolski, A., González Rouco, J.F., Jansen, E., Lambeck, K., Luterbacher, J., Naish, T., Osborn, T., Otto-Bliesner, B., Quinn, T., Ramesh, R., Rojas, M., Shao, X., and Timmermann, A., 2013, Information from Paleoclimate Archives, *in* Stocker, T.F., Qin, D., Plattner, G.-K., Tignor, M., Allen, S.K., Boschung, J., Nauels, A., Xia, Y., Bex, V., and Midgley, P.M., *eds.*, Climate Change 2013: The Physical Science Basis. Contribution of Working Group I to the Fifth Assessment Report of the Intergovernmental Panel on Climate Change: Cambridge University Press, Cambridge, UK and New York, NY, USA, p. 383–464, https://doi.org/10.1017/CBO9781107415324.013.

Matthews Jr., J.V., 1987, Plant macrofossils from the Neogene Beaufort Formation on Banks and Meighen Islands, District of Franklin: Geological Survey of Canada, Current Research, Part A, Paper 87-1A, p. 73–87.

Matthews Jr., J.V., and Fyles, J.G., 2000, Late Tertiary plant and arthropod fossils from the High Terrace Sediments on the Fosheim Peninsula of Ellesmere Island (Northwest Territories, District of Franklin): Geological Survey of Canada Bulletin, v. 529, p. 295–317.

Matthews Jr., J.V., and Ovenden, L.E., 1990, Late Tertiary plant macrofossils from localities in Arctic/Subarctic North America: a review of the data: Arctic, v. 43, p 364–392, https://doi.org/10.14430/arctic1631.

McNeil, D., Duk-Rodkin, A., Dixon, J., Dietrich, J., White, J., Miller, K., and Issler, D., 2001, Sequence stratigraphy, biotic change, $^{87}Sr/^{86}Sr$ record, paleoclimatic history, and sedimentation rate change across a regional late Cenozoic unconformity in Arctic Canada: Canadian Journal of Earth Sciences, v. 38, p. 309–331, https://doi.org/10.1139/e00-098.

Mitchell, W.T., Rybczynski, N., Schröder-Adams, C., Hamilton, P.B., Smith, R., and Douglas, M., 2016, Stratigraphic and paleoenvironmental reconstruction of a Mid-Pliocene fossil site in the High Arctic (Ellesmere Island, Nunavut): Evidence of an ancient peatland with beaver activity: Arctic, v. 69, p. 185–204, https://doi.org/10.1038/nclimate2940.

Murray, A.M., Cumbaa, S.L., Harington, C.R., Smith, G.R., and Rybczynski, N., 2009, Early Pliocene fish remains from Arctic Canada support a pre-Pleistocene dispersal of percids (Teleostei: Perciformes): Canadian Journal of Earth Sciences, v. 46, p. 557–570, https://doi.org/10.1139/E09-037.

Pagani, M., Liu, Z., LaRiviere, J., and Ravelo, A.C., 2010, High Earth-system climate sensitivity determined from Pliocene carbon dioxide concentrations: Nature Geoscience, v. 3, p. 27–30, https://doi.org/10.1038/ngeo724.

Preece, S.J., Westgate, J.A., Froese, D.G., Pearce, N.J.G., and Perkins, W.T., 2011, A catalogue of late Cenozoic tephra beds in the Klondike goldfields and adjacent areas, Yukon Territory. Yukon Geological Survey Contribution 010: Canadian Journal of Earth Sciences, v. 48, p. 1386–1418, https://doi.org/10.1139/e10-110.

Roth-Nebelsick, A., 2005, Reconstructing atmospheric carbon dioxide with stomata: possibilities and limitations of a botanical pCO_2-sensor: Trees, v. 19, p. 251–265, https://doi.org/10.1007/s00468-004-0375-2.

Rybczynski, N., Gosse, J.C., Harington, R.C., Wogelius, R.A., Hidy, A.J., and Buckley, M., 2013, Mid-Pliocene warm-period deposits in the High Arctic yield insight into camel evolution: Nature Communications, v. 4, p. 1550, https://doi.org/10.1038/ncomms2516.

Salzmann, U., Dolan, A.M., Haywood, A.M., Chan, W.-L., Voss, J., Hill, D.J., Abe-Ouchi, A., Otto-Bliesner, B., Bragg, F.J., Chandler, M.A., Contoux, C., Dowsett, H.J., Jost, A., Kamae, Y., Lohmann, G., Lunt, D.J., Pickering, S.J., Pound, M.J., Ramstein, G., Rosenbloom, N.A., Sohl, L., Stepanek, C., Ueda, H., and Zhang, Z., 2013, Challenges in quantifying Pliocene terrestrial warming revealed by data-model discord: Nature Climate Change, v. 3, p. 969–974, https://doi.org/10.1038/nclimate2008.

Seki, O., Foster, G.L., Schmidt, D.N., Mackensen, A., Kawamura, K., and Pancost, R.D., 2010, Alkenone and boron-based Pliocene pCO_2 records: Earth and Planetary Science Letters, v. 292, p. 201–211, https://doi.org/10.1016/j.epsl.2010.01.037.

Tedford, R.H., and Harington, C.R., 2003, An Arctic mammal fauna from the Early Pliocene of North America: Nature, v. 425, p. 388–390, https://doi.org/10.1038/nature01892.

Tozer, E.T., 1956, Geological reconnaissance, Prince Patrick, Eglington and western Melville Islands, Arctic Archipelago, Northwest Territories: Geological Survey of Canada, Paper 55-5, p. 1–32.

Tozer, E.T., and Thorsteinsson, R., 1964, Western Queen Elizabeth Islands, Arctic Archipelago: Geological Survey of Canada, Memoir 332. Ottawa, p. 1–242.

Trettin, H.P., 1989, The Arctic Islands, *in* Bally, A.W., and Palmer, A.R., *eds.*, The Geology of North America—An Overview: DNAG Volume A, Geological Society of America, p. 349–370, https://doi.org/10.1130/DNAG-GNA-A.349.

Xue, K., Yuan, M.M., Shi, Z.J., Qin, Y., Deng, Y., Cheng, L., Wu, L., He, Z., Van Nostrand, J., Bracho, R., Natali, S., Schuur, E.A.G., Lou, C., Konstantinidis, K.T., Wang, Q., Cole, J.R., Tiedje, J.M., Luo, Y., and Zhou, J., 2016, Tundra soil carbon is vulnerable to rapid microbial decomposition under climate warming: Nature Climate Change, v. 6, p. 595–600, https://doi.org/ 10.1038/nclimate2940.

Yang, J., Spicer, R., Spicer, T., and Li, C.-S., 2011, 'CLAMP Online': a new web-based palaeoclimate tool and its application to the terrestrial Paleogene and Neogene of North America: Palaeobiodiversity and Palaeoenvironments, v. 91, p. 163–183, https://doi.org/10.1007/s12549-011-0056-2.

Received November 2016
Accepted as revised March 2017

ARTICLE

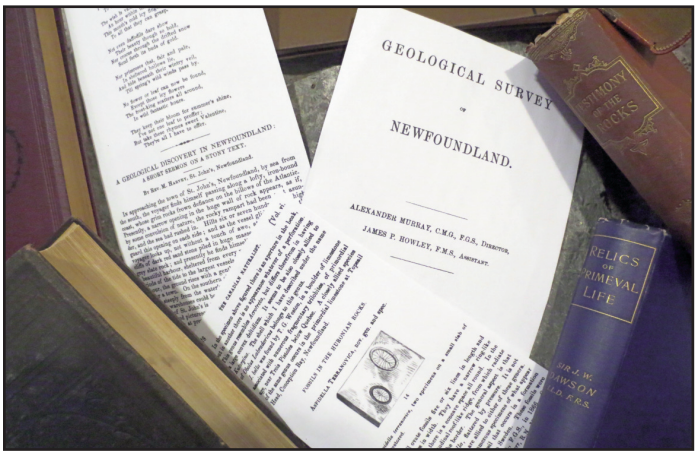

Who Was the First Person Known to Have Discovered Fossils of the Precambrian (Ediacaran) Organism *Aspidella terranovica*?

Jeffrey M. Minicucci

Barrister-at-Law, Solicitor, and Notary Public
229 Glen Park Avenue
Toronto, Ontario, M6B 2E2, Canada
E-mail: priority1mail@rogers.com

SUMMARY

This article briefly examines the possible confusion pertaining to the discoveries of Precambrian (Ediacaran) fossils made in the self-governing British colony of Newfoundland in 1868 by the amateur naturalist, the Reverend Moses Harvey, and the subsequent description and naming of the fossil organism *Aspidella terranovica* in 1872 by Elkanah Billings, the father of Canadian paleontology. Both events could be misinterpreted as one transaction that began with the former event and ended with the latter event. Accounts published by Alexander Murray, the director of the Geological Survey of Newfoundland at the time, arguably may have inadvertently exacerbated the possibility for confusion. The determination of who first discovered fossils of *A. terranovica* and whose fossil material Billings primarily relied upon when he first described and named the taxon could be placed into doubt as a consequence. Although the confusion does not affect the undisputed priority that Billings holds in having described and named *A. terranovica*, the opportunity to remedy the confusion serves to benefit the historical record. The incomplete or ambiguous ascertaining and documenting of contextual information whenever an historically significant fossil discovery is made arguably may precipitate subsequent misinterpretations, distortions or omissions in the resulting historical narrative as it develops and becomes entrenched or mythologized in its retelling.

RÉSUMÉ

Cet article examine brièvement la confusion possible concernant les découvertes de fossiles Précambriens (Ediacaran) fabriqués dans la colonie Britannique autonome de Terre-Neuve en 1868 par le naturaliste amateur, le Révérend Moses Harvey, et la description et l'appellation suivantes de l'organisme fossile *Aspidella terranovica* en 1872 par Elkanah Billings, le père de la paléontologie Canadienne. Les deux événements pourraient être mal interprétés comme une transaction qui a commencé avec l'événement précédent et s'est terminée avec le dernier événement. Les comptes publiés par Alexander Murray, le directeur de la Commission Géologique de Terre-Neuve à l'époque, ont sans doute peut-être exacerbé par mégarde la possibilité de confusion. La détermination de qui a découvert les fossiles d'abord de *A. terranovica* et dont Billings s'appuyait principalement sur le matériel fossile dont il a d'abord décrit et nommé le taxon pourrait être mis en doute en conséquence. Bien que la confusion ne porte pas atteinte à la priorité incontestée que Billings détient en ayant décrit et nommé *A. terranovica*, la possibilité de remédier à la confusion sert à bénéficier du dossier historique. La constatation et la documentation incomplètes ou ambiguës de l'information contextuelle chaque fois qu'une découverte fossilifère historiquement significative peut être faite peut précipiter des interprétations, des distorsions ou des omissions subséquentes dans le récit historique résultant au fur et à mesure qu'il se développe et devient ancré ou mythologisé dans son récit.

NEWFOUNDLAND AND THE FIRST KNOWN EDIACARAN BODY FOSSIL

Newfoundland has been recognized for its complex and fascinating early history (see, for example, Bannister 2003). It began as an English colony founded in 1610, administered by the fishing admirals, with customary law comprising an important aspect of its legal system. It evolved into a British colony with representative government in 1832 and responsible govern-

ment in 1855. It became a British dominion in 1907 (resolved at the Imperial Conference of that year and by Royal Proclamation) and finally entered into confederation with Canada as its 10th province in 1949 (United Kingdom 1949). The geological history of the province has proven to be no less varied and intriguing. In particular, the Avalon Peninsula of southeastern Newfoundland contains several spectacular Precambrian fossil deposits, including one of the richest in the world known as the Mistaken Point Konservat–Lagerstätten (Fig. 1). This United Nations Educational, Scientific and Cultural Organization (UNESCO) World Heritage Site, inscribed in 2016, was discovered in 1967 by Shiva Balak Misra, then a graduate student at Memorial University of Newfoundland, with Professor Michael Marchmont Anderson as his academic supervisor (Anderson and Misra 1968; Misra 1969, 1971; Fedonkin et al. 2007). Canada's first professional paleontologist, the Ontario lawyer Elkanah Billings, described and named the Precambrian fossil organism *Aspidella terranovica* (Fig. 2) in 1872 from material that had been discovered in Precambrian (Ediacaran) rocks of the Fermeuse Formation (St. John's Group) from Newfoundland (Billings 1872). Paleontologists have since credited Billings with having described and named the first known Ediacaran body fossil (Gehling et al. 2000).

THE REVEREND MOSES HARVEY AND HIS 1868 DISCOVERY OF FOSSILS

The Reverend Moses Harvey, an amateur naturalist and a dedicated researcher on the history of Newfoundland, reported in 1869 on some unknown, primordial fossils from Newfoundland that he had apparently discovered in 1868. He suggested that the most prominent of these might be referable to *Oldhamia radiata*, a taxon initially postulated to have been a body fossil (Kinahan 1856) but which is presently classified as an Early Cambrian ichnotaxon (trace fossil) (Herbosch and Verniers 2011). Harvey stated that he had sent photographs of the putative *O. radiata* material to the prominent geologist Alexander Murray, director of the Geological Survey of Newfoundland, and to Sir J. William Dawson of McGill University. Dawson referred the matter to Billings for study. Harvey also reported finding other fossils, which he described as "markings much resembling the whorls of shell fish" and "shell-markings, or traces of mollusca." He also found what he characterized as "*two other forms* in the same slate rock." It does not appear that he had arranged for anyone to examine any of this additional material. He concluded his 1869 report with a note that –

> *"It must be borne in mind that the fossils referred to have yet to be examined by a* professional *Palaeontologist, only photographs of them having yet been sent. I have, however, given the evidence which seems strongly to point to the conclusion that they are Cambrian forms identical with* Oldhamia*, or at all events closely allied thereto. Mr. Billings reserves his final verdict till he has examined the fossils themselves"* (Harvey 1869).

Murray made reference to Harvey's discovery in a report on the activities of the Geological Survey of Newfoundland for 1868 (Murray and Howley 1881).

ELKANAH BILLINGS AND HIS 1872 DESCRIPTION OF *ASPIDELLA TERRANOVICA*

The published literature indicates that the fossils that Billings had discussed in his 1872 publication on *A. terranovica* and those that Harvey had reported in 1869 had been discovered only two years apart near St. John's on the Avalon Peninsula and both discoveries had involved the participation of Murray and Billings. An assumption could be made that either Harvey's mollusc-like fossils or the "*two other forms*" were *A. terranovica*. It had been argued in the late 19th century that *A. terranovica* represented "problematical forms…which may be Crustaceans or Mollusks allied to the limpets" from strata "underlying the Lower Cambrian" (Dawson 1897). As exemplified by statements made in Walcott (1891), and in Fensome et al. (2014), a possibility has consequently existed that the events of both discoveries could be misinterpreted as one transaction that began with Harvey's fossil discovery in 1868 and ended with Billings' description of *A. terranovica* in 1872. Walcott (1891) stated: "…It was in this series of slates that the Rev. Moses Harvey discovered the fossil which Mr. Billings described as *Aspidella terranovica*." Fensome et al. (2014) stated: –

> *"The first inkling that Newfoundland's Avalon Peninsula had something special to contribute to our knowledge of the history of life came in the late nineteenth century. In a report published in 1881, the first Director of the Geological Survey of Newfoundland, Alexander Murray, remarked on a discovery in rocks previously thought to be barren of fossils. Murray noted, 'I have long had some obscure forms in my possession, collected [by the Rev. Mr. Harvey] in the neighbourhood of St. John's, which were suspected to be organisms of a low type, but which I could not venture to pronounce to be such without palaeontological reference.'*
>
> *That 'palaeontological reference' was Elkanah Billings, a lawyer whose passion was fossils…It was natural, then, that Murray would send Reverend Harvey's finds to Billings, Canada's first professional paleontologist.*
>
> *Billings examined the dime-sized discs and, in an 1872 publication, named them* Aspidella terranovica *(Newfoundland's little shield)…"*

Fensome et al. (2014) inserted the above parenthetical reference to Harvey within Murray's quote.

Billings' 1872 description of *A. terranovica* and Harvey's 1869 report on the purported *O. radiata* fossils, mollusc-like fossils, and "*two other forms*", do not necessarily lead to the conclusions that Harvey's work had contributed to, or formed the basis of, Billings' 1872 description of *A. terranovica* or that both publications had, in fact, concerned identical fossil material comprising *A. terranovica*. Billings made no references to Harvey's 1868 discovery or 1869 report. Billings stated that the *A. terranovica* "fossils were first discovered by A. Murray, Esq., F.G.S. in 1866. Other specimens were collected by Capt. Kerr, R.N., Mr. Howley, and Mr. Robertson" (Billings 1872). He repeated this statement in 1874 in the second volume of his renowned publication *Palaeozoic Fossils* (Billings 1874). Murray repeated the statement in his report on the activities of the Geological Survey of Newfoundland for 1872 (Murray and

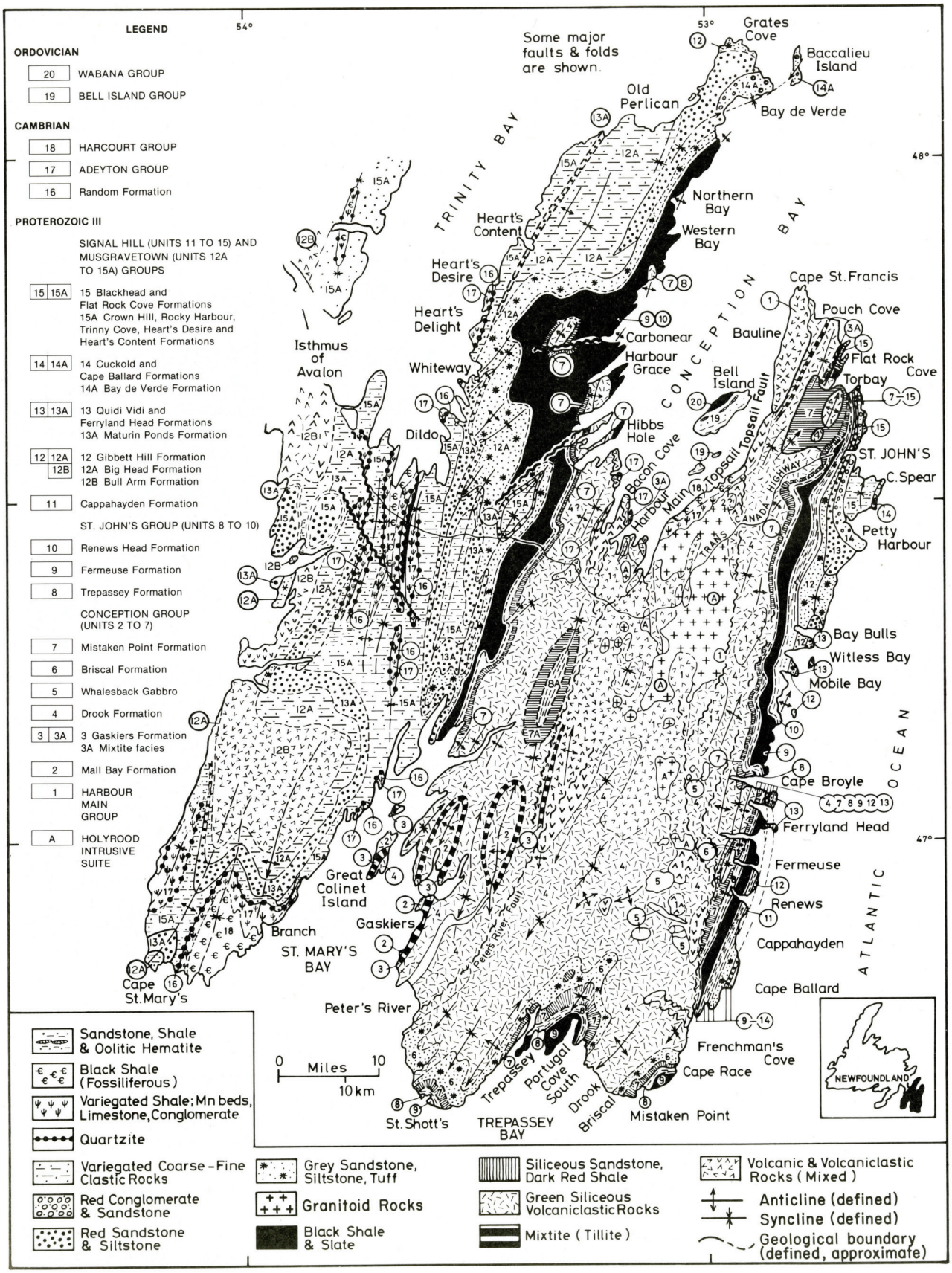

Figure 1. Geological map of the Avalon Peninsula, Newfoundland from King 1990, figure 3.

https://doi.org/10.12789/geocanj.2017.44.115

Figure 2. Remains of two individuals of *Aspidella terranovica* from Ferryland, Newfoundland. 5 cm scale bar shown. Photograph courtesy of Marc Laflamme.

Howley 1881). Billings' 1872 and 1874 discussions on *A. terranovica* both indicate that he did not knowingly examine, rely upon or make reference to any fossils that Harvey had collected in 1868 (or subsequently) and reported on in 1869.

ALEXANDER MURRAY AS A POTENTIAL SOURCE FOR CONFUSION

The potential for confusion concerning which primordial fossils from Newfoundland had first been found, when they had been found, and who had found them arguably appears to have originated with Murray, who reported in 1868: –

> *"The Rev. Mr. Harvey of this place had the good fortune to find the first well-defined specimen of these organic forms; and they, with others subsequently obtained, will doubtless be of inestimable service in finally settling the question of horizon. I have long had some obscure forms in my possession, collected in the neighbourhood of St. John's, which were suspected to be organisms of a low type, but which I could not venture to pronounce to be such without palaeontological reference. Since Mr. Harvey's discovery, I have obtained many more, all apparently of the same low order of existence; some of them so much resembling forms described by Sir Roderick Murchison, Jukes, Salter, and others, as peculiarly Cambrian, that there seems but little reason to doubt that the rocks of Avalon are the representatives of that system"* (Murray and Howley 1881).

Murray's 1868 statement that he "long had" primordial Newfoundland fossils appears to suggest that Murray had made a discovery of fossils that had predated Harvey's and agrees with Billings' assertion that Murray had been the first person known to have discovered *A. terranovica* fossils in 1866. Murray's statement "Since Mr. Harvey's discovery, I have obtained many more" appears to suggest that the additional quantities of fossils that Murray had obtained had not been discovered by Harvey. Murray did not state that anyone other than himself had collected the fossils that he had "long had" or those that he had obtained "Since Mr. Harvey's discovery". Murray also specifically stated that Harvey had discovered "the first well-defined specimen of these organic forms" (Murray and Howley 1881). Murray did not state that Harvey had been the first person known to have discovered "these organic forms." Murray arguably did not adequately distinguish to which "forms" he was referring. Was he referring to the *O. radiata* fossils, the mollusc-like fossils, the "*two other forms*" or a combination of some or all of these? Harvey reported in 1869 that he had not yet submitted the purported molluscan fossils or the "*two other forms*" to any researcher for analysis. He stated they "are yet unread…it remains for a palaeontologist to determine what they are" (Harvey 1869).

In the absence of a detailed study of the primordial Newfoundland fossils known to Harvey and Murray at the time that Murray had made his Geological Survey of Newfoundland report for 1868, Murray briefly summarized the available fossils by tentatively commenting on the collected material in a limited, generalized context. However, in a footnote added when all of the Geological Survey of Newfoundland reports were compiled, revised, and republished in England as one volume in 1881 (see the Preface in Murray and Howley 1881 for the reasons behind the compilation), Murray distinguished the Newfoundland "forms" that purportedly resembled *O. radiata* from the fossils that Billings described as *A. terranovica* in 1872. No specific reference was made in the footnote to Harvey's "*two other forms*" or mollusc-like fossils: –

> *"The forms in question were supposed to resemble the* Oldhamii *of Bray Head, but were pronounced upon examination by the late E. Billings to be undeterminable. He doubted their organic origin altogether. At a later date, however, fossils of a very low type were found, which Mr. Billings describes and names* Aspidella terranovica *and* arenicolites" (Murray and Howley 1881).

The mention of the taxon "*arenicolites*" in Murray and Howley (1881) was a reference to *Arenicolites spiralis*, an ichnotaxon that Billings briefly described in his 1872 publication on *A. terranovica* (Billings 1872). Murray's 1881 statement that *A. terranovica* fossils were found "At a later date" appears to contradict his 1868 statement that he had "long had" such fossils and Billing's 1872 statement that the first *A. terranovica* "fossils were first discovered by A. Murray, Esq., F.G.S. in 1866." The 1881 footnote did not mention or distinguish the date when the *A. terranovica* fossils had first been discovered (1866) from the date when they had first been described (1872). Perhaps Murray's footnote was referring specifically to the *A. terranovica* fossils on the slab that Billings had figured in his 1872 description (Billings 1872, figure 14). These specific fossils may have been discovered "At a later date" either by Murray or by one of the other persons ("Capt. Kerr, R.N., Mr. Howley, and Mr. Robertson") whom Billings had credited with having discovered *A. terranovica* fossils.

OTHER STUDIES OF THE FOSSILS AT ISSUE

Whitney and Wadsworth (1884) reviewed Murray's Geological Survey of Newfoundland reports and they appeared to have readily understood the differences between the discoveries of the *O. radiata* and *A. terranovica* fossil material. Weston (1896) distinguished the *A. terranovica* fossils that Billings described from the –

"…other forms found in Huronian argillite by the Rev. Mr. Harvey. At the time of the discovery of these fossil-like markings they were considered to be most important, and were supposed to belong to the genus Oldhamia*, and specimens were sent to Sir W. E. Logan. Billings would not decide one way or the other as to their organic affinity and they were handed to me. I said at once they were concretionary, and, what had not been observed by others, that these markings lay transverse to the bedding of the slate in which they were."*

With respect to *A. terranovica*, Weston expressed his doubts that the taxon represented a fossil: "I am afraid they will ultimately be classed with the concretionary forms already spoken of, collected by the Rev. Mr. Harvey" (Weston 1896). No matter what the status of *A. terranovica* may have been perceived to have been, Weston's writing arguably does not communicate an understanding that Harvey had in any way contributed to either the collection or the description of *A. terranovica* fossils. The applicable primary sources convey an overall impression that the only fossils that Harvey had ever been explicitly or implicitly recognized for having unearthed had been those interchangeably referred to in the literature as *Oldhamia radiata*, *Oldhamia* or "*Oldhamii*". In a comprehensive review of known Precambrian fossils from Canada, Hofmann (1971) discussed Murray's references to *Oldhamia* and Billings' 1872 description of *A. terranovica* under the headings macro-pseudofossils and macro-problematica. Concerning *A. terranovica*, Hofmann stated that "these structures were first collected in 1866 and reported by A. Murray (1868, pp. 11, 12) in the St. John's Formation" (Hofmann 1971).

Whitney and Wadsworth drew attention to an interesting discrepancy concerning the appearance of some particular *A. terranovica* fossils that they had examined: –

"Specimens of Aspidella *sent us by Mr. Murray, however, do not resemble in any respect the fossil figured by Mr. Billings. There are several indistinct impressions on the fragment of rock, neither of them like that fossil, and none of them necessarily of organic origin, at least so far as we are able to discover. They look more like spray markings than anything else with which we are able to compare them"* (Whitney and Wadsworth 1884).

It may be fairly stated that undoubted *O. radiata* fossils do not generally resemble fossils of *A. terranovica*, which is not even an ichnotaxon. Gehling et al. (2000) identified three predominant preservational morphs of *A. terranovica*, none of which resemble *O. radiata* fossils. *O. radiata* typically consists of radially branching structures, while *A. terranovica* remains are typically preserved as discoidal structures representing the holdfast of a sessile, frond-like organism (Gehling et al. 2000; Carbone et al. 2015). Menon et al. (2013, 2014) controversially argued that *A. terranovica* fossils may suggest evidence of vertical and horizontal movement consistent with the behaviour of cnidarians, however Retallack (2014) disputed this argument. Liu et al. (2015) argued the possibility "that *Aspidella* reflects several very different original entities, including holdfast discs, microbial colonies (cf. Grazhdankin and Gerdes, 2007), and discrete organisms (cf. MacGabhann, 2007)".

The literature arguably does not appear to offer any applicable data that could reasonably be construed to indicate that

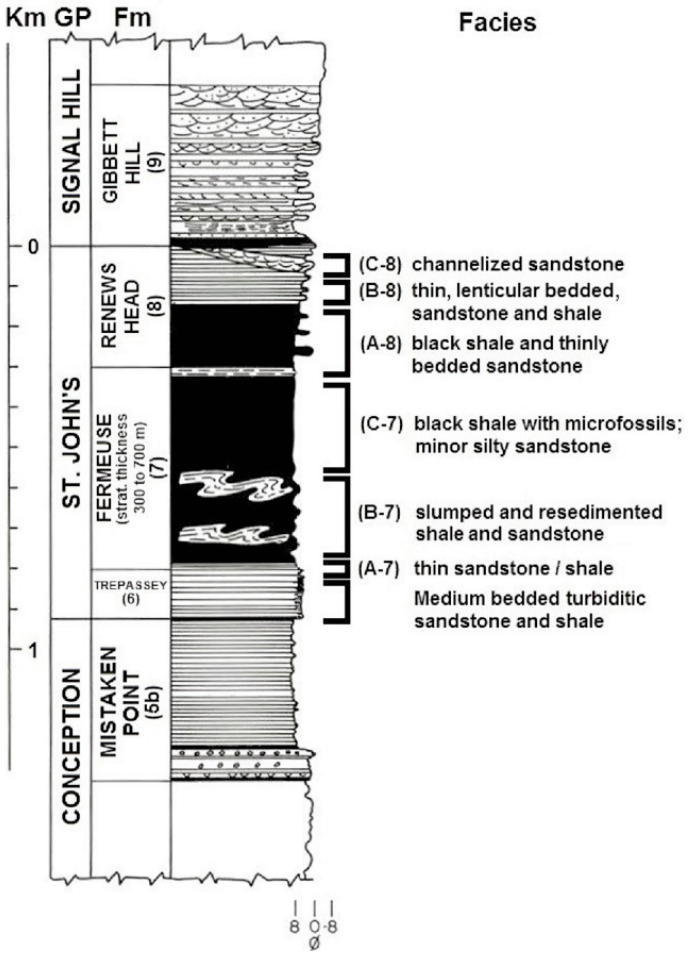

Figure 3. Composite stratigraphic section of the St. John's Group from King 1990, figure 14.

fossils of *Aspidella* and *Oldhamia* are taphonomically the same or represent the same organism. A statement was nonetheless published in Fedonkin et al. (2007) that "Some other workers suggest that *Oldhamia* may even be a body fossil, some allying it with *Aspidella* (Runnegar, 1992)". Tacker et al. (2010) cited Fedonkin et al. (2007) stating that "*Oldhamia* was originally questioned as an Ediacaran trace fossil by Runnegar (1992), who affiliated it with the body fossil *Aspidella*."

The Fermeuse Formation is one of several geologic formations on the Avalon Peninsula (Fig. 3) containing fossils of *A. terranovica*. Fossils of the Ediacaran genus *Hiemalora*, which, like *A. terranovica*, are known to occur in the Fermeuse Formation, combine what arguably could be described as a superficially *A. terranovica*-like discoidal structure with superficially *O. radiata*-like radially branching structures (see, for example, Fedonkin et al. 2007). But because neither *A. terranovica* nor *O. radiata* each exhibit a combination of such structures, it would be difficult or even implausible to argue that the purported *O. radiata* fossils that Harvey had reported in 1869 were, in fact, fossils of *Hiemalora*. Some researchers have suggested that the Ediacaran bush-like body fossil *Parviscopa bonavistensis*, which occurs along with *Hiemalora* and *A. terranovica* on the Bonavista Peninsula, Newfoundland, may display 'similarities' to the Cambrian trace

fossil *Oldhamia flabellata* (Hofmann et al. 2008; Liu et al. 2015). However, there is no evidence that Harvey's presumed *Oldhamia* fossils could have been referable to *P. bonavistensis*. Harvey had not even made his discovery of fossils on the Bonavista Peninsula.

It would be useful to contrast, compare, and conclusively identify all of the Newfoundland fossils that Harvey, Murray, and Billings had each independently studied and precisely place each of the fossils in their proper stratigraphic context. Complete stratigraphic information would be extremely important in view of the arguments presented by Herbosch and Verniers (2011). Inter alia, they argued that the ichnogenus *Oldhamia* is not definitively known from the Precambrian. The organisms responsible for creating *Oldhamia* traces were argued to have lived "probably between the earliest Cambrian and the middle Cambrian mostly in deep oceanic environments and more rarely in shallow ones." Tacker et al. (2010) argued that *O. recta* known from the Precambrian of North Carolina, U.S.A. potentially represents the body fossil of a rod-like organism and not a trace fossil falling within the scope of the ichnogenus *Oldhamia*.

Not all of the fossils at issue appear to be presently accounted for in institutional collections. The fossils that Billings had consulted in his 1872 description of *A. terranovica* were placed in the repository of the National Type Collection of Invertebrates and Plants, Geological Survey of Canada (GSC) in Ottawa, Ontario, Canada. Gehling et al. (2000, figure 4) examined the metal plastotype (GSC 221c) of the slab that Billings had figured in 1872 (Billings 1872, figure 14). It would appear that the original material on which the metal plastotype had been based was lost. Gehling et al. presumed that a small cross marked on the slab above the largest specimen of *A. terranovica* was intended to indicate the holotype, although Billings did not formally designate it as such in the literature (Gehling et al. 2000). Boyce (pers. comm. 2016) was of the opinion that the putative holotype of *A. terranovica* was transferred to the Canadian Museum of Nature in Ottawa along with a substantial amount of other material that had been held in the collections of the Geological Survey of Canada (Stewart 2015). Additional fossils that Boyce and Reynolds (2008) documented are in the Provincial Museum of Newfoundland and Labrador in the Rooms in St. John's.

CONCLUSIONS

It arguably appears, in the absence of clear and convincing evidence to the contrary, that the credit for having been the first person known to have discovered fossils of *A. terranovica* belongs with Murray, not Harvey, and that the discovery of the fossils occurred in 1866. Furthermore, even if it were proven that Harvey discovered fossils of *A. terranovica* prior to Murray, it nonetheless appears evident that such a discovery had not been recognized, and it was Murray's discovery of *A. terranovica* fossils that had influenced Billings' 1872 description of what constituted the first known Ediacaran body fossil. The priority that Billings holds in having described and named *A. terranovica* is not at issue and, of course, remains undisputed.

From whom did Billings obtain the information that Murray first discovered fossils of *A. terranovica* in 1866 and that "Capt. Kerr, R.N., Mr. Howley, and Mr. Robertson" subsequently discovered additional quantities of *A. terranovica* fossils? If Billings obtained the information from any or all of these persons, could Billings have either misunderstood any of them or could any of them have been faulty in their recollections at the time during which Billings had prepared his description of *A. terranovica* for publication in 1872? The available evidence does not appear to support these possibilities. It is sincerely hoped that further information may elucidate the matter.

The incomplete or ambiguous ascertaining and documenting of contextual information whenever an historically significant fossil discovery is made arguably may precipitate subsequent misinterpretations, distortions or omissions in the resulting historical narrative as it develops and becomes entrenched or mythologized in its retelling.

AN UNEXPECTED NEXUS BETWEEN RESEARCHERS

Billings and Harvey shared an ironic and unexpected connection with one another in their respective studies on primordial Newfoundland fossils and in the fact that they each independently had dealings with the American researcher Addison Emery Verrill, the first professor of zoology at Yale University and one of the first curators of the Yale Peabody Museum. Teuthologists remember Verrill as a prominent investigator of occurrences of the giant squid *Architeuthis dux* off the coast of Newfoundland. Harvey became a kind of local folk hero and a legendary figure in *Architeuthis* lore for his work on the cephalopod (especially in 1873) and for his concomitant collaboration with Verrill (Ellis 1998; Frank 2015; Conniff 2016). In 1866, Billings challenged Verrill's misinterpretation of Billings' research on the fossil organism *Pasceolus halli* (Minicucci 2016). For an excellent photograph of Billings, see City of Ottawa Archives (2015); for Murray, see The Rooms (2016); and for Harvey, see Heritage Newfoundland and Labrador (2001).

ACKNOWLEDGEMENTS

I offer my sincere appreciation to the staff at *Geoscience Canada*, especially Andrew Kerr, Scientific Editor, Cindy Murphy, Managing Editor, and Rob Raeside, Copyeditor, who each handled the manuscript and to R. Frank Blackwood and an anonymous reviewer, who both reviewed it. All offered extremely helpful recommendations and advice on improving the manuscript. W. Douglas Boyce of the Newfoundland and Labrador Department of Natural Resources, Geological Survey is sincerely thanked for providing information pertinent to this article. Marc Laflamme of the National Museum of Natural History, Smithsonian Institution; the Royal Ontario Museum; and the University of Toronto, Mississauga is sincerely thanked for providing the image of *A. terranovica* fossils (Fig. 2). Christopher Pereira of the Newfoundland and Labrador Department of Natural Resources, Geological Survey is sincerely thanked for providing the images from King (1990) (Fig. 1 and Fig. 3).

REFERENCES

Anderson, M.M., and Misra, S.B., 1968, Fossils found in the Pre-Cambrian Conception Group of southeastern Newfoundland: Nature, v. 220, p. 680–681, https://doi.org/10.1038/220680a0.

Bannister, J., 2003, The Rule of the Admirals: Law, Custom, and Naval Government in Newfoundland, 1699–1832: University of Toronto Press for The Osgoode Society, Toronto, 423 p.

Billings, E., 1872, On some fossils from the Primordial rocks of Newfoundland:

Canadian Naturalist and Quarterly Journal of Science, v. 6, p. 465–479.
Billings, E., 1874, Palaeozoic Fossils, Volume 2, Part 1: Dawson Brothers, Montreal, 144 p., 9 pl.
Boyce, W.D., and Reynolds, K., 2008, The Ediacaran fossil *Aspidella terranovica* Billings, 1872 from St. John's Convention Centre Test Pit CjAe-33, *in* Pereira, C.P.G., and Walsh, D.G., *eds.*, Current Research: Government of Newfoundland Labrador, Department of Natural Resources, Mines Branch, Report 08–1, p. 55–61.
Carbone, C.A., Narbonne, G.M, Macdonald, F.A., and Boag, T.A., 2015, New Ediacaran fossils from the uppermost Blueflower Formation, northwest Canada: disentangling biostratigraphy and paleoecology: Journal of Paleontology, v. 89, p. 281–291, https://doi.org/10.1017/jpa.2014.25.
City of Ottawa Archives, 2015, Portrait of Elkanah Billings, 1862 / MG002-22-037 / CA000423 / taken by William Notman, http://ottawa.ca/en/residents/arts-heritage-and-culture/city-ottawa-archives/exhibitions/billings-family-virtual-1-1#elkanah-billings-1820-1876; accessed February 3, 2017.
Conniff, R., 2016, House of Lost Worlds: Dinosaurs, Dynasties, and the Story of Life on Earth: Yale University Press, New Haven, 352 p.
Dawson, J.W., 1897, Relics of Primeval Life: Hodder and Stoughton, London, 336 p.
Ellis, R., 1998, The Search for the Giant Squid: The Lyons Press, New York, 322 p.
Fedonkin, M.A., Gehling, J.G., Grey, K., Narbonne, G.M., and Vickers-Rich, P., 2007, The Rise of Animals: Evolution and Diversification of the Kingdom Animalia: The Johns Hopkins University Press, Baltimore, 344 p.
Fensome, R., Williams, G., Achab, A., Clague, J., Corrigan, D., Monger, J., and Nowlan, G., *editors*, 2014, Four Billion Years and Counting: Canada's Geological Heritage: Nimbus Publishing for the Canadian Federation of Earth Sciences, Halifax, 402 p.
Frank, M.G., 2015, Preparing The Ghost: An essay concerning the giant squid and its first photographer: Liverlight Publishing Corporation, division of W.W. Norton & Company Ltd., New York, 297 p.
Gehling, J.G., Narbonne, G.M., and Anderson, M.A., 2000, The first named Ediacaran body fossil, *Aspidella terranovica*: Palaeontology, v. 43, p. 427–456, https://doi.org/10.1111/j.0031-0239.2000.00134.x.
Grazhdankin, D., and Gerdes, G., 2007, Ediacaran microbial colonies: Lethaia, v. 40, p. 201–210, https://doi.org/10.1111/j.1502-3931.2007.00025.x.
Harvey, M., 1869, A Geological Discovery on Newfoundland: A Short Sermon on a Stony Text: Stewart's Quarterly Magazine, v. 3, p. 51–60.
Herbosch, A., and Verniers, J., 2011, What is the biostratigraphic value of the ichnofossil *Oldhamia* for the Cambrian: A review: Geologica Belgica, v. 14, p. 229–248.
Heritage Newfoundland and Labrador, 2001, Portrait of The Reverend Moses Harvey, undated: Photo by S.H. Parsons. Courtesy of the Reverend Ian Wishart, http://www.heritage.nf.ca/articles/society/presbyterian.php; accessed February 3, 2017.
Hofmann, H.J., 1971, Precambrian fossils, pseudofossils, and problematica in Canada: Geological Survey of Canada, Bulletin 189, 146 p., https://doi.org/10.4095/123948.
Hofmann, H.J., O'Brien, S.J., and King, A.F., 2008, Ediacaran Biota on Bonavista Peninsula, Newfoundland, Canada: Journal of Paleontology, v. 82, p. 1–36, https://doi.org/10.1666/06-087.1.
Kinahan, J.R., 1856, The Genus Oldhamia (Forbes): Its character, probable affinities, modes of occurrence, and a description of the nature of the localities in which it occurs in the Cambrian rocks of Wicklow and Dublin: Transactions of the Royal Irish Academy, v. 23, p. 547–561.
King, A.F., 1990, Geology of the St. John's Area: Newfoundland Department of Mines and Energy, Geological Survey Branch, Report 90-2, 88 p.
Liu, A.G., Kenchington, C.G., and Mitchell, E.G., 2015, Remarkable insights into the paleoecology of the Avalonian Ediacaran macrobiota: Gondwana Research, v. 27, p. 1355–1380, https://doi.org/10.1016/j.gr.2014.11.002.
MacGabhann, B.A., 2007, Discoidal fossils of the Ediacaran biota: a review of current understanding, *in* Vickers-Rich, P., and Komarower, P., *eds.*, The Rise and Fall of the Ediacaran Biota: Geological Society, London, Special Publications, v. 286, p. 297–313, https://doi.org/10.1144/SP286.21.
Menon, L.R., McIlroy, D., and Brasier, M.D., 2013, Evidence for Cnidaria-like behavior in ca. 560 Ma Ediacaran *Aspidella*: Geology, v. 41, p. 895–898, https://doi.org/10.1130/G34424.1.
Menon, L.R., McIlroy, D., and Brasier, M.D., 2014, Evidence for Cnidaria-like behavior in ca. 560 Ma Ediacaran *Aspidella*: REPLY: Geology, v. 42, p. e324, https://doi.org/10.1130/G35387Y.1.
Minicucci, J.M., 2016, Elkanah Billings: The lawyer who revealed the ancient life of the past: Geoscience Canada, v. 43, p. 211–222, https://doi.org/10.12789/geocanj.2016.43.101.
Misra, S.B., 1969, Late Precambrian(?) fossils from southeastern Newfoundland: Geological Society of America Bulletin, v. 80, p. 2133–2140, https://doi.org/10.1130/0016-7606(1969)80[2133:LPFFSN]2.0.CO;2.
Misra, S.B., 1971, Stratigraphy and depositional history of Late Precambrian coelenterate-bearing rocks, southeastern Newfoundland: Geological Society of America Bulletin, v. 82, p. 979–988, https://doi.org/10.1130/0016-7606(1971)82[979:SADHOL]2.0.CO;2.
Murray, A., and Howley, J.P., *editors*, 1881, Geological Survey of Newfoundland: Edward Stanford, London, 536 p.
Retallack, G.J., 2014, Evidence for Cnidaria-like behavior in ca. 560 Ma Ediacaran *Aspidella*: COMMENT: Geology, v. 42, p. e323, https://doi.org/10.1130/G34895C.1.
Runnegar, B., 1992, Proterozoic fossils of soft-bodied metazoans (Ediacaran faunas), *in* Schopf, J.W., and Klein, C., *eds.*, The Proterozoic Biosphere. A Multidisciplinary Study: Cambridge University Press, Cambridge, UK, p. 999–1008.
Stewart, K., 2015, Cabinets, cabinets everywhere: Getting ready to welcome new collections from Geological Survey of Canada: Canadian Museum of Nature: http://canadianmuseumofnature.wordpress.com/2015/05/24/cabinets-cabinets-everywhere-getting-ready-to-welcome-new-collections-from-geological-survey-of-canada/; accessed February 3, 2017.
Tacker, R.C., Martin, A.J., Weaver, P.G., and Lawver, D.R., 2010, Trace fossils versus body fossils: *Oldhamia* recta revisited: Precambrian Research, v. 178, p. 43–50, https://doi.org/10.1016/j.precamres.2010.01.008.
The Rooms, 2016, Portrait of Alexander Murray, undated: Public Archives of Canada, C-88097, http://www.therooms.ca/the-geological-survey-of-newfoundland; accessed February 3, 2017.
United Kingdom, 1949, Newfoundland Act, 1949, 12 & 13 Geo. VI, c.22 (U.K.).
Walcott, C.D., 1891, Correlation Papers: Cambrian: Bulletin of the United States Geological Survey, n. 81, p. 1–447.
Weston, T.C., 1896, Notes on the geology of Newfoundland: Proceedings and Transactions of the Nova Scotia Institute of Science, v. 9, p. 150–157.
Whitney, J.D., and Wadsworth, M.E., 1884, The Azoic System and its proposed subdivisions: Bulletin of the Museum of Comparative Zoology, Harvard University, v. 7 (geological series v. 1), p. 1–565.

Received October 2016
Accepted as revised March 2017

GEOLOGICAL ASSOCIATION OF CANADA
(2016-2017)

CORPORATE MEMBERS

PLATINUM

MEMORIAL UNIVERSITY

GOLD

AngloAmerican

Anglo American Exploration (Canada) Ltd.

Northwest Territories Geological Survey

SILVER

ROYAL TYRRELL MUSEUM

YUKON GEOLOGICAL SURVEY

BRITISH COLUMBIA GEOLOGICAL SURVEY

OFFICERS

President
Graham Young

Vice-President
Stephen Morison

Past President
Victoria Yehl

Secretary-Treasurer
James Conliffe

COUNCILLORS

Ihsan Al-Aasm
Alwynne Beaudoin
Oliver Bonham
James Conliffe
Louise Corriveau
Andy Kerr
Stephen Morison
David Pattison
Sally Pehrsson
Liz Stock
Dène Tarkyth
Chris White
Victoria Yehl
Graham Young

STANDING COMMITTEES

Communications: Sally Pehrsson

Finance: Dène Tarkyth

GAC Lecture Tours: Alwynne Beaudoin

Publications: Chris White

Science Program: Louise Corriveau

GEOSCIENCE CANADA

JOURNAL OF THE GEOLOGICAL ASSOCIATION OF CANADA
JOURNAL DE L'ASSOCIATION GÉOLOGIQUE DU CANADA

GAC Medallist Series **1**
Logan Medallist 4
Large-Scale Impact and Earth History
R.A.F. Grieve

Article **27**
Applying Phase Equilibria Modelling to Metamorphic and Geological Processes: Recent Developments and Future Potential
C. Yakymchuk

PoLAR-FIT: Pliocene Landscapes and Arctic Remains—Frozen in Time **47**
J.C. Gosse, A.P. Ballantyne, J.D. Barker, A.Z. Csank, T.L. Fletcher, G.W. Grant, D.R. Greenwood, R.D.E. MacPhee and N. Rybczynski

Who Was the First Person Known to Have Discovered Fossils of the Precambrian (Ediacaran) Organism *Aspidella terranovica*? **55**
J.M. Minicucci

2017 VOLUME 44 GSCNA7 44 1-62
PRINT EDITION ISSN 0315-0941
ONLINE EDITION ISSN 1911-4850